



Western Michigan University  
ScholarWorks at WMU

---

Dissertations

Graduate College

---

12-2007

## Adsorption of Lead on Single and Mixed Solid Systems

Soumya Das  
*Western Michigan University*

Follow this and additional works at: <https://scholarworks.wmich.edu/dissertations>



Part of the Geochemistry Commons, and the Geology Commons

---

### Recommended Citation

Das, Soumya, "Adsorption of Lead on Single and Mixed Solid Systems" (2007). *Dissertations*. 849.  
<https://scholarworks.wmich.edu/dissertations/849>

This Dissertation-Open Access is brought to you for free and open access by the Graduate College at ScholarWorks at WMU. It has been accepted for inclusion in Dissertations by an authorized administrator of ScholarWorks at WMU. For more information, please contact [wmu-scholarworks@wmich.edu](mailto:wmu-scholarworks@wmich.edu).



ADSORPTION OF LEAD ON SINGLE AND MIXED SOLID SYSTEMS

by

Soumya Das

A Dissertation  
Submitted to the  
Faculty of The Graduate College  
in partial fulfillment of the  
requirements for the  
Degree of Doctor of Philosophy  
Department of Geosciences  
Dr. Carla M. Koretsky, Advisor

Western Michigan University  
Kalamazoo, Michigan  
December 2007

## ADSORPTION OF LEAD ON SINGLE AND MIXED SOLID SYSTEMS

Soumya Das, Ph.D.

Western Michigan University, 2007

Metal oxy-hydroxides and phyllosilicate minerals play a significant role in the fate and transport of heavy metals in the environment (Bertsch and Seaman, 1999). Chemical speciation of metals affects their bioavailability and chemical reactivity (Stumm and Morgan, 1996). Surface complexation models (SCMs) based on equilibrium thermodynamic principles have been successfully used to quantify adsorption of heavy metals on pure solid minerals, including phyllosilicates and oxy-hydroxides. For natural sediments with mixed mineralogy, Davis et al. (1998) suggested two different SCM approaches, namely, the component additivity and generalized composite models. In this study, adsorption of lead on pure HFO, silica and kaolinite and on binary and ternary assemblages of HFO, silica and kaolinite have been measured as a function of pH (~2-9), total metal concentration ( $10^{-4}$  to  $10^{-6}$  M Pb), ionic strength of the electrolyte (0.1 to 0.001 M  $\text{NaNO}_3$ ) and solid-to-solid ratio. Results of the single solid systems show that HFO is by far the strongest adsorbent for Pb of the three solids at any given pH. Adsorption of Pb is not affected by ionic strength for HFO, but adsorption decreases strongly with increasing ionic strength for silica and kaolinite systems. This suggests that Pb forms strong inner-sphere complexes on HFO surfaces in contrast to weaker outer-sphere complexes with both silica and kaolinite. Data for the single solid systems are used to derive best fit DLM

thermodynamic stability constants for Pb adsorption and are used to predict adsorption edges for binary and ternary solid mixtures at varying sorbent ratios. Predictions made using the thermodynamic data with a simple component additivity approach are in excellent agreement with experimental data for binary mixtures containing HFO and silica. Fits are poorer when kaolinite is a component in the system. Results for two ternary systems show that the component additivity approach can predict Pb adsorption very. Therefore, this study suggests that if a single solid system has been studied well enough to adequately derive stability constants for a robust surface complexation model, then predictions based on the single systems can provide reasonable estimates of adsorption behavior for systems with mixed mineralogy.

UMI Number: 3293162

### INFORMATION TO USERS

The quality of this reproduction is dependent upon the quality of the copy submitted. Broken or indistinct print, colored or poor quality illustrations and photographs, print bleed-through, substandard margins, and improper alignment can adversely affect reproduction.

In the unlikely event that the author did not send a complete manuscript and there are missing pages, these will be noted. Also, if unauthorized copyright material had to be removed, a note will indicate the deletion.

**UMI**<sup>®</sup>

---

UMI Microform 3293162

Copyright 2008 by ProQuest Information and Learning Company.

All rights reserved. This microform edition is protected against unauthorized copying under Title 17, United States Code.

ProQuest Information and Learning Company  
300 North Zeeb Road  
P.O. Box 1346  
Ann Arbor, MI 48106-1346

Copyright by  
Soumya Das  
2007

## ACKNOWLEDGMENTS

First, I would like to acknowledge to my advisor, Dr. Carla M. Koretsky for her suggestion of this dissertation topic and all of her guidance thorough out this project. I am indebted to her insight and assistance, which has been invaluable throughout my research work. She also helped to answer many questions, which I encountered during researching and writing this dissertation. Not only that, she also provided her sincere help and suggestions during the course of my study here at Western Michigan University. I am also thankful to her for providing me summer research assistantships for the past five years.

I am also grateful to NSF, for the generous funding they provided during this project. I would also like to thank Dr. Johnson R. Haas, Dr. Alan E. Kehew, and Dr. John Miller who provided careful reviews of my dissertation. Dr. Haas provided me many important suggestions and guidance during my research work. I am also thankful to Mrs. Kathryn Wright and Ms. Beth Steele for their sincere care and for everything. I am also thankful to the Department of Geosciences, College of Arts and Sciences, Western Michigan University, for providing me teaching assistantships during these five years.

I would also like to take the opportunity to show my sincere gratitude to my parents (Mr. Gopal Chandra Das and Mrs. Runu Das), to my beloved grandma (Mrs. Pushpa Bala Das), to my late grandpa (Late Chandi Charan Das), to my aunt (Miss

## Acknowledgments—continued

Kalpana Das), my mother-in-law, Mrs. Rekha Seth and to my other family members, whose support, inspiration and sincere care helped me to complete this work.

I also owe special thanks and gratitude to my loving and caring wife, Anushna Das, whose unrelenting mental support, inspiration and encouragement provided me to maintain the intensity, vigor, and effort to the advancement in finishing up my dissertation work. I would also like to recognize and appreciate the sacrifices she has made during my grad-student life and sharing all of the hardships during last couple of years.

Lastly, but not the least, I would also thank my fellow lab mates (Keith, Tracy, Hailachin, Terry, Chris, Kelley) for their sincere help during research work and my friends (Tammy, Sam, Polly, Duane, Tina, Andy, Tracy, Steve, Jodie, Dallas) for their friendship and support.

Soumya Das

## TABLE OF CONTENTS

ACKNOWLEDGMENTS .....	ii
LIST OF TABLES .....	viii
LIST OF FIGURES.....	x
CHAPTER	
I. INTRODUCTION.....	1
Lead in the environment .....	1
Health and toxicity effects.....	1
Natural and anthropogenic sources of lead.....	3
Bioavailability and mobility .....	4
The importance of adsorption in an environmental context.....	6
Surface complexation models.....	9
Adsorption models.....	11
Review of pertinent previous work.....	13
Adsorption of lead on iron oxides and hydroxides .....	13
Adsorption of lead on kaolinite.....	19
Adsorption of lead on silica .....	26
Adsorption of lead onto natural soils and mineral mixtures .....	28
Applicability of Component Additivity (CA) and Generalized Composite (GC) models .....	30
This study: purpose and goals .....	31
Scientific contribution and importance .....	32

Table of Contents—continued

CHAPTER	
II.	MATERIALS AND METHODS..... 33
	Preparation of HFO (Hydrous Iron Oxide) ..... 33
	Kaolinite ..... 34
	Silica..... 34
	Surface area analyses ..... 35
	Preparation of Pb stock solution..... 37
	Batch experiments..... 38
	Kinetics experiment ..... 41
	Kinetics experiment using a dialysis bag ..... 42
III.	RESULTS AND DISCUSSION..... 44
	Single solid phase systems..... 44
	Adsorption of Pb on HFO..... 44
	Adsorption of Pb on silica ..... 45
	Adsorption of Pb on kaolinite..... 50
	Adsorption of Pb on Ward's kaolinite..... 50
	Adsorption of Pb on kaolinite (KGa-1B) ..... 52
	Comparison between Ward's kaolinite and KGa-1B..... 54
	Kinetics experiments in batch solution ..... 56
	Dialysis bag experiments..... 58
	Kinetics experiments using dialysis bags ..... 58
	Pb adsorption of HFO in dialysis bag ..... 59

Table of Contents—continued

CHAPTER		
	Comparison of Pb adsorption among the three different single solid systems: HFO, silica and kaolinite .....	62
	Binary systems.....	66
	Adsorption of Pb on HFO+silica systems .....	66
	HFO+kaolinite (KGa-1B) system .....	69
	Kaolinite (KGa-1B)+silica system.....	72
	Ternary Systems .....	75
IV.	MODELING OF EXPERIMENTAL DATA .....	77
	Single solid systems.....	77
	Adsorption of Pb on HFO.....	77
	Adsorption of Pb on silica .....	90
	Adsorption of Pb on KGa-1B .....	98
	Binary systems.....	107
	HFO+silica system .....	107
	HFO+kaolinite (KGa-1B) system .....	117
	Kaolinite (KGa-1B)+silica system.....	129
	Ternary Systems .....	138
V.	SUMMARY AND CONCLUSION .....	145

Table of Contents—continued

APPENDICES

A. Adsorption of Pb on HFO .....	152
B. Adsorption of Pb on silica .....	155
C. Adsorption of Pb on Ward's kaolinite .....	157
D. Adsorption of Pb on KGa-1B .....	159
E. Adsorption of Pb on HFO+silica .....	161
F. Adsorption of Pb on HFO+KGa-1B .....	164
G. Adsorption of Pb on KGa-1B+silica .....	168
H. Adsorption of Pb on HFO+KGa-1B+silica .....	171
BIBLIOGRAPHY .....	172

## LIST OF TABLES

1.1. Parameters of Pb adsorption onto different iron oxides and hydroxides.....	14
1.2. Experimental parameters used in studies of Pb adsorption onto kaolinite .....	20
1.3. Modeling parameters used in studies of Pb adsorption onto kaolinite.....	20
2.1. Surface areas (in m <sup>2</sup> /g) of solids used in this study.....	37
2.2. Amount of sorbent (in g) used for various binary kaolinite and HFO experiments.....	39
2.3. Amount of sorbent (in g) used for various binary silica and HFO experiments.....	39
2.4. Amount of sorbent (in g) used for various binary kaolinite and silica experiments.....	39
2.5. Amount of sorbents (in g) used in ternary mixtures.....	40
3.1. Experimental conditions for adsorption of Pb on HFO.....	44
3.2. Experimental conditions for adsorption of Pb on silica .....	45
3.3. Experimental conditions for Pb adsorption onto KGa-1B.....	52
3.4. Adsorption of Pb on the four single solids. All experiments were completed with 10 <sup>-5</sup> M Pb, 0.01M NaNO <sub>3</sub> , and 2 g/L total solid.....	64
3.5. A comparison of the pH at which various percents of Pb adsorption occur for pure HFO and silica systems, as well as for the various binary mixtures. All experiments conducted with 10 <sup>-5</sup> M Pb, 0.01M NaNO <sub>3</sub> , and 2 g/L total solid.....	67
3.6. A comparison of the pH at which different percentages of Pb adsorption occur for the pure HFO and silica systems, as well as for the various binary mixtures. All experiments conducted with 10 <sup>-5</sup> M Pb, 0.01M NaNO <sub>3</sub> , and 2 g/L total solid .....	70
3.7. pH values at which a given the percentage of Pb adsorption occurs for the pure silica and kaolinite systems, together with the mixed systems .....	73

List of Tables—continued

3.8. pH at which a given the percent Pb adsorbed occurs on the pure solids and the 1:1:1 ratios of the solids.....	75
4.1. Exchange capacities of strong and weak sites on ferrihydrite surfaces as proposed by Dzombak and Morel (1990) .....	78
4.2. Site densities of three sites on ferrihydrite surface as proposed by Swedlund et al. (2003) .....	80
4.3. Comparison between stability constants for Pb surface complexes on ferrihydrite from Dzombak and Morel (1990) and Swedlund et al. (2003) .....	80
4.4. Best-fit log stability constants for Pb adsorption on the HFO strong site for each of adsorption experiments.....	82
4.5. A comparison of stability constants used to describe Pb adsorption on HFO.....	83
4.6. Best-fit log Ks for Pb adsorption on silica for each adsorption edge measured in this study.....	92
4.7. Exchange capacities for two site kaolinite surface, as proposed by Benyahya and Garnier (1999) .....	100
4.8. Best-fit log Ks for Pb adsorption on kaolinite based on 2-site DDLM.....	102
4.9. Stability constants for Pb adsorption used for modeling of binary mixtures.....	108
4.10. Best-fit log stability constants for Pb adsorption on HFO and kaolinite.....	117
4.11. Stability constants for Pb adsorption on kaolinite and silica derived for the single solid systems and used for the binary system speciation calculations.....	129
4.12. Stability constants derived for single solid systems and used for modeling ternary mixtures.....	138

## LIST OF FIGURES

3.1. Percentage adsorption of Pb on HFO as a function of pH, sorbate/sorbent ratio and background electrolyte.....	46
3.2. Percent adsorption of Pb on silica as function of pH. All experiments were completed in NaNO <sub>3</sub> using 2 g/L silica with a BET surface area of 9.4 m <sup>2</sup> /g.....	49
3.3. Adsorption of Pb on Ward's kaolinite with Pb concentrations varied from 10 <sup>-4</sup> to 10 <sup>-6</sup> M. The concentration of the background electrolyte was kept constant (0.01M NaNO <sub>3</sub> ), as was the amount of sorbent (2 g/L) .....	51
3.4. Percent adsorption of Pb on kaolinite KGa-1B as a function of pH. Experiments were completed with 10 <sup>-5</sup> or 10 <sup>-6</sup> M Pb, a background electrolyte of 0.01 or 0.1M NaNO <sub>3</sub> and 2 g/L kaolinite .....	53
3.5. Comparison of Pb adsorption as a function of pH between Ward's kaolinite and KGa-1B for 10 <sup>-5</sup> and 10 <sup>-6</sup> M Pb, 2 g/L kaolinite and 0.01M NaNO <sub>3</sub> .....	55
3.6. Kinetics experiments showing the percentage of Pb adsorbed as a function of time. The adsorption experiments was completed at pH~10 and the desorption experiment at pH~2. Both experiments were completed using 2 g/L of kaolinite KGa-1B, 0.01M NaNO <sub>3</sub> and 10 <sup>-5</sup> M Pb.....	57
3.7. Kinetics of Pb adsorption and desorption on HFO contained within a dialysis bag. The adsorption experiment was initiated by increasing the pH to ~10 and desorption by dropping the pH to ~2.....	60
3.8. Comparison between the percentage of Pb adsorbed to HFO as a function of pH with 10 <sup>-5</sup> M Pb, 2 g/L HFO and 0.01M NaNO <sub>3</sub> with and without a dialysis bag .....	63
3.9. Comparison of Pb adsorption as as function of pH among the three adsorbents: HFO, silica and kaolinite (KGa-1B and Ward's) for 10 <sup>-5</sup> M Pb, 0.01M NaNO <sub>3</sub> and 2 g/L solid.....	65

List of Figures—continued

3.10. Percentage of Pb adsorption on binary mixtures of HFO+silica with six different solute-to-solute ratios as function of pH. All experiments were completed with $10^{-5}$ M Pb, 0.01M NaNO <sub>3</sub> and 2 g/L total solid .....	68
3.11. Percent of Pb adsorbed on binary mixtures of HFO+kaolinite (KGA-1B) with seven different kaolinite:HFO ratios as a function of pH. All experiments were completed with $10^{-5}$ M Pb, 0.01M NaNO <sub>3</sub> and 2 g/L total solid.....	71
3.12. The percentage of Pb adsorbed as a function of pH in kaolinite and silica systems with $10^{-5}$ M Pb, 0.01M NaNO <sub>3</sub> and 2 g/L total solid .....	74
3.13. Pb adsorption for ternary systems containing all these three pure mineral phases in a ratio of 1:1:1 by surface area as well as by mass as a function of pH. All experiments were completed with $10^{-5}$ M Pb, 0.01M NaNO <sub>3</sub> and 2 g/L total solid.....	76
4.1. Comparison of fits to experimental data ( $10^{-4}$ M Pb, 0.01M NaNO <sub>3</sub> ) produced using the parameters from the DLM proposed by Dzombak and Morel (1990) and Swedlund et al. (2003) and using the modified average stability constant for Pb adsorption on the strong site from this study .....	84
4.2. Comparison of fits to experimental data ( $10^{-5}$ M Pb, 0.01M NaNO <sub>3</sub> ) produced using the parameters from the DLM proposed by Dzombak and Morel (1990) and Swedlund et al. (2003) and using the modified average stability constant for Pb adsorption on the strong site from this study .....	85
4.3. Comparison of fits to experimental data ( $10^{-6}$ M Pb, 0.1M NaNO <sub>3</sub> ) produced using the parameters from the DLM proposed by Dzombak and Morel (1990) and Swedlund et al. (2003) and using the modified average stability constant for Pb adsorption on the strong site from this study .....	86
4.4. Comparison of fits to experimental data ( $6.8 \cdot 10^{-7}$ M Pb, 0.1M NaNO <sub>3</sub> ) produced using the parameters from the DLM proposed by Dzombak and Morel (1990) and Swedlund et al. (2003) and using the modified average stability constant for Pb adsorption on the strong site from this study .....	87

## List of Figures—continued

4.5. Comparison of fits to experimental data ( $6.10^{-8}$ M Pb, 0.001M NaNO <sub>3</sub> ) produced using the parameters from the DLM proposed by Dzombak and Morel (1990) and Swedlund et al. (2003) and using the modified average stability constant for Pb adsorption on the strong site from this study .....	88
4.6. Model fits using the average stability constant for Pb adsorption on the strong site for the 2-site model derived in this study for all experiments .....	89
4.7. Experimental data (squares) for $10^{-5}$ M in 0.1M NaNO <sub>3</sub> and best DLM fit achieved by adjusting the log K for Pb adsorption on a single silica surface site.....	94
4.8. Experimental data (squares) for $10^{-5}$ M in 0.01M NaNO <sub>3</sub> and best DLM fit achieved by adjusting the log K for Pb adsorption on a single silica surface site.....	95
4.9. Experimental data (squares) for $10^{-6}$ M in 0.01M NaNO <sub>3</sub> and best DLM fit achieved by adjusting the log K for Pb adsorption on a single silica surface site.....	96
4.10. Model fits for all three experiments using the average log K for Pb adsorption derived from the three edges.....	97
4.11. Experimental data (squares) for $10^{-5}$ M in 0.01M NaNO <sub>3</sub> and best DLM fit achieved by adjusting the log Ks for Pb adsorption on a two surface site model of kaolinite .....	103
4.12. Experimental data (squares) for $10^{-5}$ M in 0.1M NaNO <sub>3</sub> and best DLM fit achieved by adjusting the log Ks for Pb adsorption on a two surface site model of kaolinite .....	104
4.13. Experimental data (squares) for $10^{-6}$ M in 0.01M NaNO <sub>3</sub> and best DLM fit achieved by adjusting the log Ks for Pb adsorption on a two surface site model of kaolinite .....	105
4.14. Model fits for all three experiments using the average log K for Pb adsorption derived from the three edges.....	106
4.15. Predicted fit for a mixture of silica and HFO of 1:1 with $10^{-5}$ M Pb in 0.01M NaNO <sub>3</sub> based on thermodynamic parameters derived for the single solid systems .....	109

List of Figures—continued

4.16. Predicted fit for a mixture of silica and HFO of 5:1 with $10^{-5}$ M Pb in 0.01M NaNO <sub>3</sub> based on thermodynamic parameters derived for the single solid systems .....	110
4.17. Predicted fit for a mixture of silica and HFO of 10:1 with $10^{-5}$ M Pb in 0.01M NaNO <sub>3</sub> based on thermodynamic parameters derived for the single solid systems .....	111
4.18. Predicted fit for a mixture of silica and HFO of 50:1 with $10^{-5}$ M Pb in 0.01M NaNO <sub>3</sub> based on thermodynamic parameters derived for the single solid systems .....	112
4.19. Predicted fit for a mixture of silica and HFO of 100:1 with $10^{-5}$ M Pb in 0.01M NaNO <sub>3</sub> based on thermodynamic parameters derived for the single solid systems .....	113
4.20. Predicted fit for a mixture of silica and HFO of 500:1 with $10^{-5}$ M Pb in 0.01M NaNO <sub>3</sub> based on thermodynamic parameters derived for the single solid systems .....	114
4.21. Predicted fit for a mixture of silica and HFO of 1:1, 5:1, and 10:1 with $10^{-5}$ M Pb in 0.01M NaNO <sub>3</sub> based on thermodynamic parameters derived for the single solid systems.....	115
4.22. Predicted fit for a mixture of silica and HFO of 50:1, 100:1, and 500:1 with $10^{-5}$ M Pb in 0.01M NaNO <sub>3</sub> based on thermodynamic parameters derived for the single solid systems.....	116
4.23. Predicted fit for a mixture of kaolinite and HFO of 1:1 with $10^{-5}$ M Pb in 0.01M NaNO <sub>3</sub> based on single systems thermodynamic parameters.....	120
4.24. Predicted fit for a mixture of kaolinite and HFO of 5:1 with $10^{-5}$ M Pb in 0.01M NaNO <sub>3</sub> based on single systems thermodynamic parameters.....	121
4.25. Predicted fit for a mixture of kaolinite and HFO of 10:1 with $10^{-5}$ M Pb in 0.01M NaNO <sub>3</sub> based on single systems thermodynamic parameters .....	122
4.26. Predicted fit for a mixture of kaolinite and HFO of 50:1 with $10^{-5}$ M Pb in 0.01M NaNO <sub>3</sub> based on single systems thermodynamic parameters .....	123

List of Figures—continued

4.27. Predicted fit for a mixture of kaolinite and HFO of 100:1 with $10^{-5}$ M Pb in 0.01M NaNO <sub>3</sub> based on single systems thermodynamic parameters .....	124
4.28. Predicted fit for a mixture of kaolinite and HFO of 500:1 with $10^{-5}$ M Pb in 0.01M NaNO <sub>3</sub> based on single systems thermodynamic parameters .....	125
4.29. Predicted fit for a mixture of kaolinite and HFO of 5000:1 with $10^{-5}$ M Pb in 0.01M NaNO <sub>3</sub> based on single systems thermodynamic parameters .....	126
4.30. Predicted fit for a mixture of kaolinite and HFO of 1:1, 5:1, 10:1, and 50:1 with $10^{-5}$ M Pb in 0.01M NaNO <sub>3</sub> based on single systems thermodynamic parameters .....	127
4.31. Predicted fit for a mixture of kaolinite and HFO of 100:1, 500:1, 5000:1 with $10^{-5}$ M Pb in 0.01M NaNO <sub>3</sub> based on single systems thermodynamic parameters .....	128
4.32. Predicted fit for a mixture of kaolinite and silica of 1:1 with $10^{-5}$ M Pb in 0.01M NaNO <sub>3</sub> based on single systems thermodynamic parameters.....	131
4.33. Predicted fit for a mixture of kaolinite and silica of 10:1 with $10^{-5}$ M Pb in 0.01M NaNO <sub>3</sub> based on single systems thermodynamic parameters .....	132
4.34. Predicted fit for a mixture of kaolinite and silica of 50:1 with $10^{-5}$ M Pb in 0.01M NaNO <sub>3</sub> based on single systems thermodynamic parameters .....	133
4.35. Predicted fit for a mixture of kaolinite and silica of 0.1:1 with $10^{-5}$ M Pb in 0.01M NaNO <sub>3</sub> based on single systems thermodynamic parameters .....	134
4.36. Predicted fit for a mixture of kaolinite and silica of 0.02:1 with $10^{-5}$ M Pb in 0.01M NaNO <sub>3</sub> based on single systems thermodynamic parameters .....	135
4.37. Predicted fits for mixtures of kaolinite and silica 1:1, 10:1 and 50:1 ratios with $10^{-5}$ M Pb in 0.01M NaNO <sub>3</sub> .....	136

List of Figures—continued

4.38. Model fits for mixtures of kaolinite and silica 1:1, 0.1:1 and 0.02:1 ratios with $10^{-5}$ M Pb in 0.01M NaNO <sub>3</sub> .....	137
4.39. Model fit for 1:1:1 ratio by mass with $10^{-5}$ M Pb in 0.01M NaNO <sub>3</sub> .....	140
4.40. Model fit for 1:1:1 by surface areas with $10^{-5}$ M Pb in 0.01M NaNO <sub>3</sub> .....	141
4.41. Model fits for ternary systems for all ratios with $10^{-5}$ M Pb in 0.01M NaNO <sub>3</sub> .....	142
4.42. Percentage of adsorbed Pb species for a 1:1:1 mixture by mass.....	143
4.43. Percentage of adsorbed Pb species for a 1:1:1 mixture by surface areas .....	144

## CHAPTER I

### INTRODUCTION

#### Lead in the environment

##### Health and toxicity effects

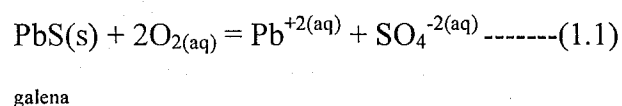
Heavy metal toxicity, or heavy metal poisoning, is widespread in the world today. Ground water and sediment contamination by toxic metals poses a major problem worldwide. Approximately 1300 sites in the United States are identified as “Superfund” sites, which are highly contaminated by various heavy metals and metal bearing phases (Bethke and Brady, 1999). About 75% of all Superfund sites have been identified as being contaminated by metals. The most common of metals found in these Superfund sites are lead, chromium, arsenic, zinc, cadmium, copper and mercury, of which lead contamination has been far more severe than any other metals. As of 1996, according to the US EPA, 460 sites had been contaminated by lead whereas chromium, which is also a severe threat to human beings, had been found to occur in 306 Superfund sites (Evanko and Dzombak, 1997). Exposure to excessive quantities of heavy metals can cause cardiovascular disease, high blood pressure, insomnia, and other illnesses, as well as radical damage, which leads to heart attacks, strokes and cancer. Moreover, water polluted by heavy metals can cause deadly diseases like Melanosisce (scattered brown spots on human skin), bronchitis, conjunctivitis, skin cancer, cirrhosis of the liver, blood cancer and others, potentially causing the death of human beings (Guha Mazumdar et al., 1992). Heavy metal toxicity is frequently the result of long term, low-level exposure to

pollutants found in air, water, food, and various consumer products (Baldwin and Marshall, 1999).

Lead is one of the heavy toxic metals that cause major health problems in many places globally and throughout the United States not only in adults, but especially in children. The most severely affected states include: Alabama, Connecticut, Maine, Michigan, New York, North Carolina, Ohio, Oklahoma, Vermont, and Wisconsin (Prikle et al., 1994). Lead is highly toxic and can affect almost every system of the human body. High levels of lead can cause coma, and even death in human beings. Children with high levels of lead in their blood can sustain damage to their brain and nervous systems and may experience behavior and learning problems, nervousness, headaches, slowed growth rates, hearing problems, and so on (Baldwin and Marshall, 1999). Symptoms of lead poisoning in children mimic those of Attention Deficit Hyperactivity Disorder (ADHD). The original threshold value for adverse effect of lead in the blood was 25  $\mu\text{g}/\text{dL}$  (Schwartz, 1994). This number has been decreased to 10  $\mu\text{g}/\text{dL}$ . According to the study carried out by Federal Agencies, elevated lead has been found to occur in the blood of 8.9% (1.7 million) of American children (Brody et al., 1994). According to NHANES (National Health and Nutrition Examination Survey) lead is most dangerous to children under 6 years of age. Lead is also harmful to adults. Adults can suffer from difficulties during pregnancy, reproductive problems, high blood pressure, digestive problems, nerve disorders, memory and concentration problems, muscle and joint pain, and so on. The EPA has set its most recent MCL (maximum concentration limit) for lead in drinking water at 15 ppb.

### Natural and anthropogenic sources of lead

Metals are introduced naturally into ground and surface waters through mineral weathering, atmospheric deposition, and volcanic activity. Metals, including lead, are increasingly introduced into the biosphere through anthropogenic sources. Natural processes rarely result in dangerously elevated concentrations in the environment; in fact, human activities release the most lead and frequently result in incidents of local contamination. This currently accounts for significantly more lead than is introduced naturally into the biosphere. Anthropogenic sources include industrial waste, landfill leachates, mine tailings, atmospheric deposition from burning of fossil fuels and ore processing (Hochella and White, 1990). Runoff or infiltration of water from base metal sulfide mines is problematic in many countries, and leads to pollution of nearby water sources with potentially serious ecosystem effects. Metal pollutants deriving from mining activities include copper, lead, cadmium and zinc. Sulfate, lead and zinc are produced from oxidation of galena, e.g.,



and sphalerite, which releases metals and sulfate (Younger, 2000). Industrial wastewater, sewage sludge and solid waste materials discharge metals like lead, copper, arsenic, selenium, zinc, boron, chromium, and iron into the environment. These materials can enter surface waters and subsurface aquifer systems, resulting in the pollution of irrigation and drinking water (Shivkumar et al., 1996). Other common anthropogenic sources of lead to the environment include auto body shops, electric storage batteries,

glazes for china dishes, crockery, insecticides, electric cable insulation, hose, pipe, sheet and floor coverings. Lead is associated with stained glass-work, jewelry making and antique ceramic doll painting and lead paint (White and Travers, 1990). Widespread lead contamination due to metal smelting and processing, secondary metals production, lead battery manufacturing, pigment and chemical manufacturing, and lead-contaminated wastes as well as use of lead in gasoline are the major sources of lead in soils in the United States (Evanko and Dzombak, 1997).

Natural hot springs can potentially discharge heavy metals into the environment (Craw et al., 1999). Hot springs could be one of the significant (like other natural sources including weathering and erosion, volcanoes and forest fires etc.) point sources for metals like arsenic, cadmium, mercury, zinc and lead. Most of the hot springs water contain dissolved metals at their discharge points and these metals readily enter into the soil and stream system either in solution or as precipitates. Precipitates can be further mobilized by erosion and thus enter surface waters and stream sediments. Polluted waters can percolate through the soil and mix with ground water, which can lead to severe pollution of ground water in a short period of time, as metals like As, Cd, Hg, Zn and Pb are relatively soluble in hot water and are toxic at ppb levels (Craw et al., 1999).

#### Bioavailability and mobility

There is a consensus among the scientific community that the risk to living organisms associated with the presence of heavy metals in the environment is primarily determined by the solubility and mobility of the various heavy metal-bearing phases or species present rather than by the total metal concentration (Allen et al., 1980; Anderson

and Benjamin, 1990). The toxicity of heavy metals depends on their distribution into solid, more immobile and typically less bioavailable phases versus dissolved phases, and is usually directly proportional to the free metal ion activity (Traina and Laperche, 1999; Brown and Markich, 2000). The free-ion-activity model (FIAM) was developed to describe metal-organism interactions determining the uptake and bioavailability of cationic trace metals. Free, or uncomplexed, metal ions in solution are typically more bioavailable compared to organic or inorganic metal complexes (Hudson, 1998). For example, copper is mostly associated with organic colloidal matter, lead can be present in both inorganic and organic phases, cadmium is typically present as free dissolved ion and zinc can be present in both ionic and colloidal forms (Allen et al., 1980). According to Allen et al. (1980) the stronger the metal complex, the lower the toxicity of metal ions (or bioavailability of nutrient ions). Toxicity typically increases as metal complexes dissociate (i.e., in response to changes in environmental factors like pH, Eh or temperature change) and produce free metal ions. According to Anderson and Benjamin (1990), oxides of iron, silicon, and alumina have a paramount influence on the mobility as well as the bioavailability of trace metals in aqueous systems and sediments as these oxides are the major constituents of natural sediments. Trivedi et al. (2003) also concluded that mobility and availability of heavy metals like lead and zinc is primarily controlled by sorption reactions with iron hydroxides in the environment. Appelo et al. (2002), suggested that the elevated arsenic concentrations in Bangladesh and the eastern part of India is due to hydrogeochemical reactions. In particular, it has been suggested that reduction of oxyhydroxides is a prime cause for mobilization of arsenic in ground water because arsenic was bound to these oxyhydroxides. This demonstrates that it is

important to understand the reactions between metals and minerals in sediments in order to predict metal mobility and bioavailability.

Lead is most commonly found in nature in forms of oxides and hydroxides (Evanko and Dzombak, 1997). Free  $\text{Pb}^{2+}$  and  $\text{Pb}^{2+}$ -hydroxy complexes along with Pb-carbonates and Pb-organic complexes are typically the most stable forms of dissolved lead in natural systems (Smith et al., 1995). For example, lead can form complexes with inorganic ligands such as  $\text{Cl}^-$ ,  $\text{CO}_3^{2-}$ ,  $\text{SO}_4^{2-}$ ,  $\text{PO}_4^{3-}$  and with organic ligands like humic and fulvic acids, EDTA, or amino acids. When  $\text{Pb}^{2+}$  is complexed with such ligands, these compounds tend to have low solubility (Bodek et al., 1988). Lead can also sorb on mineral surfaces and form surface precipitates such as  $\text{PbCO}_3$ ,  $\text{Pb}_2\text{O}$ ,  $\text{Pb}(\text{OH})_2$ , and  $\text{PbSO}_4$  (Evanko and Dzombak, 1997).

#### The importance of adsorption in an environmental context

Sorption is defined as any process by which mass transfer of a chemical species from solution to solid occurs. Species being removed from solution are called sorbates and the solids to which they sorb are called sorbents. Sorption of ions can occur by adsorption, or surface complexation, or via diffusion (absorption) or co-precipitation (Parks, 1990). In adsorption, a chemical species is physically or chemically bound at the mineral surface. It is often assumed that a monolayer of sorbates bind to an essentially "2-D" mineral water interface. Symbols like  $\text{>}$ ,  $\text{>S}$  or  $\equiv$  are used to represent a bond between a sorbate and the underlying crystal structure. For example, when lead is adsorbing on a mineral surface, it can be written as  $\text{Pb}^{2+} + \text{>S} = \text{>SPb}^{2+}$  (Stumm and Morgan, 1996).

Sorption is one of the most important chemical processes governing the mobility and solubility of metals. The extent of sorption in a given sediment or soil depends upon both the mineralogy and also the aqueous phase geochemistry (Stumm and Morgan, 1996). For example, it has been demonstrated that metal oxy-hydroxides minerals and phyllosilicates such as micas and clays, together with organic substances, play a significant role in metal sorption and therefore in the fate and transport of heavy metals in the environment (Bertsch and Seaman, 1999).

Dissolved metals can interact with solids by a variety of processes, including adsorption, absorption and surface precipitation. Adsorption, or complexation, is the process by which dissolved constituents become bound at the surfaces of minerals or other solid constituents. Complexation reactions at the mineral-water interface strongly affect the transportation of metals in environments (Davis and Kent, 1990). The movement of contaminants through soils or aquifers could be retarded or enhanced by surface complexation reactions (Koretsky, 2000).

Movement of contaminants greatly depends on sorption processes. When metals are attached to mineral or sediment particle surfaces, they are immobile, unless the particle itself moves (e.g., a major issue with P in the environment) but when they are desorbed, metals and other contaminants may move more freely from one point to another. For example, once lead is released to the environment either from anthropogenic or natural sources, it tends to be retained by soil and sediments (Evans, 1989). Adsorption, along with processes like ion exchange, precipitation, and complexation govern the fate and transport of lead in the environment. These processes limit the amount of lead that can be transported into the surface water or groundwater (Smith et al., 1995). The pH of the

solution, concentration of dissolved salts and the types of mineral surfaces present in an aquifer and in soils determine the amount of soluble lead that can be present in surface and ground waters (Evanko and Dzombak, 1997).

Many field studies have shown that sorption processes control the movement of many heavy metals like Zn, V, Ni, Cu, Pb and As, which are released through acid mine drainage and industrial operations (Fuller and Davis, 1989). Sorption also controls the dissolved concentrations of metals in river waters. Dissolved metals could be adsorbed onto river sediments during transportation, which could cause lower metal concentrations in solution but higher concentrations in riverine sediments. This can control the amount of metals entering into estuaries and marine systems through rivers, which feed them (Fuller and Davis, 1989). Not only in rivers, but also in lake and ocean sediments and water columns, sorption plays a major role in controlling nutrient availability for phytoplankton, filter feeders and burrowing organisms. Uptake of potentially toxic metals increases the risk to these organisms and thus affects the whole food chain (Luoma and Davis, 1983; Morel and Hudson, 1985).

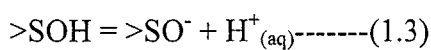
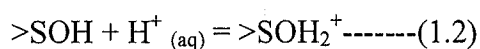
Precipitation is also another potentially important process that controls Pb mobility in the environment. For example, Martinez and McBride (1998) studied the solubility of Co, Cu, Pb and Zn in aged co-precipitates with amorphous iron hydroxides. The goal of their study was to test the efficiency of co-precipitation in limiting the solubility and mobility of these toxic metals into the environment. Previously, most co-precipitation experiments were conducted at pH ~7, but they argued that at pH ~7, most of the metals would be removed from the solution. However, if pH decreases, these co-precipitates would not be stable and might fail to limit metal solubility, ultimately increasing the availability of the

co-precipitated metals to organisms. Therefore, they conducted experiments at pH 6 and aged the co-precipitates for 200 days. Their experiments were done with known concentrations of metals together with  $\text{Fe}^{3+}$ , in a 1 M  $\text{KNO}_3$  background electrolyte, and titrated with 0.1 M KOH until pH 6. They found that the aqueous concentration of Pb in equilibrium with the solids, after aging the co-precipitates for the long period of time had decreased to <5 nM compared to original concentration ranging from 500-1500 ppm. Other metals also showed a decreasing trend of soluble concentration.

Apart from these environmental issues, adsorption could also play a major role in chemical weathering of sulfide minerals by scavenging of metals like Pb and Hg, and in influencing dissolution rates of rock forming minerals (Stumm et al., 1992) and formation of ore deposits by adsorption/reduction reactions on sulfide surfaces (Bancroft and Hyland, 1990). Sorption processes have been utilized also in metallurgical processes as well as in treatment of mine tailings and wastewater. Wastewater, which often contains a variety of metals, is sometimes passed through mineral columns on which metals are adsorbed to reduce the concentrations of metals in the water (Benjamin et al, 1982; Leake et al., 1985).

### Surface complexation models

According to Surface Complexation Models (SCMs), minerals can be approximately described as flat planes of surface hydroxyl groups ( $>\text{SOH}$ ) (Sposito, 1984; Kent et al., 1986; Davis and Kent, 1990). Variable surface charge is produced due to surface protonation or deprotonation reactions on the mineral surfaces according to the following types of reactions:



where  $>\text{SOH}$  indicates a surface hydroxyl group,  $>\text{SOH}_2^+$  is a protonated surface hydroxyl group and  $>\text{SO}^-$  is a deprotonated surface group. According to Surface Complexation Theory, metals can attach to these surface hydroxyl groups producing aqueous metal complexes (Sposito, 1984). For example, the following reaction describes the formation of a Pb complex on a mineral surface:



where  $>\text{SOPb}^+$  is a monodentate surface complex. These surface complexation reactions can be described by thermodynamic mass law equations, where the stability constant of a reaction can be calculated as, for example,

$$K^{\text{int}} = \frac{\{>\text{SOPb}^+\} \{\text{H}^+\}}{\{\text{Pb}^{2+}\} \{>\text{SOH}\}} \text{-----}(1.5)$$

where,  $\{\}$  indicates the activity of a given species and  $K^{\text{int}}$  = the intrinsic stability constant of the reaction, in this case, describing Pb adsorption on a surface hydroxyl site.

Sorbates may form different types of bonds with the mineral surfaces on which they adsorb. Charge at the mineral surfaces can be obtained in two principal ways, that is, by isomorphic substitution and surface complexation (Kehew, 2000). Charges developed due to isomorphic substitution, such as in 2:1 clay minerals, are also termed “permanent structural charge” and are assumed to be fixed. Permanent structural charge is most often associated with 2:1 clay minerals (also true for imperfect 1:1 clays like kaolinite), such as smectites and vermiculites, which have charge deficiency due to substitution of cations of lesser charge (e.g.,  $\text{Si}^{4+}$  by  $\text{Al}^{3+}$  in tetrahedral sheets, or  $\text{Al}^{3+}$  by  $\text{Mg}^{+2}$  in octahedral sheets), which is balanced by interlayer cations. In contrast, variable surface charge, with

the magnitude of the charge dependent on pH, is produced by surface complexation reactions (Kehew, 2000). For example, clay minerals have rings of siloxane groups, which are present at the basal and the interlayer regions in addition to surface hydroxyl groups (Sposito, 1989). When cations bond directly with the oxygen of the siloxane cavity, they form inner sphere complexes. This is also known as chemical or specific adsorption where the bonds are much stronger than weak van der Waals bonds and are ionic or covalent in nature (Koretsky, 2000). An outer sphere complex is formed when the sorbing cation retains waters of hydration, rather than binding directly to the mineral surface functional groups (Sposito, 1989). This is also known as “physical adsorption” as these sorbates are held on the mineral surface by weak van der Waals bonds (Koretsky, 2000).

### Adsorption models

Surface complexation models (SCMs) describing metal ion binding to oxide and other mineral surfaces have been developed based on equilibrium thermodynamic principles. Different types of SCMs have been proposed for quantifying adsorption reactions, such as the diffuse layer model (DLM), the constant capacitance model (CCM), and the triple layer model (TLM) (Hayes et al., 1991). All surface complexation models have four assumptions in common: sorption of ions takes place at specific surface sites; sorption reactions can be described by mass law equations; surface charges results from the sorption of ions; and electrostatic effects on ion binding are taken into account (Dzombak and Morel, 1990). The literature on surface complexation modeling largely describes the results of well-controlled laboratory investigations of the adsorption of

heavy metals by a variety of mineral phases. SCMs have been successfully used to investigate single metal (lead, zinc, cadmium, copper, cobalt, etc.) adsorption on a wide variety of pure solid minerals (goethite, kaolinite, quartz, etc.) (Sposito, 1984; Hayes, 1987; Davis and Hem, 1989; Dzombak and Morel, 1987, 1990).

Competitive adsorption of two metals on single mineral surfaces has also been studied using the SCM approach. For example, Christl and Kretzschmar, (1999) investigated the competitive sorption of copper and lead on oxide surfaces as a function of pH and total metal concentration. Few studies, however, have applied SCMs to metal adsorption in mixed mineral assemblages (Davis et al., 1998). Applications of SCMs to adsorption of ions by soil materials are relatively rare due in part to the complexity of natural sediments (Cowan et al., 1992; Coston et al., 1995; Bertsch and Seaman, 1999; Barnett et al., 2002). The use of equilibrium models to guide soil remediation is complicated by the heterogeneous nature of most contaminated soils.

Davis et al. (1998) suggested two different approaches for using the SCMs approach to describe environmental sorbents, namely, the component additivity and generalized composite methods. The component additivity (CA) approach attempts to predict adsorption on complex mineral assemblages using adsorption data derived for pure mineral or organic phases. No fitting of field or laboratory data is required to apply this model, although the solid phase materials must be very well described. The generalized composite (GC) approach assumes that the surface compositions of complex mineral assemblages are too complex to be quantified using just the contributions from each separate pure individual mineral phase. According to the general composite approach the adsorptive reactivity of the surface is best described by generic surface functional groups

and by fitting experimental adsorption data using sediments from a specific site. This approach is also somewhat simplified compared to the CA approach because the pH dependence of adsorption is fitted without representation of electrostatic energies. The component additivity model, if found to be generally applicable, has a great advantage over the GC model, because it does not require labor-intensive measurements of adsorption to be made for each “new” system of interest. Rather, the previously described data can be used to make quantitative predictions of metal speciation. In spite of this potentially significant advantage, the CA model has yet to be extensively tested, in either laboratory or field settings.

### Review of pertinent previous work

#### Adsorption of lead on iron oxides and hydroxides

Iron-oxides and hydroxides are one of the major constituents of most natural soils, sediments, and aquifers. These oxides and hydroxides have very high surface areas and can be present finely dispersed in sediments and coated over other minerals. Thus, they can play major role in metal ion adsorption (Samad and Watson, 1998).

Dzombak and Morel (1990) pioneered the development of a large, internally-consistent database of thermodynamic parameters characterizing the adsorption of many metals, including lead, on hydrous ferric oxide (HFO) surfaces. Dzombak and Morel (1990) proposed a two-site (one strong site, one weak site) electrostatic double layer model to describe metal sorption on HFO. Protons and metals (e.g.,  $\text{Pb}^{2+}$ ) compete for the two types of binding sites, and equilibrium is described by mass-action equations.

Activities of the surface species depend on the potential at the surface, which is due to the development of surface charge. They proposed a reactive surface area of  $600 \text{ m}^2/\text{g}$  with  $0.078 \text{ } \mu\text{mol}/\text{m}^2$  of strong sites and  $3.11 \text{ } \mu\text{mol}/\text{m}^2$  of weak sites on HFO for modeling purposes, although other workers have used different parameters to fit experimental data for Pb adsorption on HFO (Table 1.1).

Table 1.1 Parameters of Pb adsorption onto different iron oxides and hydroxides

Previous workers	Model type	Colloid type	Site type	Type of Pb-complex
Dzombak and Morel (1990)	Diffuse Double Layer (DDL)	Ferrihydrite	2 types, one strong and one weak	Inner-sphere
Coughlin and Stone (1995)	Triple Layer Model (TLM)	Goethite	One type	Both outer and inner-sphere
Christl and Kretzschmar (1999)	Triple Layer Model (TLM)	Hematite	One type SOH	Both outer and inner-sphere
Swedlund et al (2003)	Diffuse Double Layer (DDL)	Ferrihydrite	3 types, one strong, one weak and one type '0'	Inner-sphere
Dyer et al. (2003)	Triple Layer Model (TLM)	Ferrihydrite	One type SOH	Inner sphere
Trivedi et al. (2003)	Triple Layer Model (TLM)	Ferrihydrite	One type	Inner sphere

Various surface complexation models have been proposed to describe adsorption of lead on varieties of iron oxides including not just HFO (Dzombak and Morel, 1990; Benschoten et al., 1998; Swedlund et al., 2003; Trivedi et al., 2003; Dyer et al., 2003), but also hematite (Christl and Kretzschmar, 1999), goethite (Gunneriusson et al., 1994;

Coughlin and Stone, 1995; Rodda et al, 1996; Samad and Watson, 1998, Kovacevic et al., 2000) and iron oxide rich soils (Papini et al., 1999). Competitive adsorption of Pb(II) and Cu(II) on the surface of hematite has been studied by Christl and Kretzschmar (1999) as a function of pH and total metal concentration. According to their study, Cu and Pb adsorption increased sharply with increasing pH, but Pb sorbed more strongly than Cu on hematite surface at a given pH. They also found that the presence of Pb strongly reduces Cu adsorption. The presence of Cu also reduces the Pb adsorption on to hematite but it is much less pronounced compared to the influence of Cu on Pb. At higher pH values, the adsorption edges of both Pb and Cu merged together. According to Christl and Kretzschmar (1999), this is due to the precipitation of oxide and hydroxide phases of both Cu and Pb under the chosen experimental conditions.

Gunneriusson et al. (1994) studied the adsorption of lead on goethite and the influence of chloride on Pb adsorption. They found that the adsorption is enhanced in sodium chloride electrolyte when compared to data obtained using sodium nitrate. This was attributed to a decrease of surface potential by the formation of chloride complexes. According to Gunneriusson et al. (1994), Pb can form stronger complexes with chloride owing to its higher coordination number (usually 6) and can adsorb as Pb-chloro complexes at higher pH.

Coughlin and Stone (1995) have studied adsorption and desorption kinetics of metal cations including Mn, Co, Ni, Cu and also Pb on goethite surfaces. They made a slurry using 4.7  $\mu\text{M}$  of Pb and 1 g/L of FeOOH in 10 mM  $\text{NaNO}_3$ , and modeled their experimental data using a triple layer model (TLM). Their study showed that 50%

adsorption occurs at pH 4.8 for Pb, compared with 50% of Cu at 4.5, Co and Ni at 6.3 and Mn at 6.8.

The temperature dependence of Pb(II) and Zn(II) adsorption have been studied by Rodda et al (1996) on goethite surfaces at fixed pH. They chose a constant pH of 5.5 for Pb and 6.5, 7 and 7.5 for Zn and varied temperature from 10 to 70°C. Their experimental results showed that the amount of adsorption increased with increasing temperature. Adsorption of Pb increased 2-fold with an increase in temperature from 10 to 70°C whereas a 7-fold increase of zinc adsorption was noted for the same conditions. This is due to the higher entropy of the Zn adsorption reaction compared to Pb.

An XPS (X-ray photoelectron spectroscopy) study of adsorption of Pb on goethite has assessed by Samad and Watson (1998). The aim of their study was to provide information about the chemical nature of adsorbed lead. They used 0.1 M NaNO<sub>3</sub> as constant background electrolyte with 1.6 g/L goethite and 1.5 mM Pb(NO<sub>3</sub>)<sub>2</sub>. They titrated this mixture of Pb and goethite from pH 4-9 using either 0.1 M NaOH or HNO<sub>3</sub> after pre-equilibration on a shaker overnight at 25°C. After centrifuging and removing the supernatants, the residue was freeze-dried for study using XPS. They found that below pH 5.5, >FeOHPb<sup>2+</sup> is the dominant surface complex, whereas >FeOPb<sup>+</sup> dominates over pH 5.5-6.5. >FeOPbOH becomes dominant above pH 6.5 and polynuclear complexes started to form above pH 7.

The adsorption of Pb-species on goethite was also studied by Kovacevic et al. (2000) as a function of pH. Using surface complexation modeling, they suggested that Pb(II) ions are present on the goethite surface as PbOH<sup>+</sup> species bound to MO<sup>-</sup> (same as >SO<sup>-</sup>) functional groups. They performed their experiments at pH 3-6, as above pH 7

precipitates would form. They argued that it would be incorrect to interpret the adsorption data according to total Pb concentration, as the dominant aqueous species at pH 3-6 was singly charged Pb species ( $\text{PbOH}^+$ ).

Swedlund et al (2003) studied Co, Pb and Cd adsorption on ferrihydrite including how the presence of sulfate affects adsorption. They postulated the formation of ternary complexes with the stoichiometry  $>\text{FeOHMeSO}_4$ , where  $>\text{Fe}$  is an iron on ferrihydrite, and Me is the metal ion such as Pb, Co or Cd. With the addition of this ternary complex, they accurately predicted and modeled the adsorption of these cations in the presence of sulfate.

Dzombak and Morel (1990) proposed a 2-site model using a strong and weak site for Pb adsorption onto ferrihydrite. However, to model Pb adsorption on ferrihydrite, Swedlund et al (2003) added a third site with very high affinity, but low site density. They also showed that the adsorption constants proposed by Dzombak and Morel (1990) could not predict the adsorption of Pb on ferrihydrite as measured in their experiments. In all cases, the Dzombak and Morel (1990) model significantly underestimated their adsorption edges. Therefore, Swedlund et al. proposed not only the third surface site, but also a much higher stability constant for adsorption of Pb on the original strong site: 5.70, compared to 4.65 as proposed by Dzombak and Morel (1990).

Trivedi et al. (2003) used both macroscopic and spectroscopic analyses to study Pb adsorption onto ferrihydrite as function of pH, ionic strength, and adsorbate concentration. The spectroscopic study was done by XAS (X-ray absorption spectroscopy). This study demonstrated the formation of two different Pb-Fe bonds having radial distances of 3.34 and 3.89 Å at pH 4.5. This was interpreted to imply the

formation of both monodentate and bidentate complexes at the ferrihydrite surface. In contrast, it has been found that only bidentate complexes formed at pH 5 and higher with a Pb-Fe bond distance 3.34 Å. XANES study also showed that Pb forms inner-sphere complexes onto ferrihydrite and does not retain the hydration sphere during adsorption.

Pb adsorption onto 2-line ferrihydrite was studied by Dyer et al. (2003) using a combination of macroscopic and spectroscopic data. They modeled Pb adsorption on 2-line ferrihydrite as a function of pH, ionic strength and Pb concentration using the triple layer model (TLM). Macroscopic data were also in good agreement with spectroscopic data. Both these results showed that the experimental data could be fitted well using a one site model with a bidentate-mononuclear and a monodentate-mononuclear species. They ran their experiments with 50  $\mu\text{M}$  Pb and 1 g/L ferrihydrite in 0.1, 0.01 and 0.001 M  $\text{NaNO}_3$  to produce adsorption edges. Their study showed negligible ionic strength dependence of Pb adsorption, suggesting the formation of an inner-sphere complex. The spectroscopic data revealed that inner-sphere mononuclear bidentate complexes are the dominating species at pH 5.5-6.5, but at lower pH (pH at 4.5) both monodentate and bidentate mononuclear complexes predominate. These spectroscopic findings are in good agreement with the results of Trivedi et al (2003).

Benschoten et al (1998) studied lead adsorption on soils and amorphous hydrous ferric oxide (HFO) surfaces using non-electrostatic surface complexation models. They assumed that the free energy of adsorption would dominate over the coulombic attraction for strongly adsorbing metal ions, such as Pb, on the HFO surface. They showed that they could model Pb adsorption reasonably well using the non-electrostatic model.

### Adsorption of lead on kaolinite

Like iron-oxides and hydroxides, clay minerals such as kaolinite, montmorillonite, illite, and smectite are also ubiquitous in natural soils. Most of these clay minerals have large specific surface areas, negative charges on the surface at circumneutral pH and reactive surface hydroxyl groups (Adriano, 2001, Sparks, 2003). For this reason, they can play a major role in sorbing cations in natural sediments. Most of these clay minerals have permanent negative charge on basal surfaces due to isomorphic substitution in the tetrahedral and octahedral sheets, as discussed above. Along with the permanent surface charge, they also possess a pH dependent charge on edge surfaces resulting from the reactive surface hydroxyl groups (Sparks, 2003, Davis and Kent, 1990).

Although metal adsorption on kaolinite has been studied well by different workers like Carroll-Webb and Walther (1988); Puls and Bohn (1988); Schulthess and Huang (1990); Brady et al. (1996); Huertas et al. (1998); Graveling et al. (1997); Angove et al. (1998); Benyahya and Garnier (1999); Ganor et al. (2003); Payne et al. (2004), Peacock and Sherman (2005), and Lackovic et al. (2004), only a few studies have quantified Pb adsorption on kaolinite using surface complexation models. Notable contributions have come from Schindler et al. (1987); Ikhsan et al. (1999); Chantawong et al. (2003); Heidmann et al. (2005, 2005); Srivastava et al. (2005); and Hizal and Apak (2006) (Tables 1.2 and 1.3).

Table 1.2 Experimental parameters used in studies of Pb adsorption onto kaolinite

Previous workers	Type of kaolinite	Surface area m <sup>2</sup> /g	Amount of colloid g/L	Strength and type of electrolyte M
Heidmann et al. (2005)	KGa-2 Warren County, GA	23.8 N <sub>2</sub> -BET	5	0.01 NaNO <sub>3</sub>
Schindler et al. (1987)	KGa-1, Clay Mineral Society	10.2 N <sub>2</sub> -BET	1	0.1 and 0.01 NaClO <sub>4</sub>
Ikhsan et al. (1999)	acid-washed kaolinite, Ajax Chemicals	14.73 N <sub>2</sub> -BET	~6.78	0.005 KNO <sub>3</sub>
Srivastava et al. (2005)	acid-washed kaolinite, Ajax Chemicals	14.4 N <sub>2</sub> -BET	~6.68	0.01 NaNO <sub>3</sub>

Table 1.3 Modeling parameters used in studies of Pb adsorption onto kaolinite

Previous workers	Model type	Site type	Type of Pb- complex
Heidmann et al. (2005)	Basic Stern Model	2 types, surface hydroxyl and cation exchange	Inner-sphere
Schindler et al. (1987)	Combined ion-exchange and SCM	2 types, surface hydroxyl and ion exchange	Inner-sphere
Ikhsan et al. (1999)	Constant capacitance	2 types, permanent negatively charged site and one variable-charge site	Both inner and outer- sphere
Srivastava et al. (2005)	Extended Constant capacitance	2 types, permanent negatively charged site and one variable-charge site	Both inner and outer- sphere

Competitive adsorption of Pb and Cu onto kaolinite (KGa-2) has been modeled by Heidmann et al. (2005) as a function of pH and total metal concentrations using surface complexation and cation exchange reactions. Competitive adsorption experiments were done using pH 4-8 in a constant background electrolyte concentration (0.01 M NaNO<sub>3</sub>) with varying concentrations of Pb (0, 50 and 200 μM) and a fixed concentration of Cu (50 μM). Single metal adsorption experiments showed that Pb was more strongly

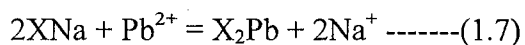
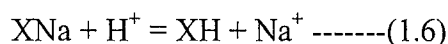
adsorbed onto kaolinite compared to Cu at a given pH. Thus, below pH 6.25, an increasing amount of lead decreased copper adsorption, due to competition between Cu and Pb for sorbing sites.

Chantawong et al. (2003) studied the adsorption characteristics of heavy metals including Cd, Cr(III), Cu, Ni, Pb and Zn onto kaolinite and ball clay. They used Langmuir and Freundlich isotherms to model their experimental data as a function of pH. Their results showed that Cr and Zn adsorbed much more readily onto kaolinite compared to other metals. Pb adsorbed least followed by Cu, Cd and Ni, in contrast to other studies, where Pb showed higher affinity for kaolinite surfaces compared to Cu and Zn (Heidmann et al., 2005; Ikhsan et al, 1999). For ball clay, Cr showed the highest affinity for sorption of the six metals. Their data could be fitted well with Langmuir and Freundlich isotherms, except for Ni, which they could only fit well with their model at low concentrations. They also found that the ball clay had a higher affinity than pure kaolinite for all the metals by approximately one order of magnitude. They postulated that this is because the majority of the ball clay is comprised of illite, which is a 2:1 type clay mineral, whereas kaolinite is 1:1 type. Due to this structural difference, the ball clay has more excess negative charge and a higher cation exchange capacity (due to greater isomorphous substitution) than kaolinite. Therefore, it tends to adsorb metals more readily than kaolinite. Chantawong et al. (2003) also found some organic matter in the ball clay, which may also have enhanced metal adsorption. They also studied the pH dependent adsorption of these metals onto kaolinite and ball clay. They found that ball clay has a higher affinity for adsorbing these heavy metals at a given pH compared to kaolinite, due to the presence of organic matter as well as the higher CEC of ball clay

(14.9 meq/100 g for ball clay, compared to 11.3 for their Thai kaolinite). They also explained this fact by the relative points of zero charge (pzc) of the two solids. The kaolinite and ball clay had pzc's of 4.34 and 3.25, respectively. As the pzc of ball clay is lower than that of kaolinite, at higher pH values the amount of negative charge is greater than for kaolinite, and accordingly the adsorption is greater on ball clay compared to kaolinite.

Schindler et al. (1987) studied Cu, Cd and Pb adsorption on kaolinite as a function of pH and strength of the electrolyte. They used Georgia kaolinite (KGa-1) from the Clay Mineral Society with a surface area of 10.2 m<sup>2</sup>/g (using BET). Their study showed that for all metals increasing pH increases metal adsorption and increasing ionic strength decreases adsorption. They used a combination of ion exchange and surface complexation models to study the nature of adsorption of the above-mentioned metals onto kaolinite-water interface. They modeled the metal adsorption behavior assuming two different kinds of binding sites on the kaolinite. One, a weak acidic group, termed an XH group, accounts for the ion exchange at low pH values, and the second site type is a surface hydroxyl group, also called an >SOH group, which accounts for adsorption at higher pH by formation of inner sphere complexes with the individual divalent metal cations.

They proposed an ion exchange reaction as follows:



They also mentioned that because kaolinite is a 1:1 type clay, it should not be assumed that ion exchange will occur. However, some small impurities of 2:1 type clay in the

kaolinite might affect the adsorption phenomena. Therefore, they introduced the ion exchange site to model their data. A previous study by Schindler and Stumm (1987) showed that the surface hydroxyl groups are comprised of  $>\text{SiOH}$  and  $>\text{AlOH}$  groups that can deprotonate and form surface complexes. However, Schindler et al. (1987) suggested that the  $>\text{SOH}$  group on their kaolinite is predominantly Al-OH type rather than Si-OH type, and that the  $>\text{AlOH}$  site is responsible for specific adsorption and formation of inner-sphere complexes on the kaolinite surface.

A comparative study of the adsorption of transition metals like Pb, Cu, Zn, Co and Mn onto kaolinite was completed by Ikhsan et al. (1999). They used acid-washed kaolinite from Ajax Chemicals with a surface area of  $14.73 \text{ m}^2/\text{g}$  and an XRD pattern that did not indicate any significant impurities. They carried out their metal adsorption experiments in a background electrolyte of  $0.005 \text{ M KNO}_3$ . They used  $100 \text{ }\mu\text{M}$  of each metal and  $\sim 6.78 \text{ g/L}$  ( $100 \text{ m}^2/\text{L}$ ) of kaolinite, which was titrated from pH 3-10. Their results revealed that in all experiments, adsorption of metals increased with increasing pH, but the shape of the adsorption edges and the amount of adsorption was different for each metal. For Cu and Pb, the adsorption edges are sigmoidal, but for Zn, Co and Mn, the edges have distinct steps after around 40% adsorption. At any given pH, the Pb adsorbed most, followed by Cu, Zn, Co, Mn. Adsorption of Pb started at pH  $\sim 3$  with 100% adsorption at pH of  $\sim 7.5$ , very similar to that of Cu which adsorbed 100% at pH  $\sim 8.0$ . The adsorption of both Pb and Cu increased steadily from around pH of 3.5 (10%) to 6.5 (90%). This experimental data was modeled using a constant capacitance surface complexation model and assuming that a bidentate complex formed at the kaolinite surface. Ikhsan et al. (1999) proposed two different types of adsorption sites, one

permanent negatively charged site on the tetrahedral silica sheet and one variable-charge site on crystal edges and the octahedral alumina sheet. For Pb and Cu, adsorption to the variable surface charge sites started before pH 5.5, after the fixed charge sites are completely filled, compared to Co, Zn and Mn, where no significant adsorption onto variable surface charges until pH 6 or more.

Competitive adsorption behavior of Cd, Cu, Pb and Zn onto kaolinite has been studied by Srivastava et al. (2005) as a function of pH and metal concentration in a constant background electrolyte solution (0.01 M NaNO<sub>3</sub>). They used acid-washed kaolinite from Ajax Chemicals with a surface area of 14.4 m<sup>2</sup>/g. XRD showed that this kaolinite does not contain any significant impurities, so they used this kaolinite without any further cleaning treatment. They titrated slurries of kaolinite and single-element (133 μM) or multi-elements (33 μM) from pH 3.5 to 10. The results of the single-element work showed that Zn and Cd have a plateau region in their adsorption edge between pH of 6-6.5. Srivastava et al. (2005) proposed that this is because ion exchange is the dominant mechanism at low pH values and as the pH increases a bidentate outer sphere complex starts to form for Zn or Cd. The adsorption edges of Cu and Pb are somewhat different compared to Zn and Cd because Cu and Pb hydrolyze at lower pH and can therefore interact with the surface hydroxyl groups more readily at lower pH. In the single element system, Cu adsorbed most readily, followed by Zn, Pb, and Cd. Srivastava et al. (2005) argued that using a constant capacitance model (CCM), as proposed by previous workers (Ikhsan et al., 1999; Schindler et al., 1987), to describe adsorption on kaolinite is problematic, as it does not account for ion exchange phenomena. However, at low pH, ion exchange is the dominant mechanism of metal uptake on kaolinite, not

complexation at hydroxyl surface groups. Therefore, Srivastava et al. (2005) proposed an “extended” constant capacitance model to describe adsorption of these heavy metals onto kaolinite, which includes an exchange site for adsorption.

Hizal and Apak (2006) studied the adsorption of Cu and Pb onto clay minerals individually and in the presence of humic acid as a function of pH. They used three different types of clay minerals having similar structures to kaolinite, and different surface areas (clay I = 17.8, clay II = 26.68, and clay III = 14.13 m<sup>2</sup>/g) as measured by N<sub>2</sub> BET) as well as differing chemical compositions. They carried out metal adsorption experiments using 10 ppm of each cation in 0.1 M NaClO<sub>4</sub>, at a pH of 2-7, maintaining a solid/liquid ratio of 50 g/L. The maximum adsorption of both metals occurred on the clay containing the highest amount of organic carbon. They noted that most of the adsorption occurs at a pH range of 5-7. They attributed this to the fact that the metal ions are partially hydrolyzed, but still remains positively charged at this pH range, while the clay surface is negatively charged, because this pH range is higher than the clay PZC. This promotes adsorption of metal hydroxo species (MOH<sup>+</sup>). Incorporation of humic acid enhanced the metal adsorption for both copper and lead and created much steeper adsorption edges, especially at lower pH. The reason behind this observation is that like fulvic acid (Heidmann et al., 2005), humic acid also behaves as a chelating agent and thus increases the number of sorbing sites via phenolic groups. These phenolic groups can act as chelating agents and thus promote adsorption.

### Adsorption of lead on silica

Like iron oxides and hydroxides along with clay minerals, amorphous silica/quartz is also an important constituent of many natural soils. Silica can occur in various forms and size fractions ranging from sand sized particles to very fine fractions in most aquifers. Studies have shown that in some aquifers and some muddy soils, the fraction of silica is up to 70-85% by weight (Janusz et al, 2003; Bertsch and Seaman, 1999). Amorphous silica is most abundant in marine settings, where it originates from the skeletal remains of microorganisms. In the unsaturated zone of aquifer systems, quartz is typically the most abundant form of silica and is often coated by other minerals (Elzinga and Sparks, 2002). Although quartz has a very low surface area, it is a major constituent of most natural soils, and thus can play a major role in adsorbing heavy metals (Elzinga and Sparks, 2002). Because quartz and silica have very similar surface reactivity and metal adsorbing behavior, except that quartz typically has a lower surface area compared to silica and different Si-O-Si bond angles, amorphous silica is often regarded as analogous to quartz (Manceau et al, 1999). Unfortunately, however, very few studies have assessed or quantified the nature of metal adsorption and surface reactivity of silica. Some notable studies have come from the works of Janusz et al, (2003), Dixit and Van Cappellen, (2002), Chen et al. (2005), Elzinga and Sparks (2002), Prelot et al. (2002), and Sarkar et al. (1999). Of these, only three workers studied Pb adsorption at the quartz/silica-water interface.

Adsorption of Sr, Co, and Pb onto quartz has been studied by Chen et al. (2005). They carried out batch experiments in three different electrolytes namely,  $\text{NaNO}_3$ ,  $\text{NaCl}$ , and  $\text{NaClO}_4$  but keeping the strength of electrolyte constant (0.01 M). They also kept the

metal concentration constant ( $10^{-5}$  M) for the Pb experiments. They used Min-U-Sil 5 from U.S. Silica (Berkeley Springs, WV) after baking it at  $550^{\circ}\text{C}$ , boiling in 4N HCl and finally rinsing in  $\text{CO}_2$  free Milli-Q water several times to purify the silica surface. The X-ray diffraction pattern showed that the Min-U-Sil 5 was  $\alpha$ -quartz, and  $\text{N}_2$  gas adsorption demonstrated a surface area of  $4.00 \pm 0.02 \text{ m}^2/\text{g}$ . There was dependence on electrolyte type for Pb adsorption edges at ionic strength 0.01 M. Pb adsorption was also not affected by increasing the strength of electrolyte for  $\text{NaClO}_4$  or  $\text{NaNO}_3$ . However, increasing the concentration of NaCl from 0.01 to 0.1 M, decreased Pb adsorption as a function of pH, shifting the adsorption edge to the right. Elzinga and Sparks (2002) used EXAFS to show that Pb forms covalent polynuclear Pb species at high pH and that  $\text{ClO}_4^-$  does not change the coordination structure of Pb on silica. Their spectroscopic study is in good agreement with the macroscopic study results of Chen et al. (2005). They also showed that Pb adsorption on silica is not affected by increasing concentrations of  $\text{ClO}_4^-$  even at very high  $\text{ClO}_4^-$  concentrations (0.5 M).

Elzinga and Sparks (2002) studied Pb adsorption onto hydrous amorphous  $\text{SiO}_2$  as function of pH and ionic strength using XAS to identify the products that are formed on the silica surface. The silica they used was Zeo49 from J. M. Huber Corporation with a BET surface area of  $280 \text{ m}^2/\text{g}$  and an average particle diameter of  $9 \mu\text{m}$ . This surface area is very high compared to the Min-U-Sil 5 used by Chen et al. (2005) and also used in the present study. Moreover, the Zeo49 amorphous silica contains some Al impurities. Elzinga and Sparks ran their batch experiments at two different electrolyte strengths (0.1 and 0.005 M  $\text{NaClO}_4$ ), with a constant concentration of silica (7.0 g/L) and a constant Pb concentration (2000  $\mu\text{M}$ ). They titrated the suspension from pH 3.6-7.5 with incremental

addition of 0.1 M NaOH. Results showed that there is a strong ionic strength dependence of Pb adsorption onto the silica surface. The adsorption edge shifted to the right, indicating less adsorption at higher ionic strength. 50% adsorption occurred at a pH of ~3.8 for 0.005 M, whereas the same amount of adsorption occurred at ~5.8 for 0.1 M experiments. They attributed this to the formation of outer sphere, rather than chemically-bound inner sphere, Pb complexes on the silica surface. They also mentioned that Na<sup>+</sup> ions could also be competing with Pb for the surface sites.

#### Adsorption of lead onto natural soils and mineral mixtures

Unlike the great abundance of Pb adsorption onto pure single minerals data, a very few studies have assessed the adsorption of Pb onto natural sediments and mineral mixtures using surface complexation modeling. Few notable examples have cited here. Papini et al. (1999) studied the adsorption of Pb onto a natural porous medium and modeled their data using surface complexation modeling as a function of pH and total lead concentration. They used Italian volcanic soil, which is composed mainly of SiO<sub>2</sub>, Al<sub>2</sub>O<sub>3</sub>, Fe<sub>2</sub>O<sub>3</sub>, FeO, MgO, CaO, K<sub>2</sub>O and Na<sub>2</sub>O, and they sieved to use only the size fraction <200 μm. They conducted adsorption experiments with a constant electrolyte strength of 0.1 M NaCl in a 50 mL slurry with 0.5 g of the solid phase and the amount of Pb varying from  $8.8 \times 10^{-5}$  to  $7.3 \times 10^{-4}$  M. NaOH and HCl were added to maintain the desired pH (from 3.5-6.5). Model results showed that at low pH a one site model could fit their data, but at higher pH, a 2-site model was required.

Coston et al (1995) studied Pb and Zn adsorption on aquifer sand and gravel coated with iron and aluminum oxides. The composition of the aquifer materials was mostly

quartz, with some alkali feldspar and minor iron bearing phases. They studied the adsorption of lead and zinc on various size fractions of the aquifer materials. They found that Zn adsorption is not controlled by grain size, but grain size has a strong influence on Pb adsorption. Pb has a strong preference to adsorb on grains smaller than 64  $\mu\text{m}$ . Removal of the iron coating from the grains, decreased Pb adsorption, Zn adsorption remained the same. From this, Coston et al. (1995) concluded that adsorption of Pb is increased in the smaller grain sizes due to the greater abundance of iron bearing surfaces in the smaller size fractions. Because these iron bearing coatings have a high reactive surface area and abundance of iron hydroxyl surface sites, which strongly bind Pb, Pb preferentially adsorbed onto the smaller size fractions. Coston et al. (1995) also compared adsorption onto the smallest size fraction with the Fe-coating and pure quartz of the same size. Adsorption starts at  $\sim\text{pH}$  4.0 with 100% adsorbed at  $\sim\text{pH}$  6.0 on the Fe-coated quartz, compared to 6.0 and 8.0 respectively for the pure quartz surface.

In another study, competitive adsorption of Cu and Pb onto kaolinite-fulvic acid has been assessed by Heidmann et al. (2005). Experimental isotherms were produced and compared to assess the interaction between kaolinite and fulvic acid during adsorption. They modeled their data using a Linear Additivity Model (LAM), which assumes that the mixture of kaolinite and fulvic acid behave as a physical mixture of two independent separate phases and do not interact with each other. Their Cu adsorption data could be very well fitted using a LAM, but the LAM did not predict Pb adsorption properly onto kaolinite-fulvic acid surfaces. In all experimental condition, Pb adsorption was underestimated compared to the model fit generated by LAM. Their study also showed that addition of fulvic acid greatly increased the sorption of Cu and Pb onto kaolinite, by

up to one order of magnitude at pH 4 and 6. This is due to the adsorption of fulvic acid onto kaolinite at acidic conditions. This adsorption behavior was not observed at pH 8. However, at pH 8, the enhancement of adsorption of both these metals was still significant compared to pure kaolinite surfaces.

#### Applicability of Component Additivity (CA) and Generalized Composite (GC) models

Davis et al. (1998) proposed two models, termed the component additivity and generalized composite surface complexation approaches, for prediction of adsorption on complex mineral assemblages. They studied adsorption of  $Zn^{2+}$  on natural sediments, which were collected from Cape Cod, MA, U.S.A. The composite sediment had a surface area of  $0.44 \text{ m}^2/\text{g}$  (BET) and consisted mainly of medium to coarse sand, composed mainly of quartz and feldspars with very low concentrations of iron-bearing materials, along with organic carbon ranging from 0.01-0.05% by weight. They ran batch experiments over a pH range of 4.90-7.37, with a Zn concentration varied from  $1.7 \cdot 10^{-7}$ - $10^{-4}$ M. The amount of colloid varied from 400 to 50 g/L in a 0.05 M artificial groundwater solution (AGW). They found that adsorption of Zn on this composite sediment did not show a strong dependence on pH, compared to adsorption on pure hydrous oxide surfaces. They attributed this difference to the heterogeneous surface functional groups present in natural sediments, along with some organo and phosphato ligands, which are present on sediment surfaces. They concluded that the component additivity model could not fit the experimental data set well. To use model their data successfully with the component additivity approach, they had to manipulate the surface areas and site densities of the minerals present in the sediments. In contrast, the

generalized composite approach could produce a good fit of the experimental data. Davis et al. (1998) also pointed out that the generalized composite approach requires much less information about the sediment mineralogy than the component additivity approach, making it a more practical modeling approach for natural sediments compared to the component additivity approach. They suggested that further research is needed to characterize more precisely the sorbents and the surface coatings of natural sediments to use a component additivity approach.

#### This study: purpose and goals

In this study, adsorption of lead is measured on single as well as mixed solid assemblages of HFO, kaolinite and silica (in binary and ternary solid systems), as a function of pH, total metal concentration, ionic strength of the electrolyte and mineral-to-mineral ratio and is modeled using a thermodynamic component additivity surface complexation approach. The data resulting from single metal-single mineral experiments is used to derive thermodynamic stability constants for each individual metal-mineral system. These stability constants have been added to the database of the speciation code JCHESS, which uses an equilibrium thermodynamic framework to solve multi-component, multi-phase speciation problems by using mass balance and mass-action relations for individual reactions. Using the JCHESS speciation code and results from binary and ternary solid phase experiments, the following hypothesis is addressed: adsorption of lead on complex natural sediments can be modeled as a function of pH and total metal concentration using the component additivity surface complexation thermodynamic approach.

### Scientific contribution and importance

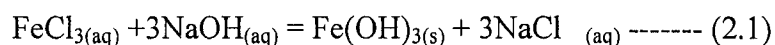
Metals do not biodegrade, so elevated concentrations of metals in near-surface environments can create a great long-term risk to human health. To reduce the potential for human exposure to toxic metals, it is important to understand and to be able to accurately model the fate and transport pathways of these metals in the environment, especially in soils and groundwater aquifers. The reactive surface phases of soil and aquifer materials are typically comprised of sand, clay and other metal hydroxides, along with humic substances, which play a major role in the fate and transport of heavy metals in the environment. Much of the knowledge regarding contaminant-mineral interaction comes from the extensive study of model mineral systems. These investigations have provided an understanding of the reactive surface functional groups on individual mineral phases, but may not allow extrapolation to predict metal interactions with surfaces in complex natural soil and aquifer systems. A goal of this study is to provide better and more accurate predictions of metal ion mobility in the environment by improving surface complexation modeling of heavy metals in the mixed environment. Specifically, the results of this study will be used to assess whether adsorption of Pb on mixed solid assemblages can be accurately modeled using a component additive approach.

## CHAPTER II

### MATERIALS AND METHODS

#### Preparation of HFO (Hydrous Iron Oxide)

HFO was synthesized in the lab by reacting anhydrous ferric chloride ( $\text{FeCl}_3$ ) and sodium hydroxide ( $\text{NaOH}$ ) using a method proposed by Cornell and Schwertmann (1991), with HFO precipitate forming according to the following equation:



#### Ferrihydrite

The procedure is as follows. First, around 10 grams of ferric chloride (anhydrous  $\text{FeCl}_3$ , Fisher scientific) is weighed into a beaker. DDI water is added and the mixture stirred well until all of the crystals dissolve completely. A pH electrode (Denver instrument/model 2.5) is calibrated and placed into the beaker containing the ferric chloride solution. Next,  $\text{NaOH}$  is slowly added with constant stirring until a pH of around 7.0 (6.5-7.5 is acceptable) is reached, and HFO precipitate forms. The solution with the precipitate is transferred into a plastic centrifuge tube and centrifuged (Eppendorf centrifuge 5810) for 15 minutes at 2500 rpm. The supernatant liquid is separated from the precipitate, DDI water is added to wash  $\text{NaCl}$  from the remaining precipitate and the mixture is centrifuged again for 5 minutes. This procedure is repeated 5-6 times to produce a chloride free HFO precipitate. The centrifuge tube of precipitate is frozen over night to prepare it for freeze-drying. The tube with frozen precipitate is attached to the freeze-dryer (Freeze dry system/Freezone 4.5, Labconco) for 72 hours to produce the dry HFO used for the experiments.

### Kaolinite

Powdered kaolinite (KGa-1B) was purchased from The Clay Minerals Society, Clay Minerals Repository. KGa-1B is a natural kaolinite from Washington County, Georgia, U.S.A. Pruett and Webb (1993) analyzed this kaolinite and found that it contains higher titanium levels than KGa-1. It also has better crystallinity compared to KGa-1. It has a slightly smaller grain size but other chemical impurities are very similar. KGa-1B contains 45.2% SiO<sub>2</sub>, 39.1% Al<sub>2</sub>O<sub>3</sub>, 1.64% TiO<sub>2</sub> and trace amounts of Fe<sub>2</sub>O<sub>3</sub>, MgO, CaO, Na<sub>2</sub>O and K<sub>2</sub>O (Pruett and Webb, 1993). To insure a pure kaolinite surface, samples were baked in an oven at 50°C for 72 hours prior to use in experiments. This process should volatilize any organic impurities.

Powdered kaolinite was purchased from Ward's Natural Science Establishment, Inc. X-Ray diffraction data shows that the Ward's kaolinite contains ~1% muscovite (data courtesy of Dr. Ray Ferrell at Louisiana State University). In comparison, the KGa-1B kaolinite from the Clay Minerals Society (KGa-1B) does not contain any phyllosilicate impurities (Pruett and Webb, 1993). It has a CEC of 3.0 meq/100g (Borden and Giese, 2001). Similar pretreatment to that conducted for KGa-1B was used for the Ward's kaolinite to purify the kaolinite surface.

### Silica

Silica used in the experiments is a fine-grained powder, commercially available as "Min-U-Sil 5", purchased from U.S. Silica (Berkeley Springs, WV). It is a natural crystalline quartz, ground to produce a fine powder with an average grain size of 1.7 µm. It is 98.3% quartz with minor impurities of iron, aluminum and other trace metals

according to the U.S. Silica Company. To create a clean quartz surface, the silica was first baked at 500°C, then acid refluxed 4 times in 4M HNO<sub>3</sub>, rinsed with D.I. ( $\geq 17.3$  megaOhm) water 8 times, centrifuged and dried for 48 hrs at 37°C. This procedure, proposed by Coston et al. (1995), oxidizes residual organic materials and removes other impurities from the silica.

### Surface area analyses

The surface area of each mineral was measured using an 11-pt BET-Nitrogen isotherm (NOVA 2200e-surface and pore size analyzer, Quantachrome Instruments). This procedure allows the surface area of a mineral, as also called the 'specific surface area', to be assessed. However, the BET surface area is not always equivalent to the reactive surface area of a mineral available for adsorbing solutes (Davis and Kent, 1990). The estimation of surface area by the BET-nitrogen (Brunauer-Emmett-Teller) method is based on a Langmuir isotherm model (Brunauer et al., 1938). This method assumes that (a) gas molecules can physically adsorb on a solid to produce infinite layers and all the adsorption sites are identical; (b) there is no interaction between each adsorption layer; and (c) the Langmuir theory can be applied to each layer. This method generally works well, except for those minerals that have a very high density of small pores (Davis and Kent, 1990).

The measured BET-N<sub>2</sub> surface area of HFO was 220 m<sup>2</sup>/g. According to Cornell and Schwertmann (1991), ferrihydrite has a large amount of internal surface area, which is not available for adsorbing gas. Therefore, the HFO surface area measured by BET gives a surface area much lower than the reactive surface area. Moreover, freezing HFO

suspensions, followed by thawing at room temperature has been shown to produce porosities of up to 73% (Hofmann et al., 2004). Due to these problems of microporosity and internal surface area, for modeling purposes, a surface area of 600 m<sup>2</sup>/g is used for HFO as proposed by Dzombak and Morel (1990).

The surface area of both types of kaolinite, namely KGa-1B and Ward's kaolinite were also measured using BET. The Ward's kaolinite has a higher specific surface area (25.7 m<sup>2</sup>/g) compared to the KGa-1B (13.6 m<sup>2</sup>/g). The BET measurements for silica indicate that the silica has the lowest surface area of the pure mineral phases used in this study, with an average specific surface area of 9.4 m<sup>2</sup>/g. For kaolinite and silica, the measured BET surface areas were used for the modeling (see Chapter IV).

Surface areas can also be estimated based on average particle size and geometric considerations. The geometric surface area is defined as  $A' = 6 \times 10^{-4} / \rho d$ , where  $\rho$  is the density of the mineral species (g/cm<sup>3</sup>) and  $d$  is the diameter of the mineral grain (cm) (Davis and Kent, 1990). The calculated surface areas based on geometric considerations, were somewhat lower compared to BET measurements. For kaolinite, assuming an average density of 2.6 g/cm<sup>3</sup> and an average grain size of 753 nm diameter (product data from Wards Scientific), yields a calculated surface area of only 3.06 m<sup>2</sup>/g compared to 25.7 and 13.6 m<sup>2</sup>/g as measured by BET. The calculated surface area for silica was also low at only 1.05 m<sup>2</sup>/g (based on an average density of 0.57 g/cm<sup>3</sup> and an average grain size of 1600 nm diameter (product data from U.S. Silica), compared to the somewhat higher surface area of 9.4 m<sup>2</sup>/g measured by BET. Table 2.1 shows the estimated surface areas of the four solids.

Table 2.1 Surface areas (in m<sup>2</sup>/g) of solids used in this study

Solids	BET S.A	Geometric S.A	Used for modeling
HFO	220	Not calculated	600
Silica	9.4	1.05	9.4
KGa-1B	13.6	3.06	13.6
Ward's kaolinite	25.7	3.06	25.7

#### Preparation of Pb stock solution

PbCl<sub>2</sub> powder (98%) purchased from Aldrich was used to make a stock solution of Pb. For a 10<sup>-3</sup> M PbCl<sub>2</sub> stock solution (10<sup>-4</sup> M was the highest Pb concentration used for adsorption experiments), 0.002781 grams of PbCl<sub>2</sub> (formula weight of PbCl<sub>2</sub> is 278.1 gram) was weighed into a 1 L volumetric flask, which was filled to the mark with DDI water up to the 1 L mark and stirred for 48 hours at 25°C so that all crystals of PbCl<sub>2</sub> dissolved completely. This yields a stock solution of lead chloride with a concentration of 10<sup>-3</sup> M. This stock solution was acidified and preserved in a teflon bottle for experiments. For lower concentrations, the quantity of stock solution needed to make a slurry containing a desired lead concentration is calculated by the following equation:

$$C_1V_1 = C_2V_2,$$

where C<sub>1</sub> = concentration of stock solution (10<sup>-3</sup> M), V<sub>1</sub> = 500 ml (or total volume of slurry), C<sub>2</sub> = desired lead concentration, and V<sub>2</sub> = amount of stock solution needed.

### Batch experiments

The pH dependent adsorption of lead ( $\text{Pb}^{2+}$ ) on hydrous ferric oxide (HFO), silica and kaolinite and binary and ternary mixtures of these solids was investigated using batch experiments as a function of pH, total Pb concentrations, strength of the electrolyte and solid to solid ratio. The total concentration of colloids in all experiments, including single solid and binary or ternary mixtures, was held constant (2g/L). The total lead concentration was kept constant for a given set of measurements (as a function of pH) at  $10^{-4}$ ,  $10^{-5}$  or  $10^{-6}$  M. A separate set of experiments, as a function of pH and at constant lead concentration was performed in 0.1, 0.01 or 0.001M  $\text{NaNO}_3$  with  $10^{-5}$  M  $\text{Pb}^{+2}$  for most of the single colloids.

Three different binary mixtures were made to run Pb adsorption experiments, namely HFO+silica, HFO+kaolinite and kaolinite+silica. The amount of both the kaolinite and silica were varied to produce mixtures containing 1:1, 5:1, 10:1, 50:1, 100:1, 500:1 and up to 5000:1 (by mass) for HFO:kaolinite (Table 2.2) and HFO:silica (Table 2.3) systems, to evaluate the effect of even very small quantities HFO on Pb adsorption. Five experiments were performed for binary mixtures containing kaolinite and silica, such that the ratio of kaolinite:silica was 1:1, 10:1, 50:1, 0.1:1 and 0.02:1 (by mass) (Table 2.4). Two ternary mixtures were made in such a way that the ratios of the three solids were either 1:1:1 by mass or by surface area (Table 2.5). For binary and ternary mixtures, the concentration of lead ( $10^{-5}$  M) and electrolyte strength (0.01 M  $\text{NaNO}_3$ ) were kept constant.

Table 2.2 Amount of sorbent (in g) used for various binary kaolinite and HFO experiments

Colloid (g)	1:1	5:1	10:1	50:1	100:1	500:1	5000:1
Kaolinite	1	1.666	1.818	1.960	1.980	1.996	1.9996
HFO	1	0.333	0.181	0.0392	0.0198	0.00399	0.000399

Table 2.3 Amounts of sorbent (in g) used for various binary silica and HFO experiments

Colloid (g)	1:1	5:1	10:1	50:1	100:1	500:1
Silica	1	1.666	1.818	1.960	1.980	1.996
HFO	1	0.333	0.181	0.0392	0.0198	0.00399

Table 2.4 Amount of sorbent (in g) used for various binary kaolinite and silica experiments

Colloid (g)	1:1	10:1	50:1	0.1:1	0.02:1
	K:S	K:S	K:S	K:S	K:S
Kaolinite	1	1.818	1.960	1.818	1.960
Silica	1	0.181	0.0392	0.181	0.0392

Table 2.5 Amount of sorbents (in g) used in ternary mixtures

Colloid (g)	1:1:1	1:1:1
	by mass	by S.A
HFO	0.6666	0.01836
Kaolinite	0.6666	1.1775
Silica	0.6666	0.8036

Batch experiments were completed in a 500 mL polyethylene bottle with a stir bar to create a homogenous mixture. Each batch slurry contained Pb and colloids in the desired concentration of  $\text{NaNO}_3$  background electrolyte. The Pb and background electrolyte were first added to a volumetric flask (500 mL) to create the desired  $\text{Pb}^{2+}$  concentration. Before adding colloid to the batch reactor, a 10 mL aliquot was removed and kept as a control. This control sample was later analyzed to determine the exact initial concentration of Pb. After the control sample was taken, colloid was added with a stir bar, and the slurry was equilibrated under constant stirring (in air) for 24 hours. After this preequilibration period, the pH of the mixture was adjusted using trace metal grade nitric acid so that pH dropped to around  $\sim 2$  for HFO and  $\sim 4$  for silica and kaolinite (as the immersion pH of all the systems were above pH 4), then slowly titrated with trace metal grade sodium hydroxide to measure the adsorption edge. The pH was first dropped rapidly to  $\sim 2$ -3 using trace metal grade nitric acid and then was typically increased from  $\sim 2$  to 9 in  $\sim 0.25$  pH increments by addition of small volumes of trace metal grade sodium hydroxide or nitric acid (in cases where pH increased more than 0.5 units with the base addition). Ten minutes after each base addition (i.e., after the desired pH value was

reached, e.g. 2.25, 2.5 and so on) and stable ( $\pm 0.05$  unit deviation of pH for 10 minutes), a 10 mL aliquot of solution was removed from the slurry and further equilibrated for 24 hours at room temperature on a rotating shaker (Barnstead/Thermodyne, Labquake). After the 24 hr equilibration period the pH was remeasured, and the aliquots centrifuged for 20 minutes at 1000 rpm. The supernatants were syringe-filtered (through a 0.2  $\mu\text{m}$  nylon membrane), diluted, acidified with nitric acid and spiked with an internal standard ( $\sim 100$  ppb, Bi, Ho, In, Li, Sc, Tb, Y) and analyzed for lead via ICP-MS (ThermoElectron) or ICP-OES (Perkin Elmer/OES Optima 2100DV). The amount of metal ion adsorbed by HFO, silica and kaolinite was calculated by the difference between the amount of metal added (as measured by the control sample) and the concentration measured in the supernatant solution. The measured adsorption edges (% metal adsorbed vs. pH) for HFO, silica and kaolinite were used to parameterize surface complexation models (see Chapter IV).

#### Kinetics experiment

A separate experiment was performed to evaluate the reaction kinetics and reversibility of the adsorption experiments. The procedure was very similar to that of adsorption edge experiments. A slurry was made with 2 g/L of kaolinite in a 0.01 M  $\text{NaNO}_3$ . The concentration of lead was  $10^{-5}$  M. To perform the adsorption kinetics experiment, enough NaOH was added to the slurry to achieve a pH of around  $\sim 10$ , to make sure that 100% adsorption would occur. Once the pH was stable at the high pH, within 5 minutes, a 10 mL aliquot of solution was removed from the slurry and the aliquot was then centrifuged for 20 minutes at 1000 rpm without the further equilibration

used in the adsorption edge experiments. The supernatants were immediately syringe-filtered (0.2  $\mu\text{m}$  nylon membrane) to ensure that the adsorption reaction was stopped. This first aliquot was termed time '0'. This procedure was followed for 72 hours with aliquots removed at time increments from 5 to 10, 10-15, 15-20, 20-30 minutes and up to 72 hours, with longer time increments later in the experiments. This experiment was used to test the time needed to achieve 100% adsorption.

After 72 hours, enough  $\text{HNO}_3$  was added to the slurry to create a low enough pH (~2) to achieve nearly 100% desorption. A similar procedure to that executed for the timed adsorption experiment was maintained for the desorption experiment. The desorption experiment was also performed for 72 hours. Once the pH was stable at pH~2 (5 minutes after initial addition of the acid), a 10 mL aliquot of solution was removed from the slurry and the aliquot was then centrifuged for 20 minutes at 1000 rpm and syringed filtered. This aliquot was also defined as '0' minute. Aliquots were removed, centrifuged and filtered at increments of 5 minutes and then at longer intervals to 72 hours. The supernatant separated from each aliquot was then diluted, acidified with nitric acid and spiked with an internal standard (~100 ppb, Bi, Ho, In, Li, Sc, Tb, Y) and analyzed for lead via ICP-OES.

#### Kinetic experiment using a dialysis bag

A preliminary set of experiments were conducted to evaluate the speed of adsorption on HFO using a dialysis bag method. The dialysis bags ("Spectra/por Float-A-Lyzer") used for the experiments were purchased from Spectrum Labs. The bags have a diameter of 10 mm, hold a volume of 10 mL and have a length of 16 cm. The dialysis membrane is

composed of biotech cellulose ester and is sealed at one end and attached to a floatable cap at the other.

2 g/L of HFO was placed inside a dialysis bag and the pH was titrated by addition of solution outside of the bag. For these experiments, the dialysis bag was floated in a 1 L teflon bottle containing a solution of  $10^{-5}$  M  $\text{Pb}^{2+}$  in 0.01 M  $\text{NaNO}_3$  with a stir bar. The stirring rate was adjusted until the bag began to spin in a “pin-wheel” type of formation. A small stir rod was also placed inside the dialysis bag to ensure that no HFO particles clogged together within the bag. A very similar procedure was followed to the kinetics experiment without a dialysis bag as discussed in the previous section, with samples removed from outside the bag at timed intervals.

## CHAPTER III

### RESULTS AND DISCUSSION

#### Single solid phase systems

##### Adsorption of Pb on HFO

Adsorption of Pb on HFO was conducted in batch experiments with five different Pb concentrations ranging from  $10^{-4}$  M to  $6 \cdot 10^{-8}$  M, including intermediate concentrations of  $10^{-5}$ ,  $10^{-6}$  and  $6.8 \cdot 10^{-7}$  M. The concentration of the background electrolyte ( $\text{NaNO}_3$ ) was varied from 0.1 to 0.001 M. The amount of solute was kept constant for every experiment at 2 g/L. Table 3.1 shows the different Pb concentrations with corresponding electrolyte strengths.

Table 3.1 Experimental conditions for adsorption of Pb on HFO

Experiment	Pb concentration (M)	Electrolyte strength (M)
1.	$10^{-4}$	0.01
2.	$10^{-5}$	0.01
3.	$10^{-6}$	0.1
4.	$6.8 \cdot 10^{-7}$	0.1
5.	$6 \cdot 10^{-8}$	0.001

In all experiments, adsorption of Pb increases with increasing pH, as expected, with negligible effect of ionic strength (Figure 3.1). A very strong affinity for Pb was observed on HFO surfaces, with adsorption starting at pH  $\sim$ 2 for all Pb concentrations and 100% adsorption occurring at pH  $\sim$ 4.5, except for experiments with  $10^{-4}$  M Pb, where 100% adsorption was achieved at pH  $\sim$ 5. The percentage adsorption at a given pH decreased

with increasing Pb concentration, which is evident from the shifting of adsorption edges towards higher pH. For example, 50% adsorption was observed for  $10^{-5}$  M at pH~2.5 compared to pH~3 for  $10^{-4}$  M Pb experiments at the same ionic strength.

HFO was the strongest adsorbent for Pb of the three single solid systems (HFO, kaolinite, silica) studied. The shapes of the adsorption edges are much sharper compared to the generally sigmoidal shaped edges measured in the other single solid systems. This is due the nature of Pb complexes that form onto HFO surfaces as well as the very high specific surface area of HFO ( $N_2$  BET =  $220 \text{ m}^2/\text{g}$ ), as has been discussed in previous studies (Dzombak and Morel, 1990; Trivedi et al., 2003; Dyer et al., 2003) Pb forms strong inner sphere complexes on the surface of HFO, consistent with the fact that essentially no ionic strength dependence is observed for Pb adsorption on HFO.

#### Adsorption of Pb on silica

Four different adsorption experiments for Pb on silica were carried out at two different electrolyte strengths (0.1 and 0.01 M  $\text{NaNO}_3$ ). The concentration of Pb was  $10^{-4}$ ,  $10^{-5}$  or  $10^{-6}$  M, with 2 g/L silica (Table 3.2).

Table 3.2 Experimental conditions for adsorption of Pb on silica

Experiment	Pb concentration (M)	Electrolyte strength (M)
1.	$10^{-4}$	0.01
2.	$10^{-5}$	0.01
3.	$10^{-5}$	0.1
4.	$10^{-6}$	0.01

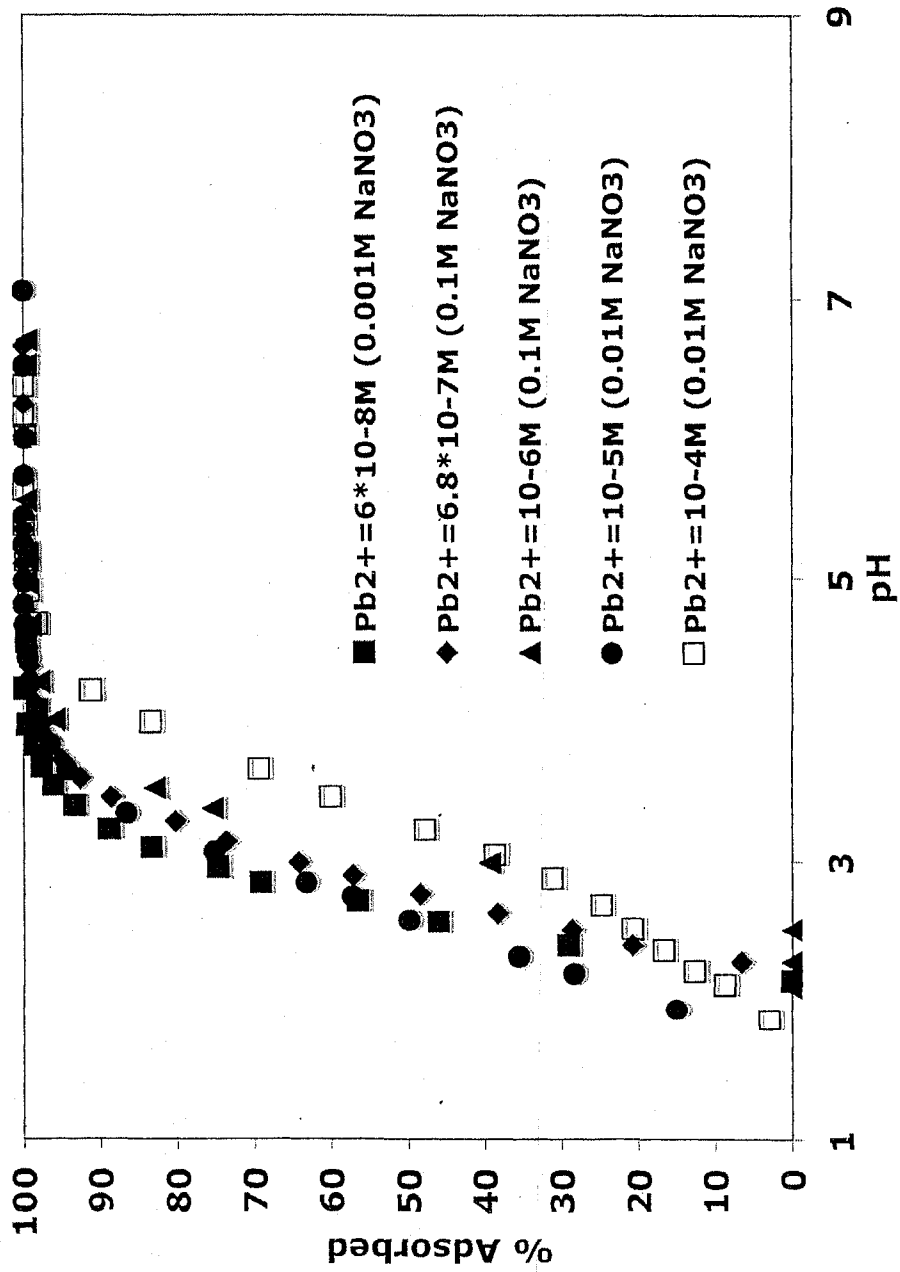


Figure 3.1. Percentage adsorption of Pb on HFO as a function of pH, sorbate/sorbent ratio and background electrolyte.

Adsorption increases with increasing pH, as expected (Figure 3.2). Pb is more weakly adsorbed on silica surfaces compared to HFO. Adsorption starts at pH~4 (compared to pH~2 for HFO) for all sorbate/sorbent ratios and 100% adsorption occurs at pH ~6.7 for  $10^{-6}$  M (compared to pH~4.3 for HFO), pH ~7.9 for  $10^{-5}$  M (compared to pH~4.5 for HFO), and pH ~8.3 for  $10^{-4}$  M (compared to pH~5 for HFO). All the adsorption edges have a very smooth sigmoidal shape, except for  $10^{-4}$  M, where the edge is nearly vertical above pH ~6.2, presumably due to precipitation of Pb on silica surfaces occurring instead of adsorption.

A strong ionic strength dependence is observed for Pb adsorption on silica. The adsorption edge shifts towards higher pH with higher ionic strength at a given Pb concentration. For example, the  $\text{pH}_{50}$  (pH value at which 50% adsorption occurs) for Pb concentrations of  $10^{-5}$  M Pb at an ionic strength of 0.01 M is noted at pH~6, compared to pH~7 for the same Pb concentration and an ionic strength of 0.1 M. In contrast, Chen et al. (2005) showed mixed results for electrolyte strength dependence of Pb adsorption. Their study showed that there is no electrolyte strength dependence on Pb adsorption on silica surfaces when  $\text{NaClO}_4$  or  $\text{NaNO}_3$  were used as background electrolytes, even changing the strength from 0.1 to 0.01M. They have also used Min-U-Sil 5, similar to this study, but their BET analysis revealed that their silica has a lower surface area of  $4.0 \text{ m}^2/\text{g}$ , compared to  $9.4 \text{ m}^2/\text{g}$  measured in this study. This contrasting result of electrolyte strength dependence presumably due to very high sorbate/sorbent ratio as used by Chen et al. (2005) in their study. They used 100 g/L colloid, compared to only 2 g/L for this study. A high sorbate/sorbent ratio would definitely increase the amount of surface area available for adsorption. So, it is possible that, there is no competition of ion for

adsorption as there are plenty of sites available. But in this study, the amount of surface area was limited. It is expected that there would be a competition of ions at silica surfaces for adsorption, which was observed in this study. They also conducted a batch experiment with 0.5 M NaClO<sub>4</sub>, and even that high background electrolyte concentration did not affect Pb adsorption. In contrast, when NaCl was used as background electrolyte, with a concentration varying from 0.1 to 0.01 M, very little dependence on ionic strength was observed. However, when the NaCl concentration was changed from 0.01 to 1M, the adsorption edge shifted towards higher pH value indicating less Pb adsorption with increasing ionic strength, as observed in this study. None of the other studies are comparable to this study due the fact that those studies have used different sorbate/sorbent ratios. Moreover they have used different types of silica for their study.

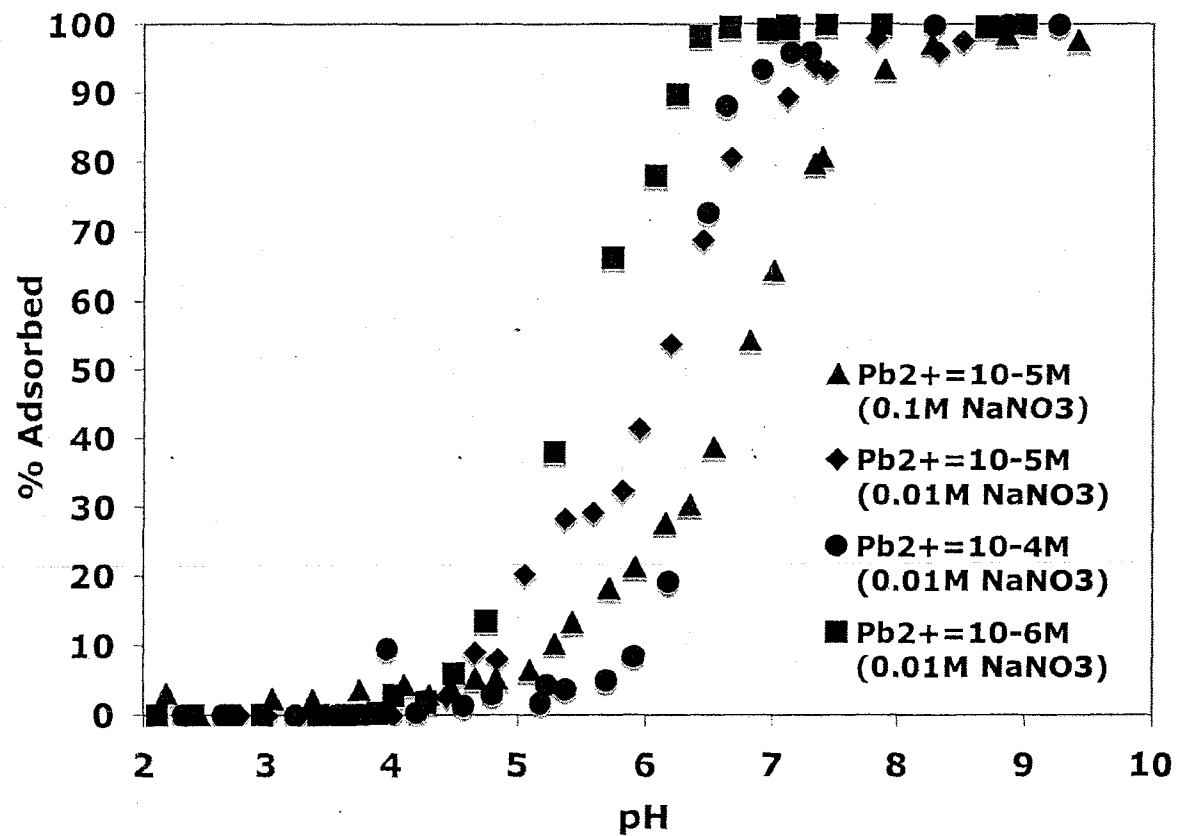


Figure 3.2. Percent adsorption of Pb on silica as a function of pH. All experiments were completed in NaNO<sub>3</sub> using 2 g/L silica with a BET surface area of 9.4 m<sup>2</sup>/g.

### Adsorption of Pb on kaolinite

Two different types of kaolinite were used for conducting Pb adsorption experiments. The first was powdered kaolinite purchased from Ward's Natural Science Establishment, Inc. The other kaolinite was powdered kaolinite (KGa-1B) from Washington County, GA purchased from The Clay Mineral Repository of the Clay Minerals Society. X-Ray diffraction data (data courtesy of Dr. Ray Ferrell at Louisiana State University) shows that the Ward's kaolinite contains ~1% muscovite or smectite impurities. The KGa-1B kaolinite of Clay Mineral Society does not contain any phyllosilicate impurities (Pruett and Webb, 1993).

### Adsorption of Pb on Ward's kaolinite

Three different concentrations of Pb ( $10^{-4}$ ,  $10^{-5}$  and  $10^{-6}$ M) were used to run the adsorption experiments, keeping the strength of the background electrolyte constant (0.01 M NaNO<sub>3</sub>) and using 2 g/L of kaolinite. Adsorption of Pb increases with increasing pH in all the systems (Figure 3.3). Adsorption starts at pH~3 for all Pb concentrations, and 100% adsorption occurs at pH~6 for both  $10^{-6}$  and  $10^{-5}$  M Pb experiments. For  $10^{-4}$  M Pb, adsorption does not reach 100% even at pH~6.7. The adsorption edges shift towards higher pH as the concentration of Pb is increased. The pH<sub>50</sub> is ~4.8 for  $10^{-6}$  M Pb compared to ~5.2 for  $10^{-5}$  M Pb and ~5.3 for  $10^{-4}$  M Pb. The adsorption edges are sharper compared to the adsorption edges for silica, but not as sharp as for HFO. For experiments with the same ionic strength and sorbate/sorbent ratio, the adsorption edges are intermediate between those measured for HFO and silica, with the most adsorption on HFO surface and the least on silica at any given pH and sorbate/sorbent ratio.

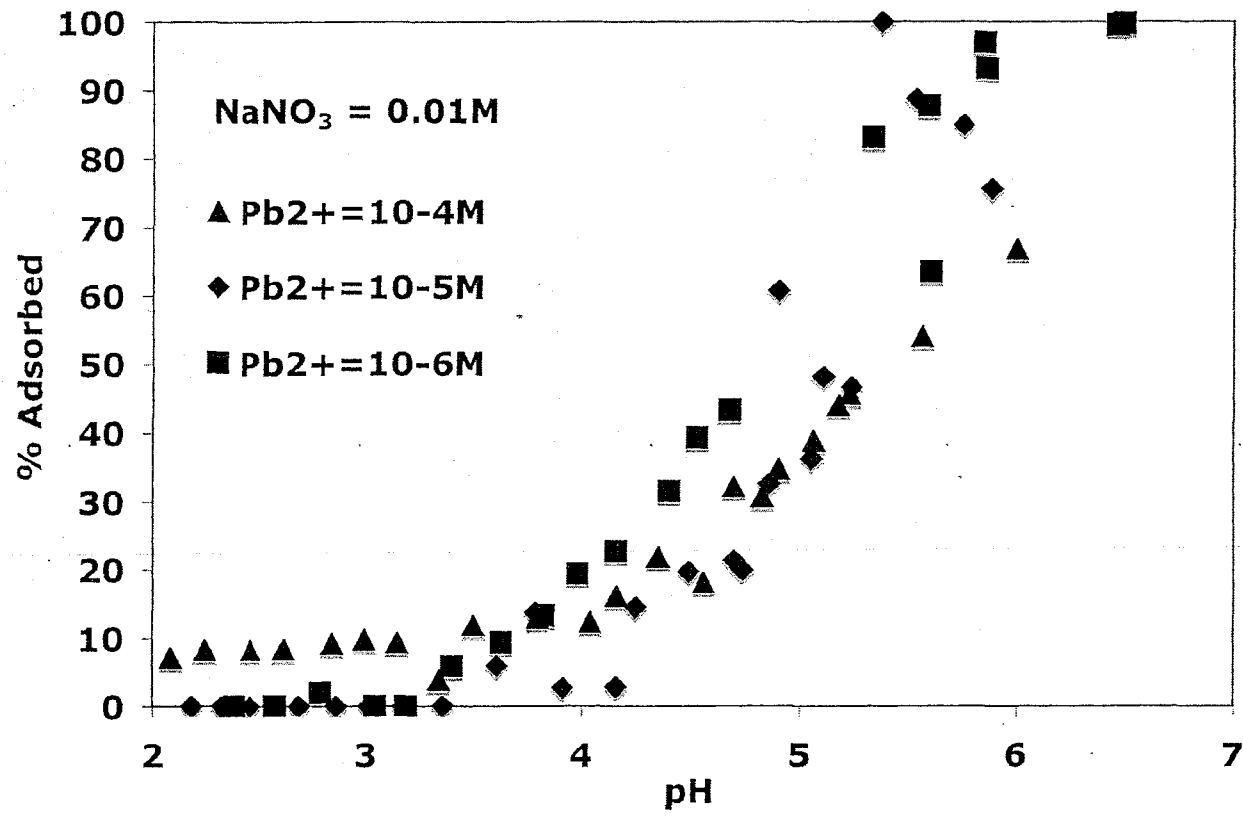


Figure 3.3. Adsorption of Pb on Ward's kaolinite with Pb concentrations varied from 10<sup>-4</sup> to 10<sup>-6</sup> M. The concentration of the background electrolyte was kept constant (0.01 M NaNO<sub>3</sub>), as was the amount of sorbent (2 g/L).

Adsorption of Pb on kaolinite (KGa-1B)

Three sets of Pb adsorption experiments were conducted on kaolinite KGa-1B with Pb concentrations of  $10^{-5}$  and  $10^{-6}$  M and the background electrolyte varied from 0.1 to 0.01 M  $\text{NaNO}_3$  (Table 3.3).

Table 3.3 Experimental conditions for Pb adsorption onto KGa-1B

Experiment	Pb concentration	Electrolyte strength
1.	$10^{-5}$ M	0.01M
2.	$10^{-5}$ M	0.1M
3.	$10^{-6}$ M	0.01M

Adsorption increases with increasing pH in all the systems studied (Figure 3.4). A greater percentage of Pb is adsorbed in the  $10^{-6}$  M system relative to the  $10^{-5}$  M system at any given electrolyte strength. Adsorption starts at pH~2 for  $10^{-6}$  M, compared to pH~4 for  $10^{-5}$  M experiments. Adsorption edges are very smooth and have a sigmoidal shape. A strong electrolyte strength dependence adsorption is noted between the two experiments conducted with  $10^{-5}$  M Pb and 0.01 versus 0.1 M  $\text{NaNO}_3$ . Higher ionic strength decreases adsorption, shifting the adsorption edge towards higher pH, such that the  $\text{pH}_{50}$  occurs at ~5.6 for 0.01 M  $\text{NaNO}_3$  compared to ~6.5 for 0.1M  $\text{NaNO}_3$  experiments.

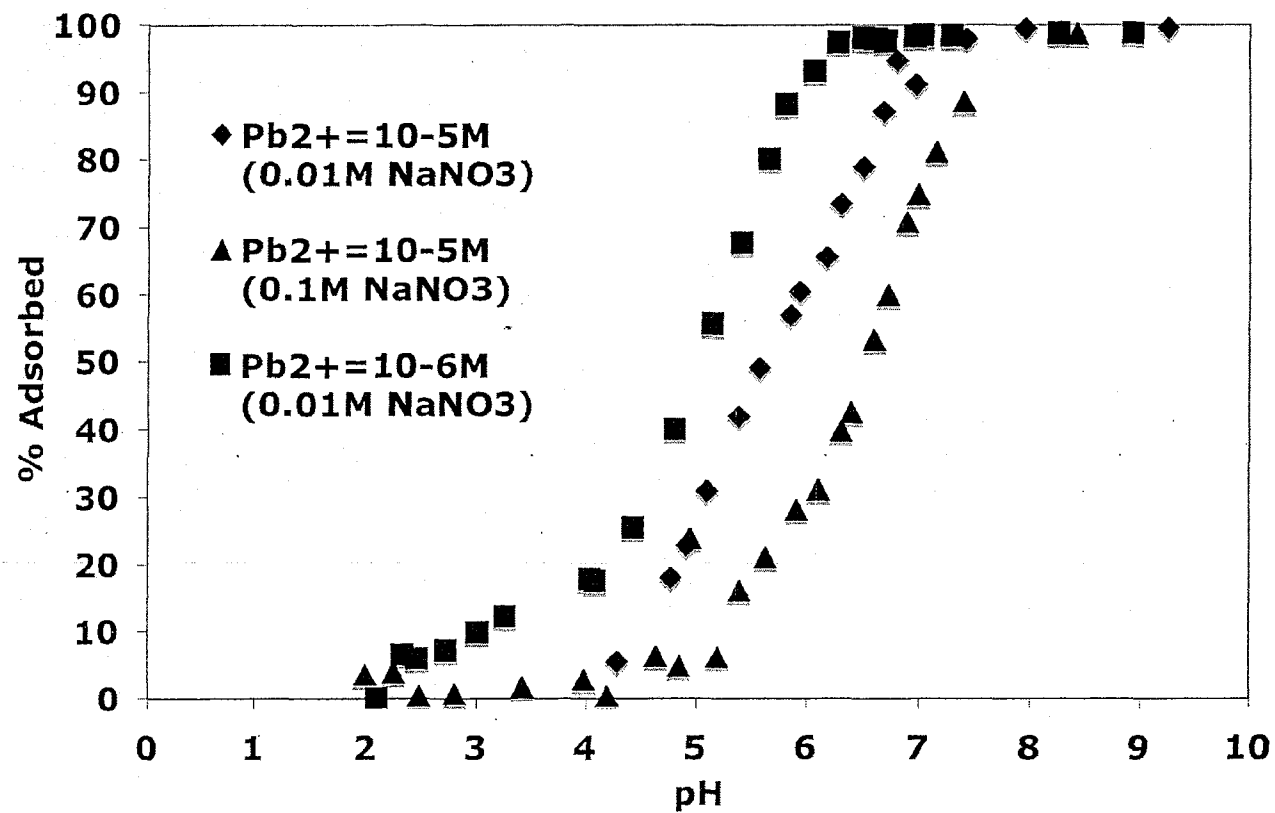


Figure 3.4. Percent adsorption of Pb on kaolinite KGa-1B as a function of pH. Experiments were completed with  $10^{-5}$  or  $10^{-6}$  M Pb, a background electrolyte of 0.01 or 0.1 M  $NaNO_3$  and 2 g/L kaolinite.

### Comparison between Ward's kaolinite and KGa-1B

For experiments with  $10^{-5}$  M Pb and 0.01 M NaNO<sub>3</sub>, adsorption initiates at lower pH for Ward's kaolinite (pH~3.5) compared to KGa-1B kaolinite (pH~4) (Figure 3.5), and the pH<sub>50</sub> for Ward's kaolinite is slightly less (~5.4) than that of KGa-1B (~5.6). The adsorption edge of KGa-1B is much smoother and more sigmoidal in shape, compared to the much more scattered edge measured for the Ward's kaolinite, especially at higher pH. Similar adsorption behavior is observed at concentrations of  $10^{-6}$  M Pb for both types of kaolinite. Adsorption starts at lower pH for KGa-1B compared to Ward's kaolinite. At pH 2.33, 6.6% adsorption is noted for KGa-1B compared to only 2% adsorption at pH 2.79 for Ward's kaolinite. 100% adsorption occurs at pH ~6.5 for Ward's kaolinite in contrast to ~6.6 for KGa-1B. Other than that, both types of kaolinite show very similar adsorption edges.

Ikhsan et al. (1999) studied adsorption of Pb on kaolinite surfaces. Though they have used different type of kaolinite (Ajax Chemicals) and amount of colloid (~6.78 g/L) compared to this study, as well as different concentration of Pb (100µM) and background electrolyte (5mM KNO<sub>3</sub>), but the sigmoidal shapes of the adsorption edges are very similar. Though adsorption starts at around pH~3 and 100% adsorption was reached at pH~7.5, compared to much less pH values for both these types of kaolinite used for this study.

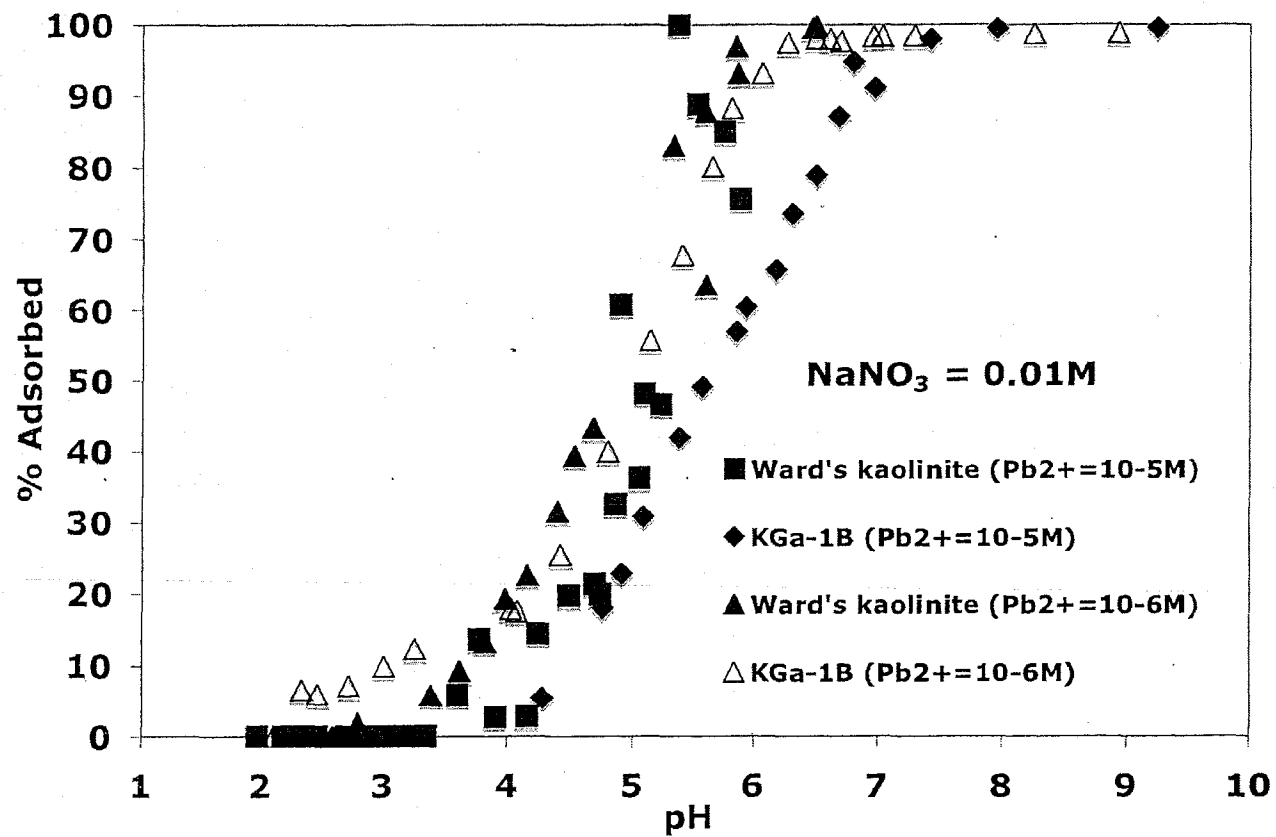


Figure 3.5. Comparison of Pb adsorption as a function of pH between Ward's kaolinite and KGa-1B for 10<sup>-5</sup> and 10<sup>-6</sup> M Pb, 2 g/L kaolinite and 0.01 M NaNO<sub>3</sub>.

### Kinetics experiments in batch solution

A separate set of experiments was performed to evaluate the reaction kinetics and reversibility of the adsorption reactions. The full procedure is described in Chapter II. Briefly, a slurry was made with 2 g/L of kaolinite in a 0.01 M  $\text{NaNO}_3$  with a Pb concentration of  $10^{-5}$  M and a time series of measurements were completed to measure the rate of Pb adsorption at pH ~10, followed by a time series of measurements to measure the rate of Pb desorption at pH ~2. Under the adsorption experiment conditions, 100% adsorption was achieved within 5 minutes after initiation of the adsorption reaction (Figure 3.6), and the adsorbed Pb remains on the kaolinite surface until the adsorption kinetics experiment is ended (72 hrs) and desorption initiated by addition of nitric acid. From this it is clear that the Pb adsorption reaction on kaolinite is very fast and the Pb remains adsorbed on the mineral surfaces as long as the pH remains stable. The desorption experiment similarly shows that 100% desorption is achieved within 5 minutes or so and the Pb remains in solution if the pH remains low enough to prevent adsorption. Thus, both the adsorption and desorption reactions are very fast and adsorption under these conditions is completely reversible.

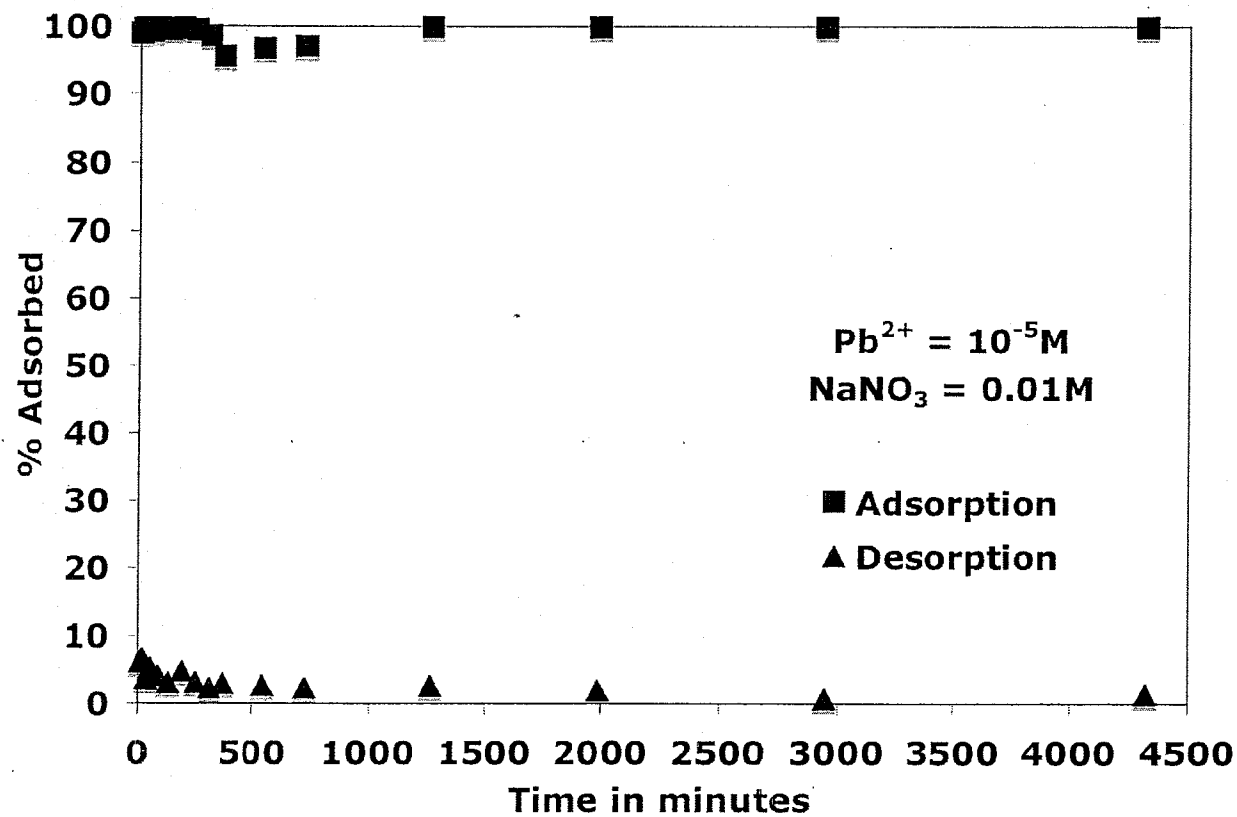


Figure 3.6. Kinetics experiments showing the percentage of Pb adsorbed as a function of time. The adsorption experiment was completed at pH ~10 and the desorption experiment at pH ~2. Both experiments were completed using 2 g/L of kaolinite KGa-1B, 0.01M NaNO<sub>3</sub> and 10<sup>-5</sup> M Pb.

### Dialysis bag experiments

Dialysis is a simple process in which small solutes diffuse from a high concentration solution to a low concentration solution across a semi-permeable membrane until equilibrium is reached. The goal of this dialysis bag experiment was to compare the speed of the adsorption reaction with or without a semi-permeable membrane. This kind of experiment is the first step in evaluating the interaction of minerals in binary or ternary assemblages where a dialysis membrane separates the minerals, so that no direct contacts between them, but Pb can move freely across the membrane. A comparison of this type of experiment with the batch experiments with minerals in contact might yield useful information regarding colloid-colloid interactions and their influence on adsorption.

### Kinetics experiments using dialysis bags

An initial set of experiments was conducted to evaluate the speed of adsorption on HFO using the dialysis bag method. The methods are fully described in Chapter II. Briefly, HFO was placed inside a dialysis bag with a diameter of 10 mm, volume of 10 mL and a length of 16 cm. The pH was titrated by addition of solution outside of the bag. The kinetics might be different than in bulk solution, as ions must move across a semipermeable membrane until equilibrium is reached. Initial adsorption was very fast with almost 90% of the adsorption occurring within 5 minutes after addition of enough base to reach pH ~10. Close to 96% of the Pb remained adsorbed on the HFO after 300 minutes. However, with increasing time, desorption took place, although the pH remained at pH ~9.15 outside of the bag. From 800 to 1500 minutes, the amount of Pb

adsorbed remained stable at ~60%. The reason for the decrease in adsorbed Pb is not clear. Although pH decreased steadily from 9.15 to 7.13 from 300 minutes to 780 minutes of total time span, 100% adsorption should be achieved at much lower pH values for HFO with  $10^{-5}$  M Pb in 0.01 M NaNO<sub>3</sub>. Therefore, the pH drop is not likely the explanation for desorption starting to occur after 300 minutes. More likely, some of the HFO within the bag began to dissolve, leaking Fe to the solution outside the bag (evident from a change in color of the solution outside the bag from clear to light reddish brown, not by measuring the amount of Fe in solution), and this may have triggered Pb desorption inside the bag, increasing the Pb concentration outside the bag. In contrast to the adsorption experiments, desorption started very quickly with 95% of the desorption occurring within the first 5 minutes after addition of enough acid to achieve a pH of ~2. The Pb remained 100% desorbed for at least 1500 minutes.

#### Pb adsorption on HFO in dialysis bag

An adsorption experiment was conducted using  $10^{-5}$  M Pb in 0.01 M NaNO<sub>3</sub> to compare adsorption as a function of pH on HFO in the presence of the dialysis bag to edges obtained in bulk solution. Although adsorption in both types of experiments started at pH~2, less adsorption occurred at higher pH values in the presence of the dialysis membrane (Figure 3.8). Although 100% adsorption occurred at pH~4 in the bulk solution experiments, even at pH~6.7, only 76% Pb is adsorbed in experiments conducted using a dialysis bag.

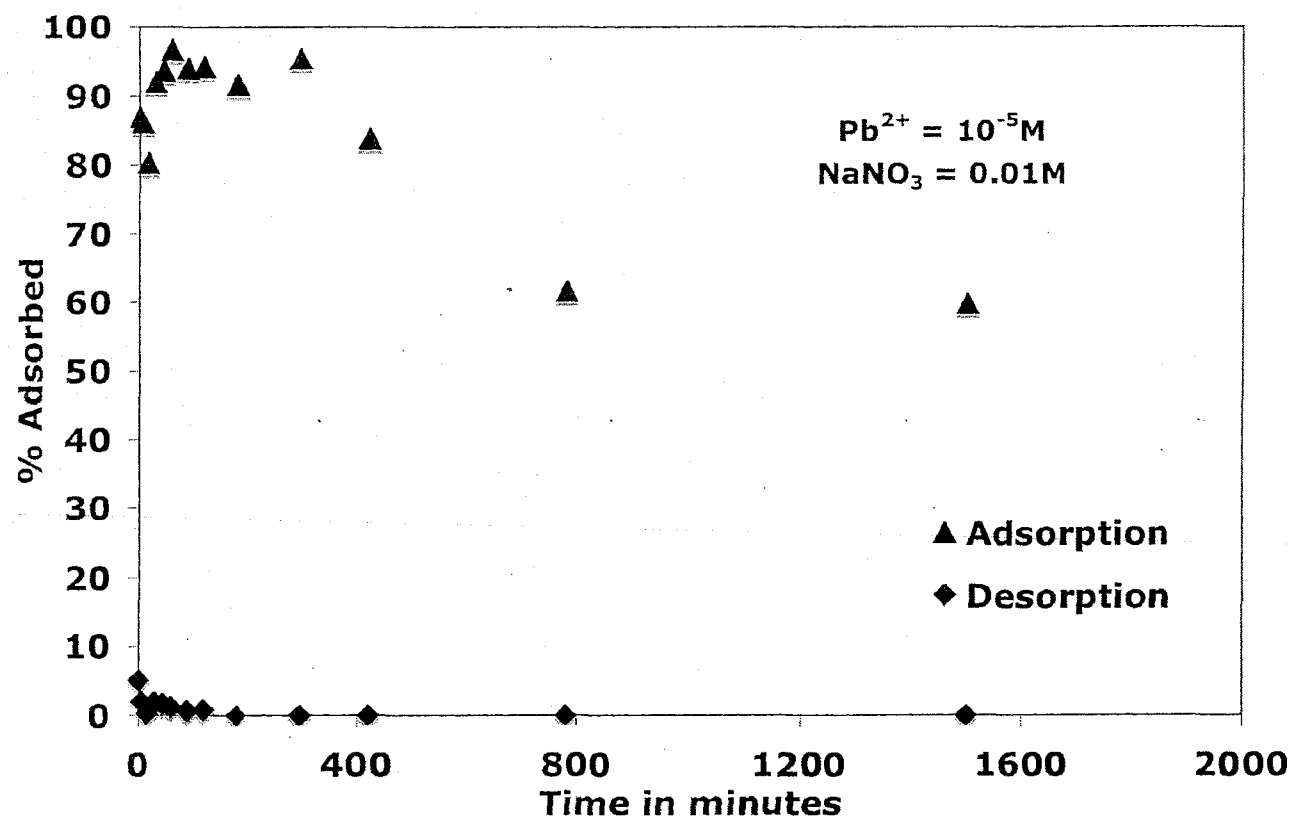


Figure 3.7. Kinetics of Pb adsorption and desorption on HFO contained within a dialysis bag. The adsorption experiment was initiated by increasing the pH to ~10 and desorption by dropping the pH to ~2.

The explanation for this adsorption behavior is unclear. Perhaps it is related to the fact that HFO began to coagulate inside the dialysis bag so that not all the surface area was available for Pb for adsorption as the reaction proceeded. During the first few hours, HFO inside the dialysis bag did not show any effect of clotting, but as the experiment proceeded, the dialysis bag became hardened as the HFO clumped and coagulated within the bag. More likely, however, some of the HFO within the bag began to dissolve, leaking Fe to the solution outside the bag (as in the kinetics experiment, evident from a change in color of the solution outside the bag from clear to light reddish brown, not by measuring amount of Fe in solution), and this may have led to Pb desorption from HFO in the bag, as Pb became adsorbed on colloids forming in the solution outside the bag. Also, using the dialysis bag might require longer than 10 minutes for the Pb to cross the membrane and equilibrate with the Pb colloids within. More study will be required to resolve the explanation for the mismatch between Pb adsorption edges measured in bulk solution compared to those measured with the dialysis bag.

I would suggest couple of ways to solve this problem. First of all, we need a larger dialysis bag with larger diameter, to provide enough space for colloids, so that HFO or any other colloids do not get clogged inside the dialysis bag. Moreover, the dialysis bag we used, were not very suitable for HFO, as after some time, HFO was started to come out from the bag and presumably started to dissolve. Therefore, we might need a better quality of dialysis bag, which can hold HFO or other colloids properly. Secondly, we could make a small tank, where a dialysis membrane put inside the tank in such a way, so that it divides the tank in half way. Instead of putting the colloids inside the bag, we could put it in the one half and put sorbates (here Pb) on the other. Therefore, the sorbate

could move freely through the membrane, but the sorbent cannot. This would definitely a much better way to resolve this issue.

Comparison of Pb adsorption among the three different single solid systems: HFO, silica and kaolinite

The adsorption behavior of Pb ( $10^{-5}$  M) in 0.01 M NaNO<sub>3</sub> on HFO, silica and kaolinite (both Ward's and KGa-1B) is shown for the four single solid systems in Figure 3.9 and is tabulated in Table 3.4. The position of the adsorption edges are strongly related to the respective surface areas of the four solids and nature of aqueous complexes produced on these four different solids surfaces. Pb forms strong inner-sphere complexes on the HFO surface compared to weakly adsorbing outer-sphere complexes for the other three solids. Moreover, HFO has the highest surface areas ( $600 \text{ m}^2/\text{g}$ ) among these pure solid phases. HFO has almost 64 times greater surface area than silica, 44 times higher than KGa-1B ( $13.6 \text{ m}^2/\text{g}$ ) and 23 times greater than Ward's kaolinite ( $25.7 \text{ m}^2/\text{g}$ ). Thus, it is not surprising that the most adsorption occurs on the HFO. Similarly, Ward's kaolinite has a surface area of  $25.7 \text{ m}^2/\text{g}$ , higher than KGa-1B ( $13.6 \text{ m}^2/\text{g}$ ). Moreover, it contains ~1% of smectite impurity, which should increase the CEC (cation exchange capacity) compared to Ward's kaolinite. This should increase adsorption compared to KGa-1B. Accordingly, Ward's kaolinite shows a slightly higher affinity for Pb compared to KGa-1B (table 3.4).

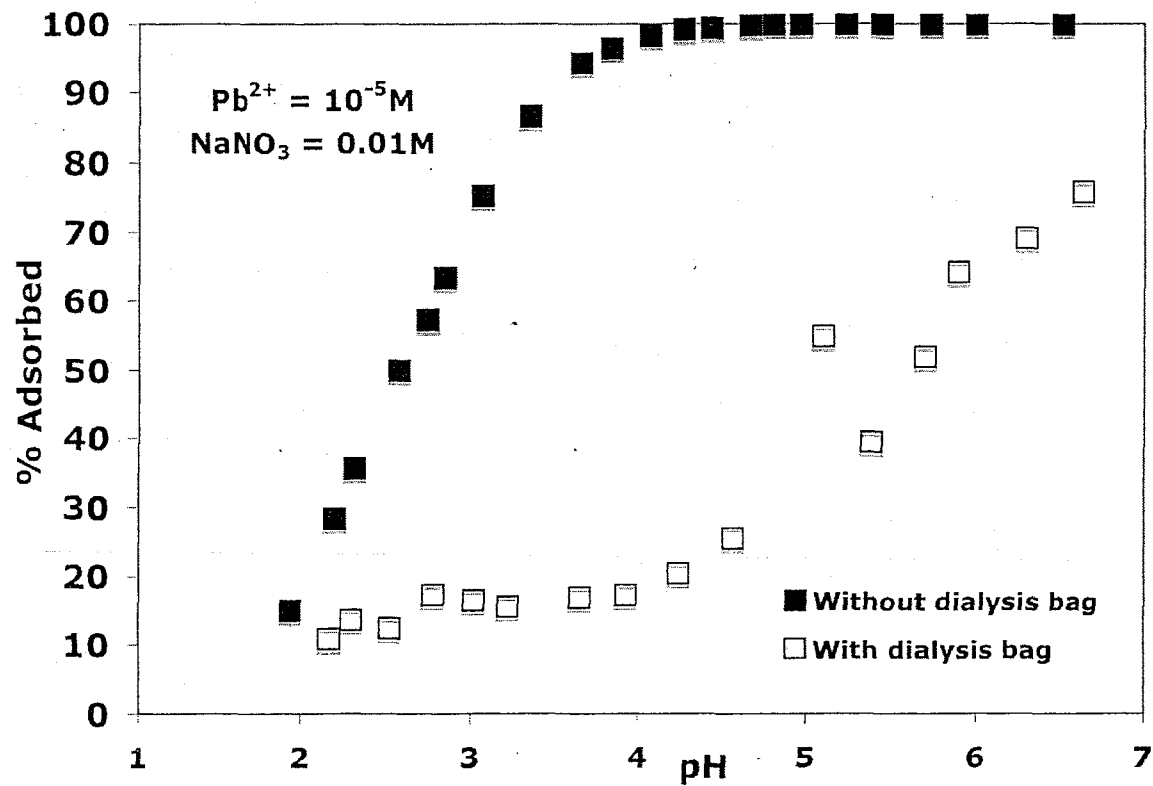


Figure 3.8. Comparison between the percentage of Pb adsorbed to HFO as a function of pH with  $10^{-5} M$  Pb, 2 g/L HFO and 0.01 M  $NaNO_3$  with and without a dialysis bag.

Table 3.4 Adsorption of Pb on the four single solids. All experiments were completed with  $10^{-5}$  M Pb, 0.01 M NaNO<sub>3</sub> and 2g/L total solid

% Adsorbed	HFO	Silica	KGa-1B	Ward's kaolinite
25	2.1	5.0	4.8	4.5
50	2.6	6.0	5.6	5.4
75	3.0	6.5	6.2	5.9
100	4.0	9.0	8.0	-

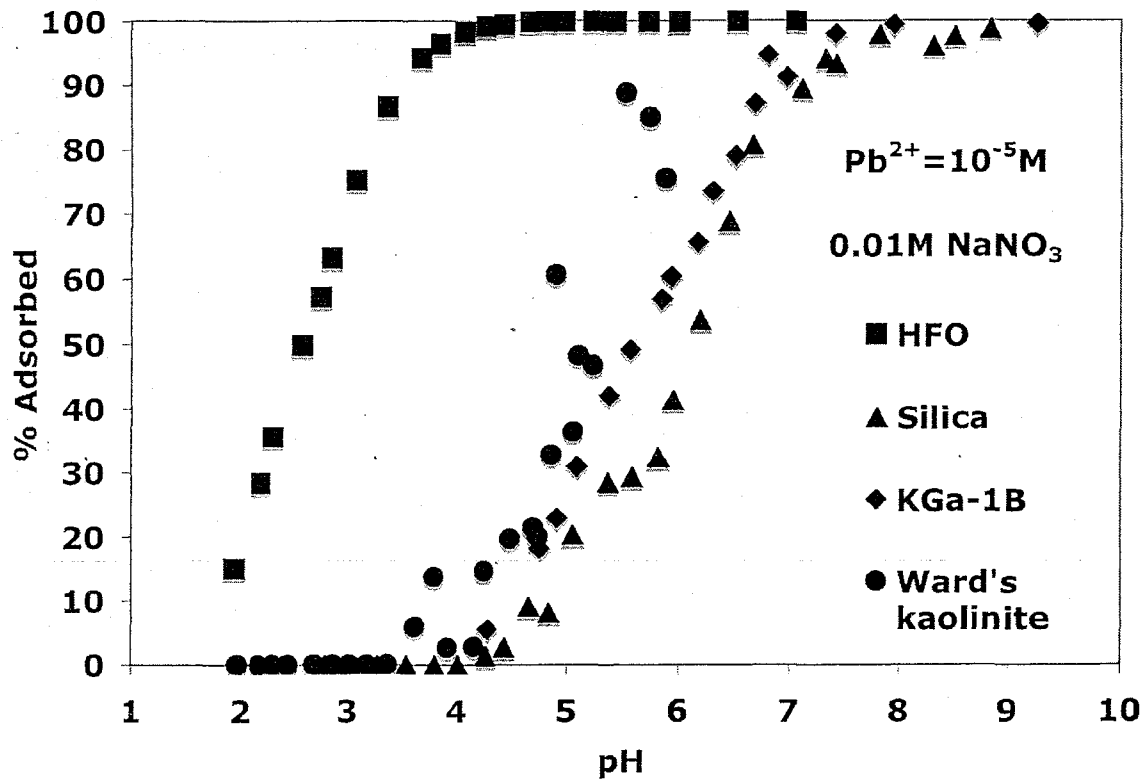


Figure 3.9. Comparison of Pb adsorption as a function of pH among the three adsorbents: HFO, silica and kaolinite (KGa-1B and Ward's) for 10<sup>-5</sup> M Pb, 0.01 M NaNO<sub>3</sub> and 2 g/L solid.

## Binary systems

### Adsorption of Pb on HFO+silica systems

Six sets of experiments were conducted to evaluate Pb adsorption on a mixture of two pure solid phases. One such binary system included HFO and silica. The concentrations of Pb, background electrolyte and total solid were held constant at  $10^{-5}$  M, 0.01M NaNO<sub>3</sub> and 2 g/L, respectively. The silica to HFO ratio was varied from 1:1 to 500:1 with intermediate ratios of 5:1, 10:1, 50:1 and 100:1. The pH edges for the mixtures are intermediate between edges measured for the pure solids (Figure 3.10, Table 3.5). As the silica to HFO ratio increases, the adsorption edges shift to higher pH, towards the pure silica edge and away from the pure HFO edge, but they never reach the pure silica edge, even at a ratio of 500:1. This suggests that Pb adsorbs strongly on available HFO surfaces, irrespective of the amount of HFO present in the system. The 50:1 and 100:1 adsorption edges are nearly identical. Other than that, all other edges show a steady shift towards the pure silica endmember with increasing silica:HFO ratio. Pb adsorption starts around pH~2 for 1:1, 5:1, 10:1 and 50:1 systems, and closer to pH 3 for the other two systems, namely 100:1 and 500:1. 100% adsorption is achieved at pH~4.6 for 1:1, ~4.9 for 5:1, ~5.0 for 10:1, ~6.4 for 50:1, ~6.9 for 100:1 and ~7.4 for 500:1.

Table 3.5 A comparison of the pH at which various percents of Pb adsorption occur for pure HFO and silica systems, as well as for the various binary mixtures. All experiments conducted with  $10^{-5}$  M Pb, 0.01 M NaNO<sub>3</sub> and 2 g/L total solid

% Adsorbed	Pure HFO	Pure silica	1:1	5:1	10:1	50:1	100:1	500:1
25	2.1	5.0	2.4	3.0	3.2	4.3	4.5	4.8
50	2.6	6.0	2.8	3.6	3.9	4.8	5.0	5.5
75	3.0	6.5	3.5	4.1	4.3	5.5	5.6	6.0
100	4.0	9.0	4.6	4.9	5.0	6.4	6.9	7.4

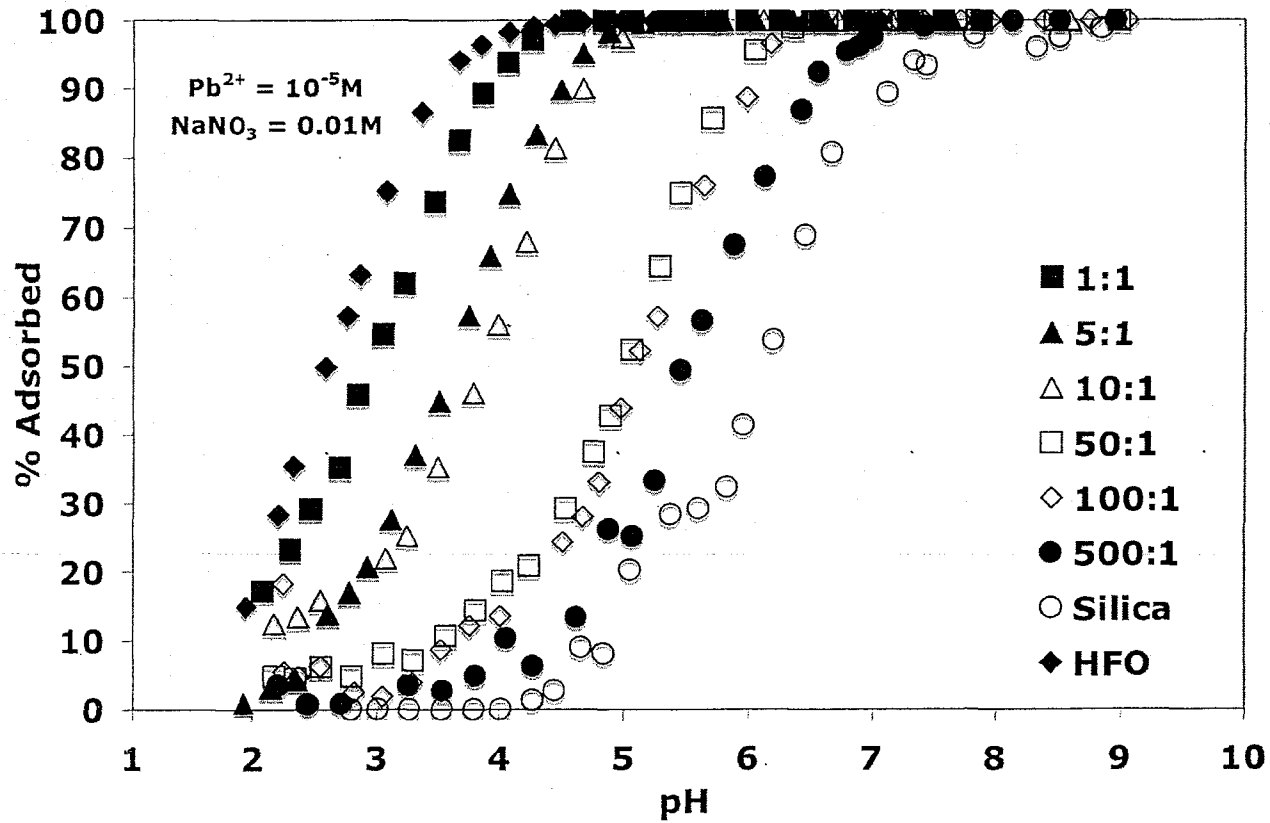


Figure 3.10. Percentage of Pb adsorption on binary mixtures of HFO+silica with six different solute-to-solute ratios as a function of pH. All experiments were completed with  $10^{-5}$  M Pb, 0.01 M  $NaNO_3$  and 2 g/L total solid.

### HFO+kaolinite (KGa-1B) system

Seven experiments were conducted to evaluate Pb adsorption in a system containing both HFO and kaolinite. The concentrations of Pb, the ionic strength and the total amount of solid were kept constant, as for the HFO+silica system, at  $10^{-5}$  M, 0.01 M NaNO<sub>3</sub> and 2 g/L, respectively. The kaolinite:HFO ratio was varied from 1:1 to 5000:1, with intermediate ratios of 5:1, 10:1, 50:1, 100:1 and 500:1. The results show that with an increasing amount of kaolinite in the system, the adsorption edges shift towards the pure kaolinite system, but never reach the pure kaolinite edge, even with 5000:1 kaolinite-to-HFO ratio (Figure 3.11, Table 3.6). This suggests that even a very small mass of HFO has a very strong influence on Pb adsorption, a very similar behavior to that noticed in the HFO+silica system. For all mixtures, adsorption starts at pH~2 and 100% adsorption occurs at pH~5.0 for the 1:1 system, ~5.2 for 5:1, ~5.6 for 10:1, 6.0 for 50:1, 100:1 and 500:1, and 6.8 for 5000:1. The adsorption edges are very similar for the 50:1, 100:1 and 500:1 systems, with the data points from the three experiments almost on top of each other. Considerable shifting of adsorption edges occurs between 1:1 and 5:1, but 5:1 to 10:1 are very similar. There is again a considerable shift noted between 10:1 and 50:1, but 50:1, 100:1 and 500:1 are very similar, as mentioned above. There was also a noticeable shift of the adsorption edges observed between the 500:1 and 5000:1 experiments.

Table 3.6 A comparison of the pH at which different percentages of adsorption occur for the pure HFO and silica systems, as well as for the various binary mixtures. All experiments conducted with  $10^{-5}$  M Pb, 0.01 M NaNO<sub>3</sub> and 2 g/L total solid

% Adsorbed	Pure HFO	Pure KGa-1B	1:1	5:1	10:1	50:1	100:1	500:1	5000:1
25	2.1	4.8	2.7	3.0	3.3	3.7	3.7	3.7	4.3
50	2.6	5.6	3.2	4.0	4.1	4.4	4.6	4.6	5.0
75	3.0	6.2	3.7	4.3	4.5	5.0	5.1	5.1	5.6
100	4.0	8.0	5.0	5.2	5.6	6.0	6.0	6.8	6.8

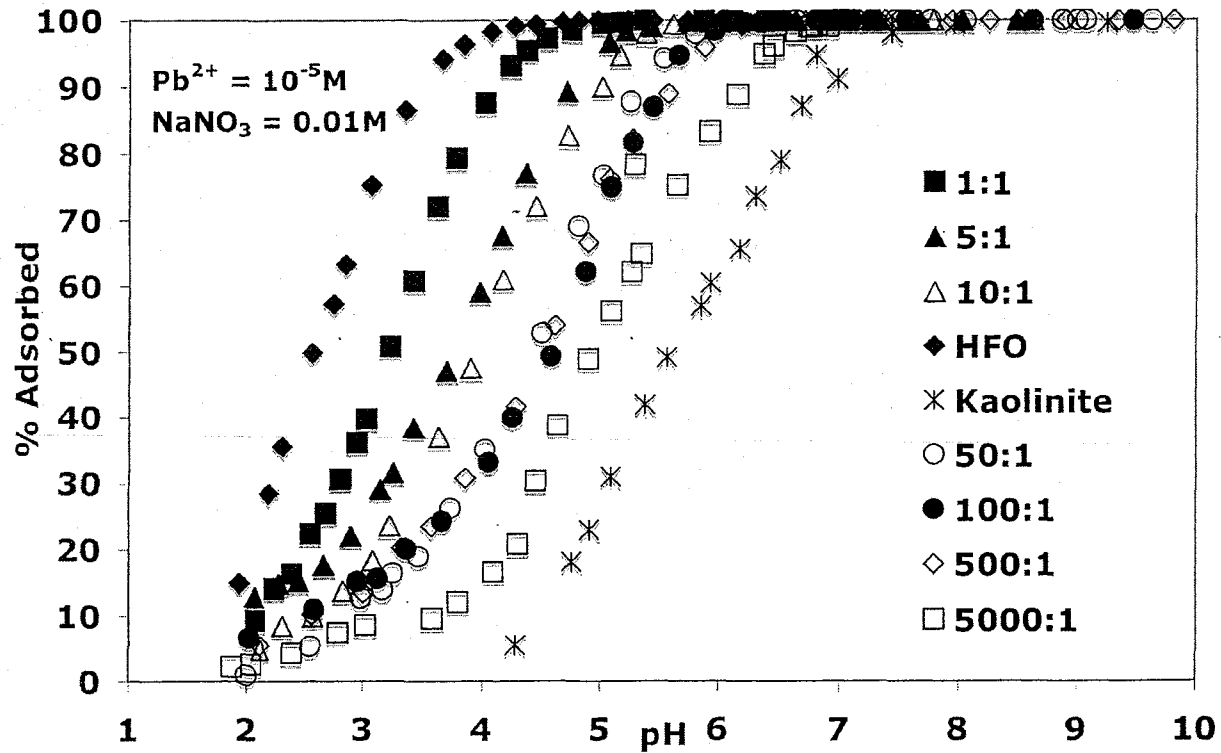


Figure 3.11. Percentage of Pb adsorbed on binary mixtures of HFO+kaolinite (KGa-1B) with seven different kaolinite:HFO ratios as a function of pH. All experiments were completed with  $10^{-5}$  M Pb, 0.01 M  $NaNO_3$  and 2 g/L total solid.

### Kaolinite (KGa-1B)+silica system

Five batch experiments were conducted to evaluate Pb adsorption on kaolinite and silica mixtures. The concentration of Pb was kept constant ( $10^{-5}$  M) in a constant background electrolyte concentration (0.01 M  $\text{NaNO}_3$ ) and with a total solid concentration of 2 g/L. The kaolinite:silica ratio was varied from 0.02:1 to 50:1, with intermediate ratios of 0.1:1, 1:1, and 10:1. For the systems with ratios of 1:1, 10:1 and 50:1, adsorption starts at pH~3, whereas for 0.02:1 or 0.1:1 ratios adsorption begins at as low as pH~4 (Figure 3.12). Adsorption edges are very similar for systems containing kaolinite:silica ratios of 1:1, 10:1 and 50:1. Curiously, these edges are all very slightly shifted to the left compared to the pure kaolinite system. The tendency of the 1:1 system to follow the pure kaolinite edge instead of being intermediate between that and the pure silica edge may be due to kaolinite coating the silica surface and blocking of the silica surface sites. Thus, the 1:1 system adsorption edge looks similar to that of pure kaolinite data. For the systems with much less kaolinite (0.1:1 and 0.02:1), adsorption starts at pH~4 and both edges are similar to that measured for pure silica. Above pH~6, the 0.1:1 edge shifts to the right, with less adsorption at a given pH compared to the 0.02:1 and pure silica systems; 100% adsorption occurs at pH~8.5 for the 0.1:1 system, compared to pH~8.0 for the 0.02:1 system.

Table 3.7 pH values at which a given the percentage of Pb adsorption occurs for the pure silica and kaolinite systems, together with the mixed systems

% Adsorbed	Pure KGa-1B	Pure silica	1:1 K:S	10:1 K:S	50:1 K:S	0.1:1 K:S	0.02:1 K:S
25	4.8	5.0	4.4	4.6	4.8	5.6	5.6
50	5.6	6.0	5.3	5.5	5.5	6.5	6.0
75	6.2	6.5	6.0	6.4	6.2	7.1	6.5
100	8.0	9.0	7.1	7.8	7.6	8.5	8.0

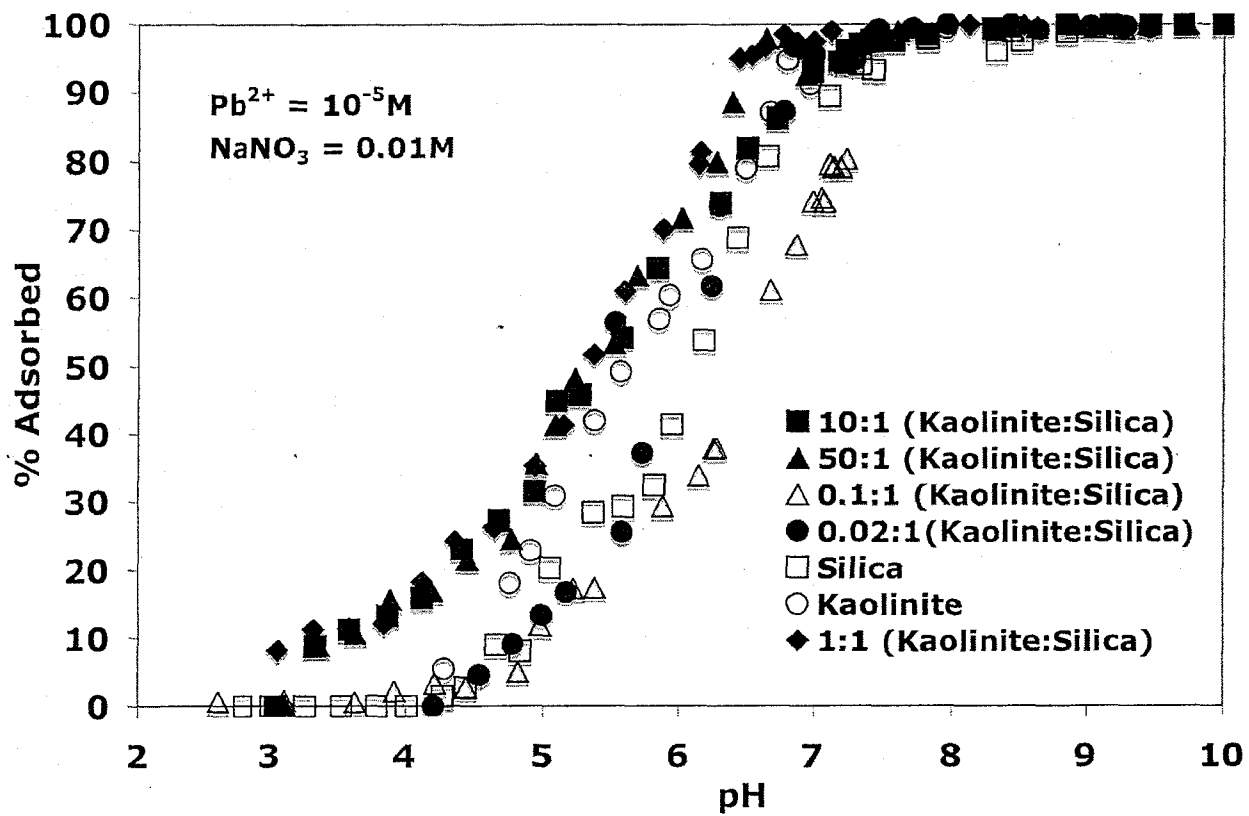


Figure 3.12. The percentage of Pb adsorbed as a function of pH in kaolinite and silica systems with 10<sup>-5</sup> M Pb, 0.01 M NaNO<sub>3</sub> and 2 g/L total solid.

### Ternary systems

Two batch experiments were conducted for ternary systems containing all three pure solid phases, namely HFO, silica and KGa-1B kaolinite. One experiment was done with a 1:1:1 ratio of the solids according to their mass and the other was 1:1:1 by surface area. The concentration of Pb was held constant ( $10^{-5}$  M) in a constant background electrolyte (0.01M NaNO<sub>3</sub>) with a total amount of sorbent of 2 g/L.

The system containing 1:1:1 by mass adsorbed Pb more strongly, as expected, than the system with 1:1:1 surface area, as the amount of HFO surface was much higher in the system with equal masses (Figure 3.13, Table 3.8). Adsorption starts at pH~2 and 100% adsorption is achieved at pH~5.0 for the 1:1:1 system by mass, compared to pH~3 and pH~6.5 respectively for the system with 1:1:1 ratio by surface area. The adsorption edge for the 1:1:1 system by mass shifts more towards pure HFO, whereas the 1:1:1 system by surface area shifts more towards the pure kaolinite edge.

Table 3.8 pH at which a given percent Pb adsorbed occurs on the pure solids and the 1:1:1 ratios of the solids

% Adsorbed	HFO	Silica	KGa-1B	1:1:1 by mass	1:1:1 by S.A
25	2.1	5.0	4.8	2.5	4.4
50	2.6	6.0	5.6	3.2	4.9
75	3.0	6.5	6.2	3.8	5.6
100	4.0	9.0	8.0	5.0	6.5

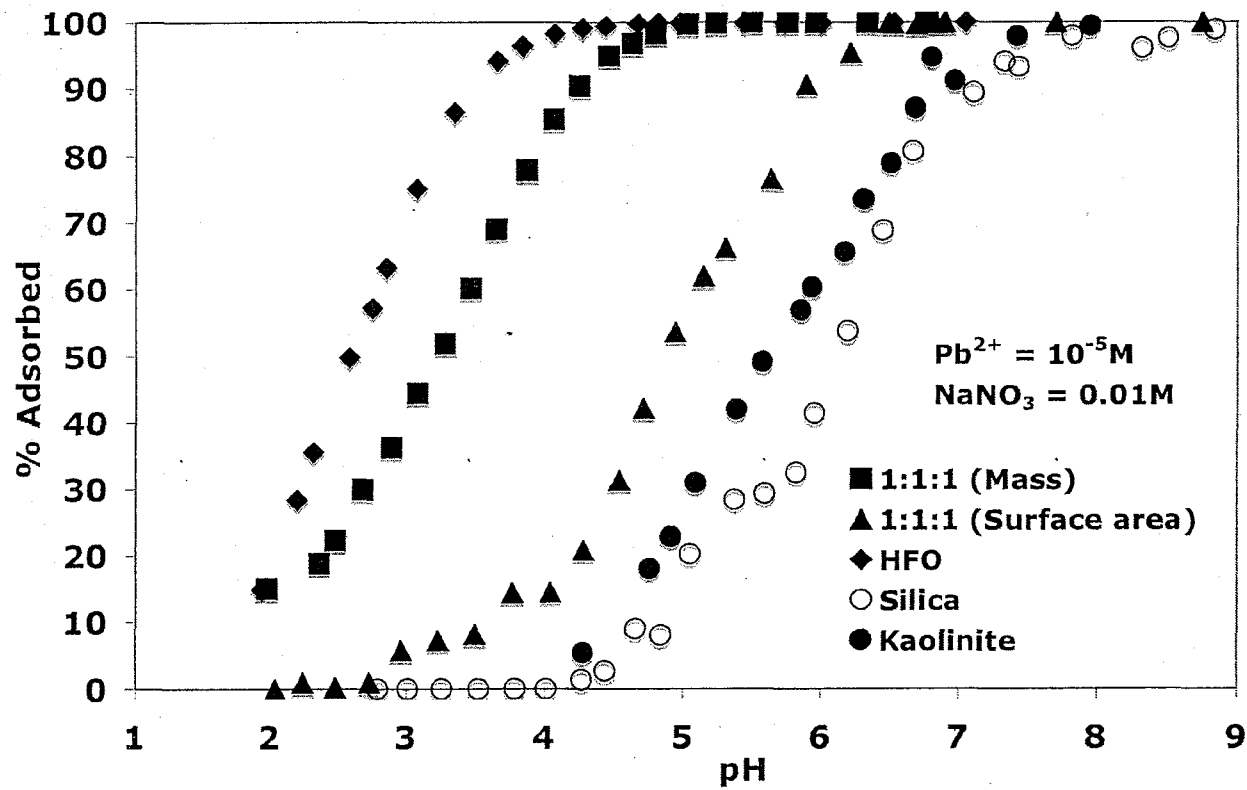


Figure 3.13. Pb adsorption for ternary systems containing all these three pure mineral phases in a ratio of 1:1:1 by surface area as well as by mass as a function of pH. All experiments were completed with  $10^{-5} M$  Pb,  $0.01 M$   $NaNO_3$  and  $2 g/L$  total solid

## CHAPTER IV

### MODELING OF EXPERIMENTAL DATA

#### Single solid systems

##### Adsorption of Pb on HFO

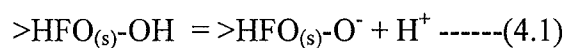
All adsorption data has been modeled using the published geochemical speciation code JCHESS, version 3.0 (van der Lee and De Windt, 2002). JCHESS is an acronym for Chemical Equilibrium with Species and Surfaces. JCHESS can be used to calculate both aqueous phase speciation and also speciation at surfaces using nonelectrostatic or constant capacitance or double layer surface complexation models. In this study, the diffuse double layer model (DDL) is used to describe experimental adsorption data, because it has the capability to model adsorption data using ion exchange, DDL, constant capacitance or nonelectrostatic surface complexation models, includes the EQ/3 database with Dzombak and Morel (1990) parameters for adsorption on HFO, and the database can be easily modified.

Pb adsorption on HFO has been described using a DDL model by Dzombak & Morel (1990). They proposed a 2-site model including a strong and weak site for Pb adsorption onto ferrihydrite. The two types of sites and their exchange capacities (site densities) are given in Table 4.1.

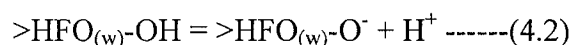
Table 4.1 Exchange capacities of strong and weak sites on ferrihydrite surfaces as proposed by Dzombak and Morel (1990)

Site	Exchange capacity
$>\text{HFO}_{(s)}\text{-OH}$	$0.078 \mu\text{mol/m}^2$
$>\text{HFO}_{(w)}\text{-OH}$	$3.11 \mu\text{mol/m}^2$

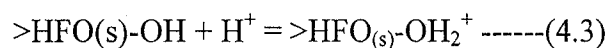
According to the Dzombak and Morel (1990) DDL model, the strong and weak HFO surface hydroxyl groups protonate and deprotonate, producing positively and negatively charged surface sites respectively, according to the following reactions:



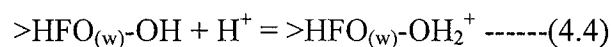
$$\log K = -8.93$$



$$\log K = -8.93$$



$$\log K = 7.29$$



$$\log K = 7.29$$

Dzombak and Morel (1990) also produced a model of Pb adsorption on HFO surfaces, based on literature values from Leckie et al. (1980). According to their model, Pb attaches to both the strong and weak HFO surface sites producing  $>\text{HFO}_{(s)}\text{-OPb}^+$  and  $>\text{HFO}_{(w)}\text{-OPb}^+$  complexes, according to the following reactions:



$$\log K = 4.65$$



$$\log K = 2.03$$

Kovacevic et al. (2000), also suggested that Pb ions are present on the goethite surface as  $\text{PbOH}^+$  species bound to  $\text{MO}^-$  (same as  $>\text{SO}^-$ ) functional groups until pH 3-6 and that the dominant aqueous species from pH 3-6 are singly charged Pb(II) species ( $\text{PbOH}^+$ ). Later, Trivedi et al. (2003) suggested that only bidentate complexes formed at pH 5 and higher on HFO. Their XANES study also supported hypothesis that inner-sphere complexes occur on ferrihydrite and that adsorbed Pb does not retain the hydration sphere during adsorption. In this study, in all experiments, Pb has adsorbed 100% at pH ~5 or lower. Therefore, it is also assumed here Pb adsorbs as a monodentate inner-sphere complex ( $\text{PbOH}^+$ ), as it never requires pH >5 or higher for 100% of the Pb to adsorb on the HFO surfaces.

A subsequent study by Swedlund et al. (2003) suggested that the stability constant for the strong site as proposed by Dzombak and Morel (1990) is much too low to accurately model experimental adsorption data, although the predicted fits do improve somewhat for higher sorbate/sorbent ratios (e.g.,  $10^{-4}$  M Pb, 2 g/L HFO). However, in all cases, the Dzombak and Morel (1990) model significantly underestimated the Pb adsorption edges of Swedlund et al. (2003). Thus, they proposed a much higher log stability constant for adsorption on the strong site: 5.70, compared to the value of 4.65 proposed by Dzombak and Morel (1990). This improved the predicted fits to their Pb adsorption data. However, they still could not fit their measured data very accurately

using the 2-site HFO model, and therefore proposed a third site with very high affinity for Pb, but a low site density ( $0.006 \mu\text{mol}/\text{m}^2$ ), called a type '0' or  $>\text{Fe}_{(0)}\text{OH}$  site. They also changed the stability constants for Pb adsorption on both the weak and strong sites to model their data. They could most accurately fit their data with the addition of the third site. Tables 4.2 and 4.3 show the different types of sites, site densities and stability constants for Pb adsorption proposed by Swedlund et al. (2003).

Table 4.2 Site densities of three sites on ferrihydrite surface as proposed by Swedlund et al. (2003)

Site	Site density
$>\text{HFO}_{(s)}\text{-OH}$	$0.078 \mu\text{mol}/\text{m}^2$
$>\text{HFO}_{(w)}\text{-OH}$	$3.11 \mu\text{mol}/\text{m}^2$
$>\text{HFO}_{(0)}\text{-OH}$	$0.006 \mu\text{mol}/\text{m}^2$

Table 4.3 Comparison between stability constants for Pb surface complexes on ferrihydrite from Dzombak and Morel (1990) and Swedlund et al. (2003)

Surface complexes	Stability constants from Dzombak and Morel (1990)	Stability constants from Swedlund et al. (2003)
$>\text{HFO}_{(s)}\text{-OPb}^+$	4.65	5.33
$>\text{HFO}_{(w)}\text{-OPb}^+$	2.03	1.99
$>\text{HFO}_{(0)}\text{-OPb}^+$	N/A	7.20

As reported by Swedlund et al. (2003), the Dzombak and Morel (1990) DLM parameters for Pb adsorption on HFO similarly do not produce a good fit to the

experimental data set from this study (Figures 4.1-4.5). Although the Swedlund et al. (2003) produces a considerably better fit to the data from this study, it is possible that only a 2-site model could provide a reasonable fit to the data from this study. Therefore, the log stability constant for Pb adsorption on the strong site of HFO was reoptimized to fit the data measured in this study. The remainder of the modeling parameters, including the log stability constant for Pb adsorption on the weak site, the protonation and deprotonation constants for the strong and weak sites, the site densities, and the specific surface area of HFO, were kept as proposed by Dzombak and Morel (1990). All calculations were made using DLM with the JCHESS 3.0 model. For each individual adsorption edge, the log stability constant for the reaction:



was iteratively adjusted to achieve the best possible fit (fits estimated by eye) for a given edge. CO<sub>2</sub> fugacity (380 ppm) was included in the speciation calculation as all the experiments were conducted in open air, although this had a negligible effect on the speciation results. This resulted in the average log stability constants shown in Table 4.4 with fits to the experimental data shown in Figures 4.1-4.5. The resulting average log stability constant for Pb adsorption on the HFO strong site is 5.87, compared to 4.65 as proposed by Dzombak and Morel (1990) and 5.70 proposed by Swedlund et al. (2003).

Table 4.4 Best-fit log stability constants for Pb adsorption on the HFO strong site for each of adsorption experiment

Pb <sup>2+</sup> conc. in M	Electrolyte (NaNO <sub>3</sub> ) conc. in M	logK >HFO <sub>(s)</sub> -OH
6.8*10 <sup>-7</sup>	0.1	6.10
6*10 <sup>-8</sup>	0.001	6.10
10 <sup>-6</sup>	0.1	5.60
10 <sup>-4</sup>	0.01	5.45
10 <sup>-5</sup>	0.01	6.10
AVERAGE:		5.87

Figures 4.1-4.5 compare the fits produced by the Dzombak and Morel (1990) and Swedlund et al. (2003) models to the fits produced with the adjusted stability constant for Pb adsorption on the HFO strong site from this study. It is clearly evident that the individually modified stability constants produce drastically improved fits to the experimental data from this study compared to the unchanged Dzombak and Morel (1990) model. The Swedlund et al. (2003) 3-site model also fits the datasets of this study accurately, except for the 10<sup>-6</sup> M Pb dataset. However, the proposed stability constants of this study can fit the data sets with similar accuracy using only a 2-site model. One can always produce a “perfect” model fit if the number of adjustable parameters is increased enough. However, this will limit the usefulness, and likely, the general applicability of the model also. The best model is the one that can reproduce the data with the smallest number of adjustable parameters. Therefore, in this study a 2-site model is used for fitting

the experimental dataset. Table 4.5 shows a comparison among the stability constants used to describe Pb adsorption on HFO including those from this study.

The predicted fits are reasonable, thus, it can be concluded that the adsorption of Pb can be very well predicted using a two site model as proposed by Dzombak and Morel with modification of only one of the stability constants.

Table 4.5 A comparison of stability constants used to describe Pb adsorption on HFO

Surface complexes	Stability constants from Dzombak and Morel (1990)	Stability constants from Swedlund et al. (2003)	Stability constants from this study
$>\text{HFO}_{(s)}\text{-OPb}^+$	4.65	5.33	5.87
$>\text{HFO}_{(w)}\text{-OPb}^+$	2.03	1.99	2.03
$>\text{HFO}_{(0)}\text{-OPb}^+$	N/A	7.20	N/A

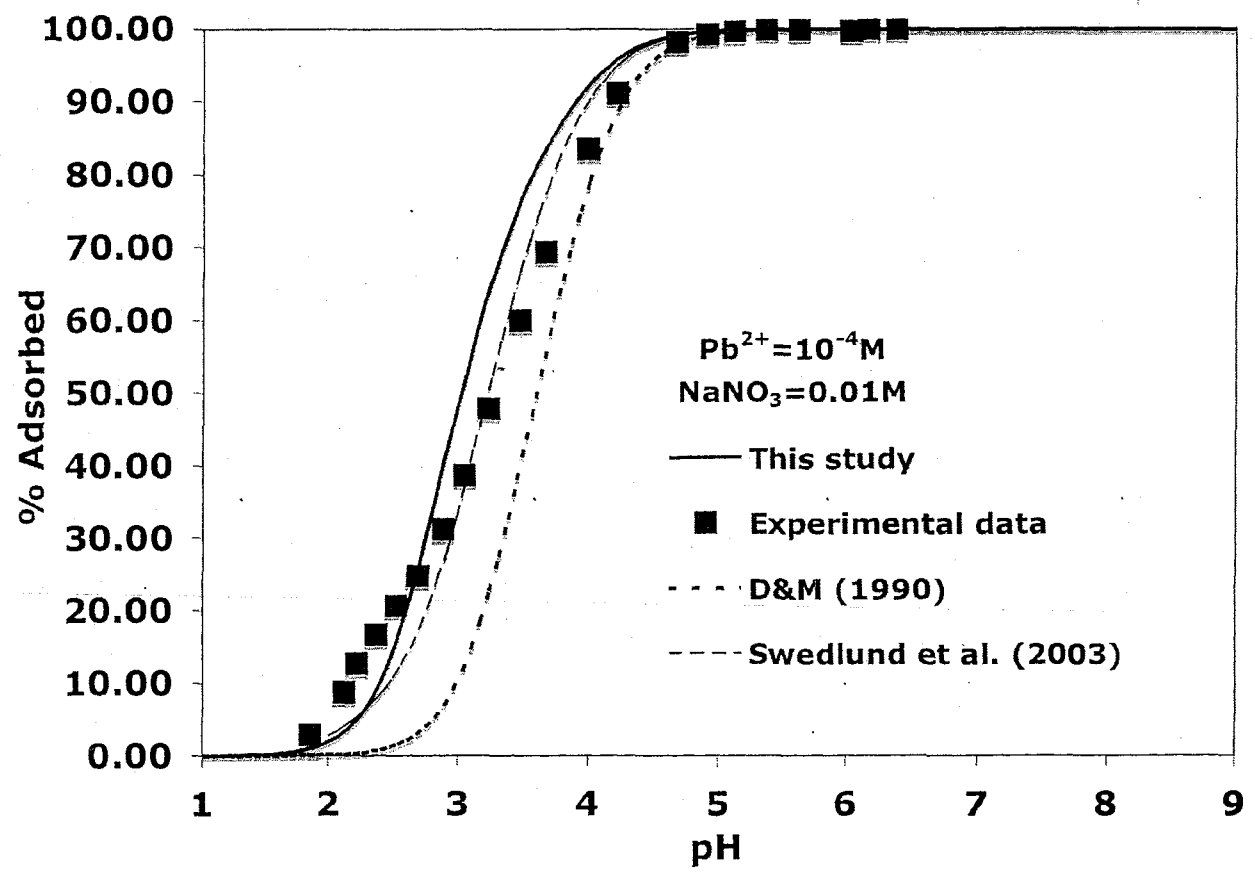


Figure 4.1. Comparison of fits to experimental data ( $10^{-4} M Pb$ ,  $0.01 M NaNO_3$ ) produced using the parameters from the DLM proposed by Dzombak and Morel (1990) and Swedlund et al, (2003) and using the modified average stability constant for Pb adsorption on the strong site from this study.

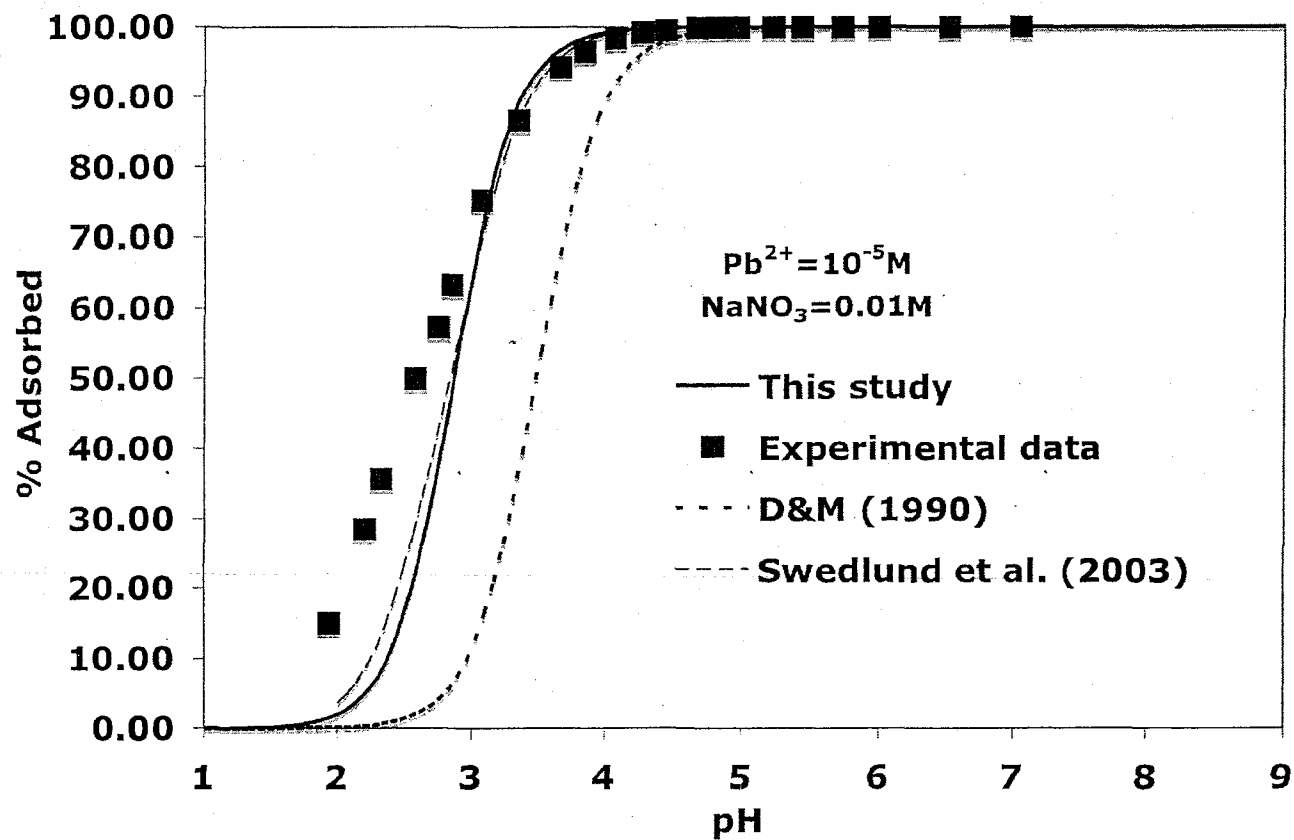


Figure 4.2. Comparison of fits to experimental data ( $10^{-5}$  M Pb, 0.01 M  $NaNO_3$ ) produced using the parameters from the DLM proposed by Dzombak and Morel (1990) and Swedlund et al. (2003) and using the modified average stability constant for Pb adsorption on the strong site from this study.

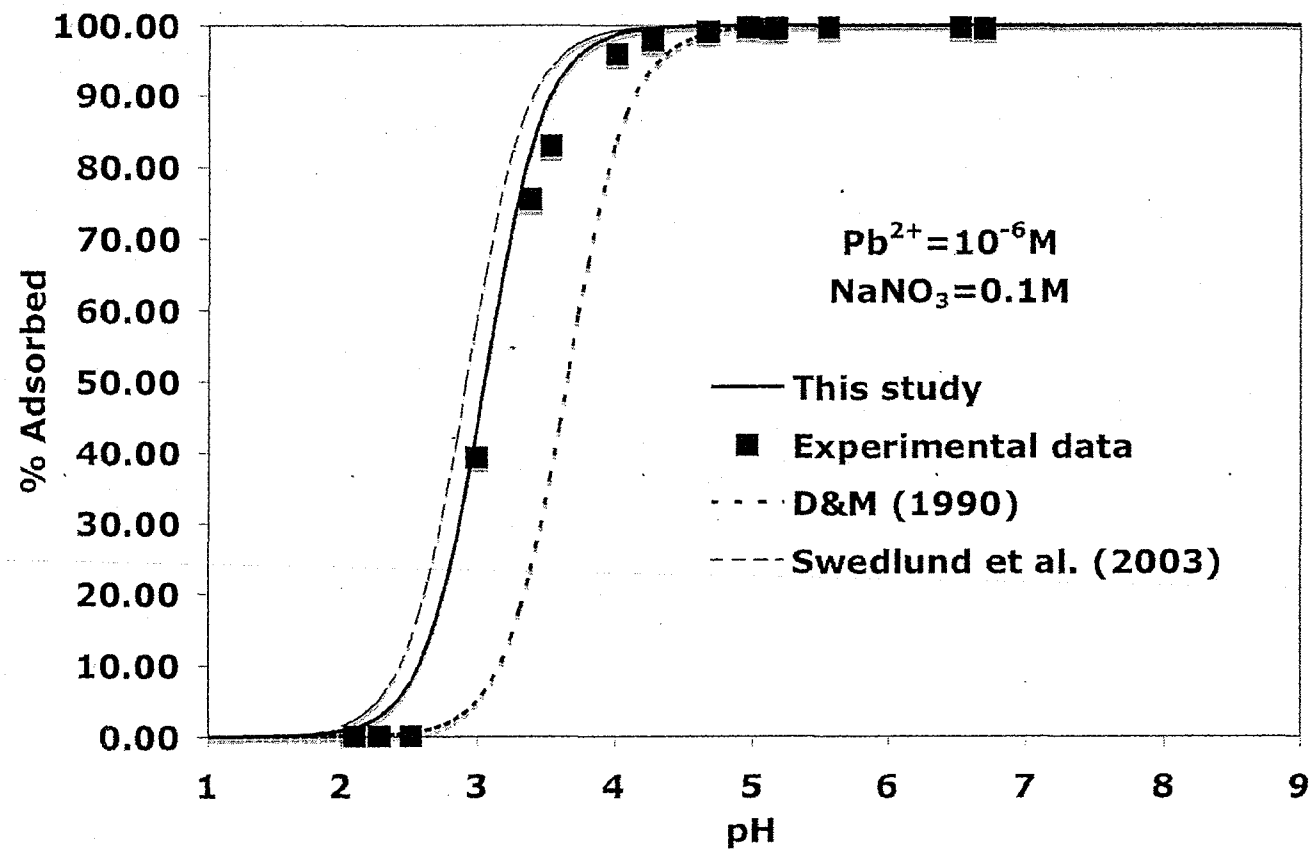


Figure 4.3. Comparison of fits to experimental data ( $10^{-6}$  M Pb, 0.1 M  $\text{NaNO}_3$ ) produced using the parameters from the DLM proposed by Dzombak and Morel (1990) and Swedlund et al. (2003) and using the modified average stability constant for Pb adsorption on the strong site from this study.

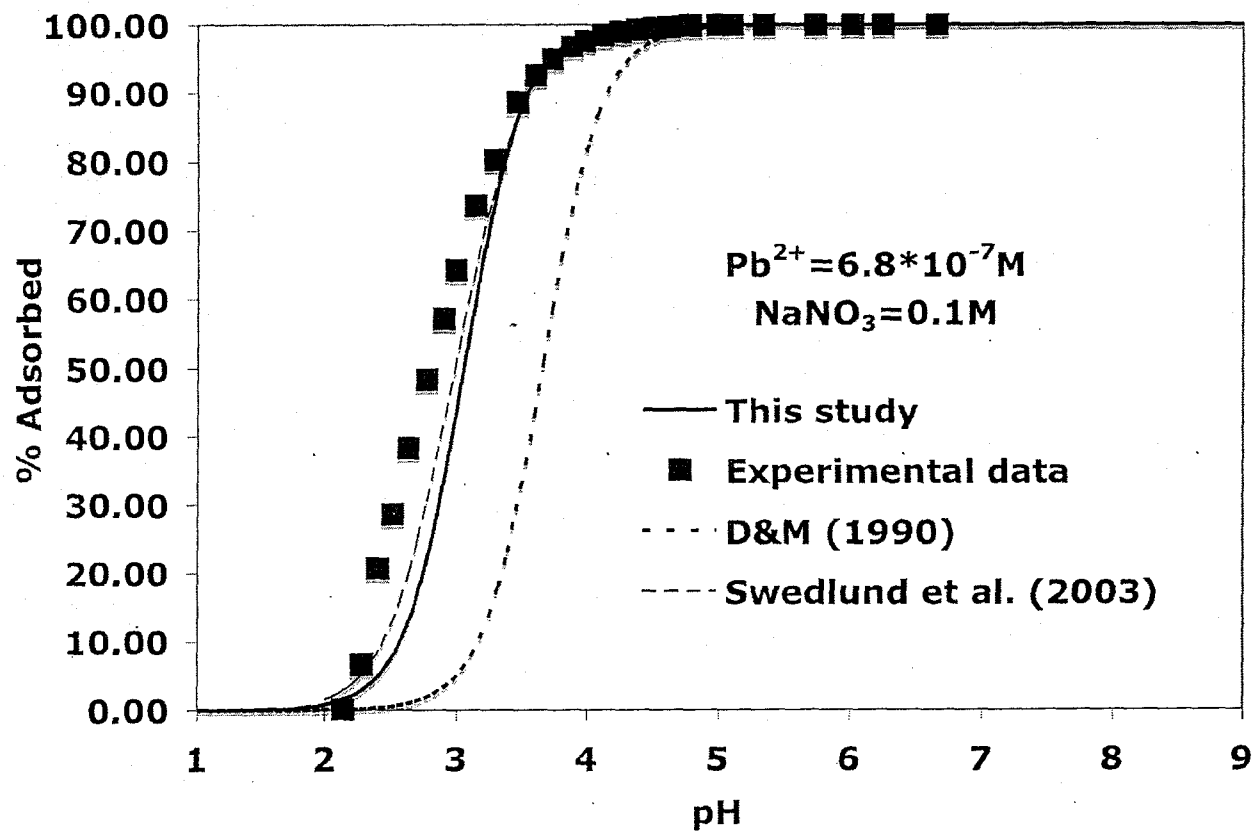


Figure 4.4. Comparison of fits to experimental data ( $6.8 \cdot 10^{-7} M Pb$ ,  $0.1 M NaNO_3$ ) produced using the parameters from the DLM proposed by Dzombak and Morel (1990) and Swedlund et al. (2003) and using the modified average stability constant for Pb adsorption on the strong site from this study.

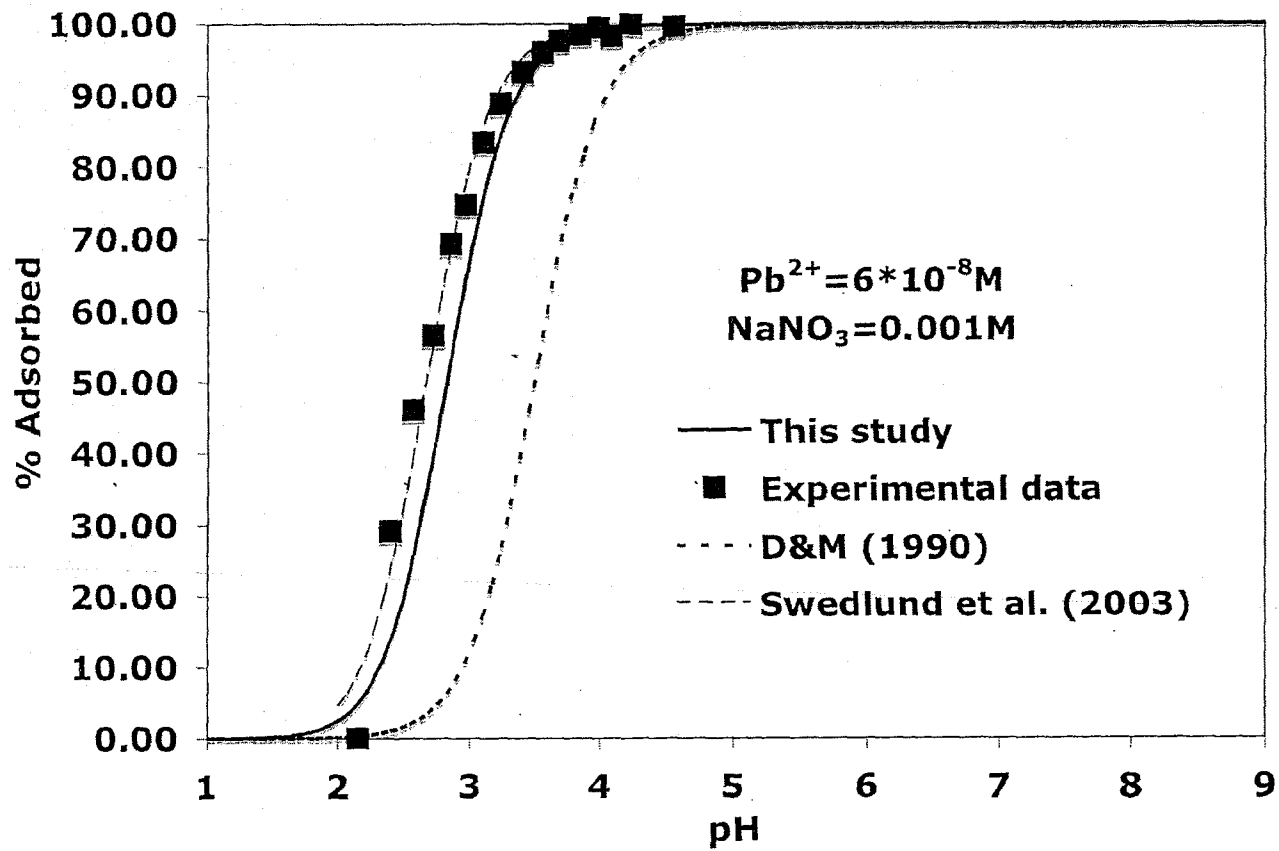


Figure 4.5. Comparison of fits to experimental data ( $6 \cdot 10^{-8} M Pb$ ,  $0.001 M NaNO_3$ ) produced using the parameters from the DLM proposed by Dzombak and Morel (1990) and Swedlund et al. (2003) and using the modified average stability constant for Pb adsorption on the strong site from this study.

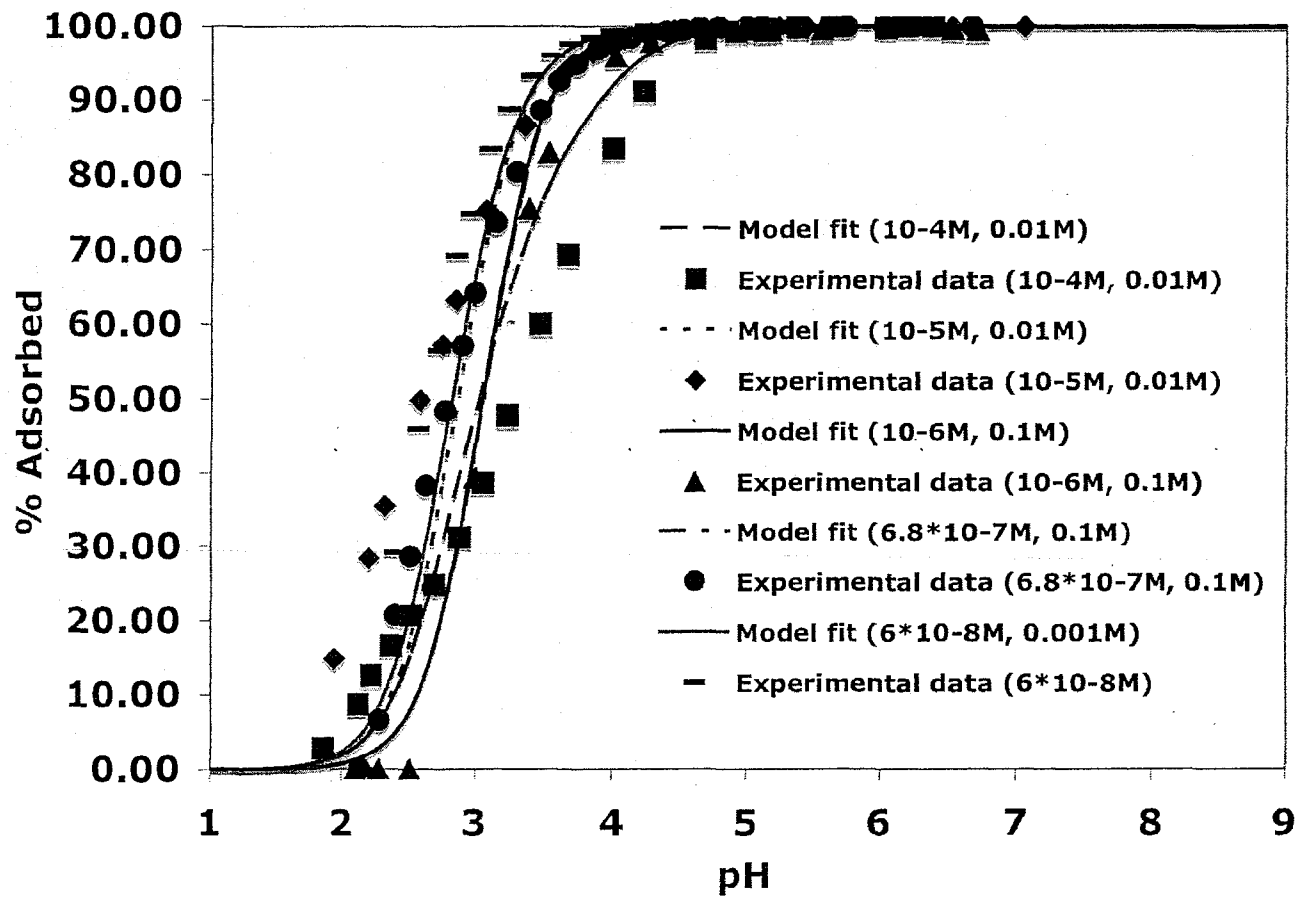


Figure 4.6. Model fits using the average stability constant for Pb adsorption on the strong site for the 2-site model derived in this study for all experiments.

### Adsorption of Pb on silica

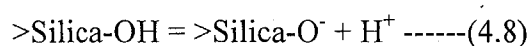
Adsorption of Pb on silica has been studied both macroscopically and spectroscopically (Chen et al., 2005; Elzinga and Sparks, 2002). In contrast, this study only assesses macroscopic data collected from batch experiments. Chen et al. (2005) studied the Pb adsorption on Min-U-Sil 5, with a surface area of  $4.0 \text{ m}^2/\text{g}$ . They conducted a series of batch experiments with different electrolytes of varying concentration, keeping Pb concentrations constant ( $10^{-5} \text{ M}$ ). Their experiments showed mixed results for electrolyte strength dependence of Pb adsorption. First of all, results of their study showed that there is no electrolyte strength dependence on Pb adsorption on silica surfaces when  $\text{NaClO}_4$  or  $\text{NaNO}_3$  are used as background electrolytes, even changing the strength from 0.1 to 0.01 M. They also conducted a batch experiment with 0.5 M  $\text{NaClO}_4$ , and even that high background electrolyte concentration did not affect Pb adsorption. In contrast, when NaCl was used as background electrolyte, with a concentration varying from 0.1 to 0.01 M, very little dependence of Pb adsorption on ionic strength was, however, when the NaCl concentration was increased from 0.01 to 1 M, the adsorption edge shifted towards higher pH, indicating less Pb adsorption.

In contrast, this study shows a strong ionic strength dependence on Pb adsorption on silica for ionic strengths of 0.01 to 0.1 M set with  $\text{NaNO}_3$ . Specifically, the adsorption edges shift towards higher pH with increased ionic strength, indicating a decrease in adsorption with increasing strength of the electrolyte. For example, 54% of the Pb was adsorbed at pH~6.8 for 0.1 M compared to pH~6.2 for 0.01 M. Therefore, in this study formation of a monodentate complex at silica surface is proposed, in contrast to the inner-sphere poly-nuclear Pb complexes as proposed by Elzinga and Sparks, (2002) according

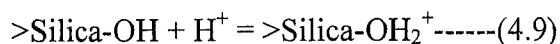
to their XAS study, which was also subsequently supported by Chen et al. (2005) by their XAS study.

There are several possible reasons for the discrepancy in ionic strength dependence and inferred form of the adsorbed Pb complex in this study compared to the previous studies of Chen et al. (2005) and Elzinga and Sparks (2002). First, in both of these studies, they have used very high sorbate/sorbent ratio. For example, Chen et al. (2005) used 100 g/L of silica compared to only 2 g/L used for this study. The silica of this study has a higher surface area (9.4 m<sup>2</sup>/g) than that used by Chen et al. (2005), and a much lower surface area than that of Elzinga and Sparks (2002), who used a totally different type of silica with very high (220 m<sup>2</sup>/g) surface area. This might change the nature of surface complexes that are produced on the silica surfaces. Because a much lower sorbate/sorbent ratio is used in this study, mononuclear complexes are more likely to form than the polynuclear complexes observed in the previous studies.

The DLM model cannot readily distinguish between inner-sphere and outer-sphere complexes, as can, for example, the TLM. For simplicity, in this study, adsorption data of Pb on silica has been modeled based on the one site DDL model as proposed by Sverjensky and Sahai (1996). They proposed a single >Silica-OH site with a site density (exchange capacity) of 16.6 μmol/m<sup>2</sup>. Based on correlation algorithms using the dielectric constant of silica and Pauling bond strength analyses, they suggest that this silica site will deprotonate or protonate according to the following reactions:



$$\log K = -8.1$$



$$\log K = -1.1$$

In this study, it is assumed that Pb can attach to the single surface site producing a monodentate Pb aqueous complex  $>\text{Silica-OPb}^+$  according to



Using the JCHESS speciation code with the appropriate conditions to describe each experimentally determined edge and using the site density, protonation and deprotonation stability constants from Sverjensky and Sahai (1996) and the measured surface area of silica (9.4 m<sup>2</sup>/g), data for three adsorption edges were used to fit for the Pb adsorption stability constant (by eye), resulting in the best-fit constants shown in Table 4.6. The fit to the experimental data produced by the average best-fit stability constant (-2.46) is shown in Figures 4.7-4.10.

Table 4.6 Best-fit log Ks for Pb adsorption on silica for each adsorption edge measured in this study

Pb <sup>2+</sup> conc. in M	Electrolyte (NaNO <sub>3</sub> ) conc. in M	Log K >Silica-OPb <sup>+</sup>
10 <sup>-5</sup>	0.1	-2.6
10 <sup>-5</sup>	0.01	-2.5
10 <sup>-6</sup>	0.01	-2.3

Excellent fits to the experimental data can be achieved using the single site model as proposed by Sverjensky and Sahai (1996), particularly for data measured with 10<sup>-5</sup> M Pb and electrolyte concentrations of 0.1 or 0.01 M (Figures 4.7-4.9). The average log K,

produces reasonably good agreement with the experimental data, slightly underestimating the 0.01 M datasets and slightly overestimating the 0.1 M dataset (Figures 4.7-4.9). A more rigorous model result could have been achieved if this study had one or two more experimental datasets. An experiment with  $10^{-4}$  M Pb in 0.01 M NaNO<sub>3</sub> was also conducted, but the higher concentration of Pb, together with the very low surface area of silica and low affinity of silica sites for Pb, likely triggered precipitation of Pb on silica surfaces (observed as a near vertical adsorption edge, close to the pH where precipitation of the mineral hydrocerrusite would be expected in aqueous solution). Therefore, the  $10^{-4}$  M data were not modeled. However, based on modeling two different Pb concentrations with two different electrolyte strengths, it appears that Pb adsorption on silica can be modeled satisfactorily using a simple one-site model, as proposed by Sverjensky and Sahai (1996).

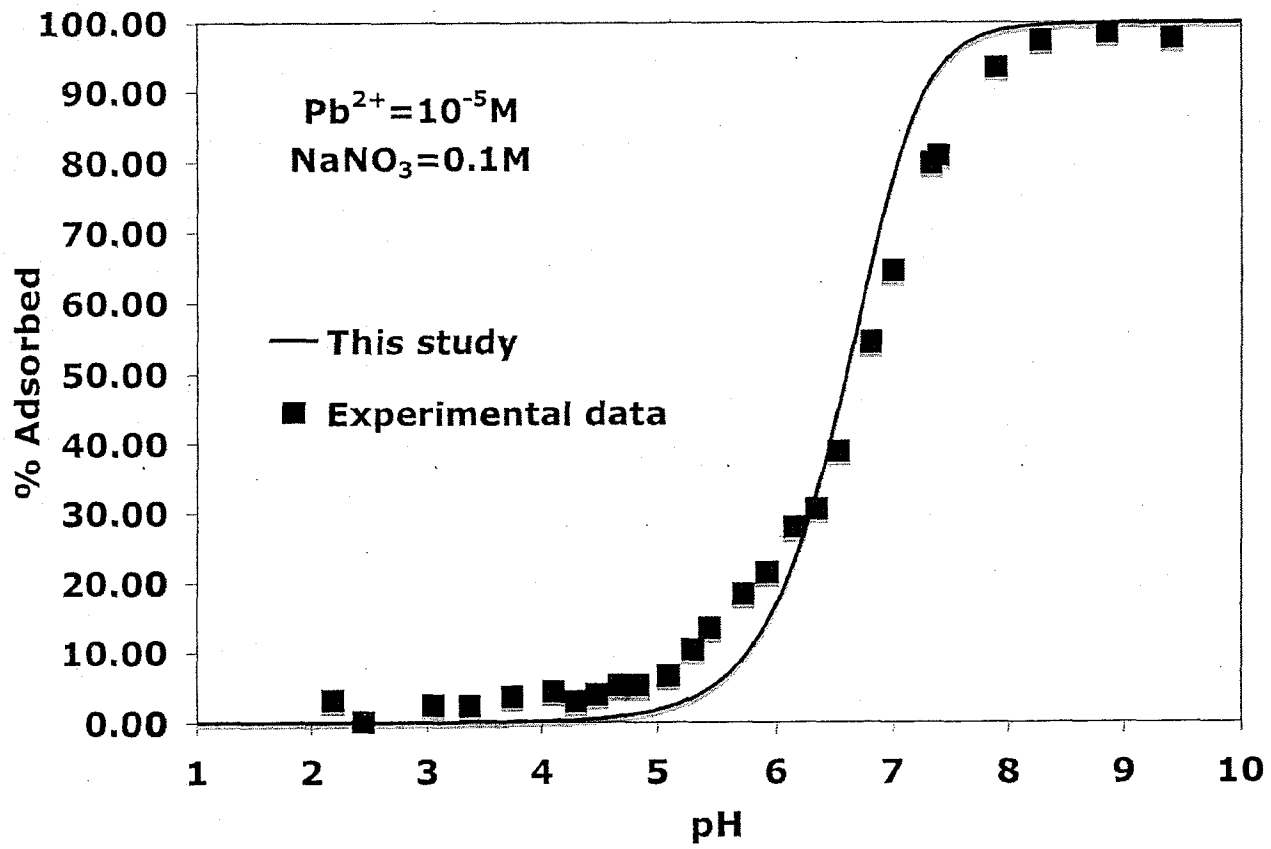


Figure 4.7. Experimental data (squares) for 10<sup>-5</sup> M Pb in 0.1 M NaNO<sub>3</sub> and best DLM fit achieved by adjusting the log K for Pb adsorption on a single silica surface site.

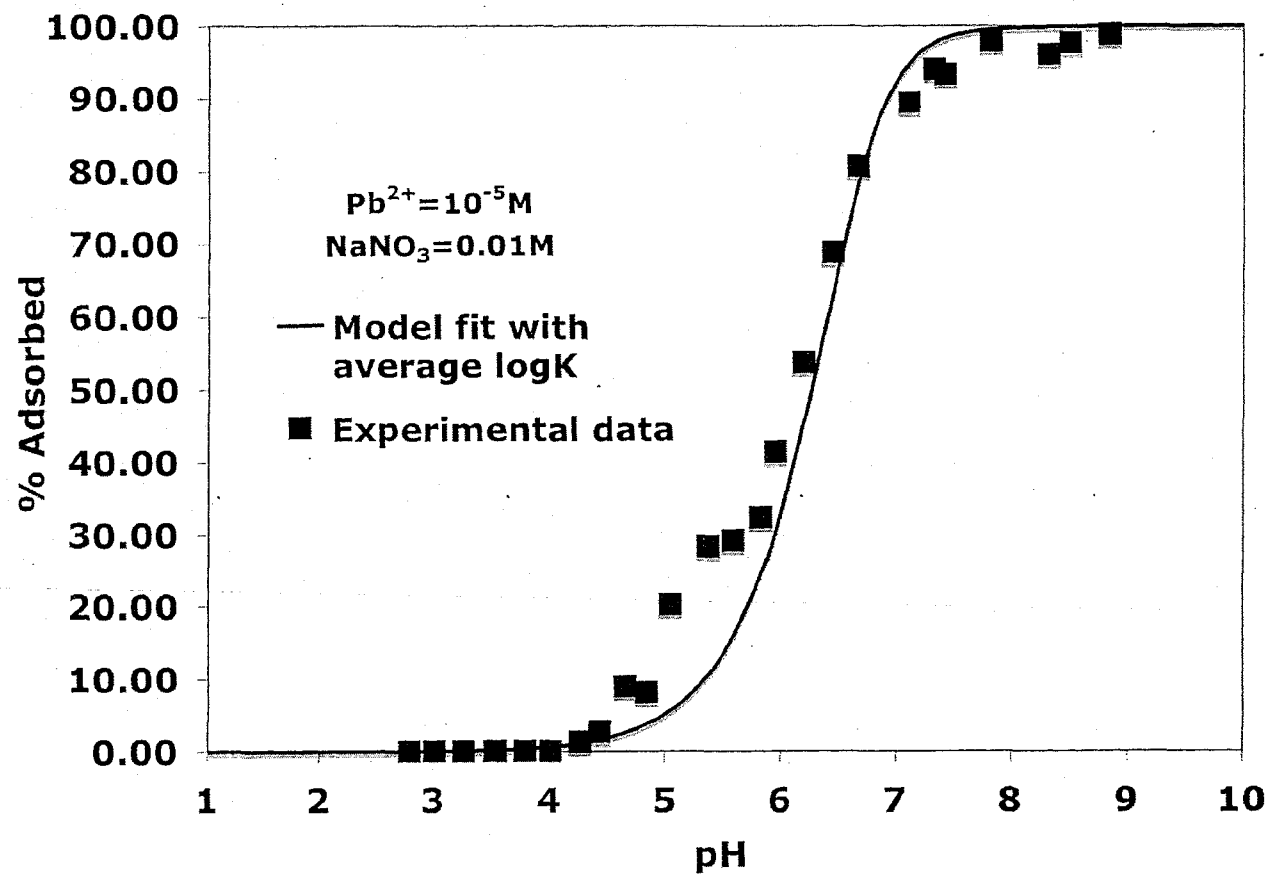


Figure 4.8. Experimental data (squares) for  $10^{-5} \text{ M}$  Pb in  $0.01 \text{ M}$   $\text{NaNO}_3$  and best DLM fit achieved by adjusting the log K for Pb adsorption on a single silica surface site.

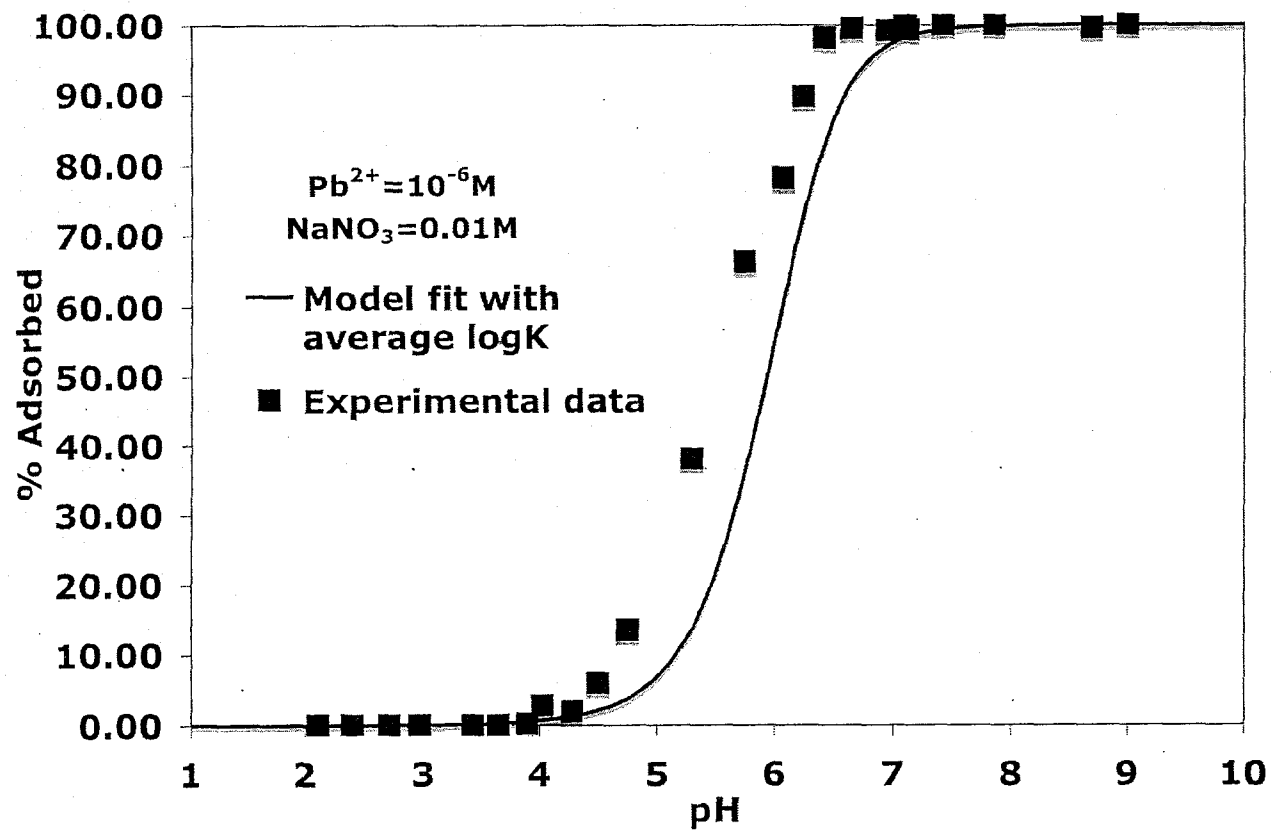


Figure 4.9. Experimental data (squares) for 10<sup>-6</sup> M Pb in 0.01M NaNO<sub>3</sub> and best DLM fit achieved by adjusting the log K for Pb adsorption on a single silica surface site.

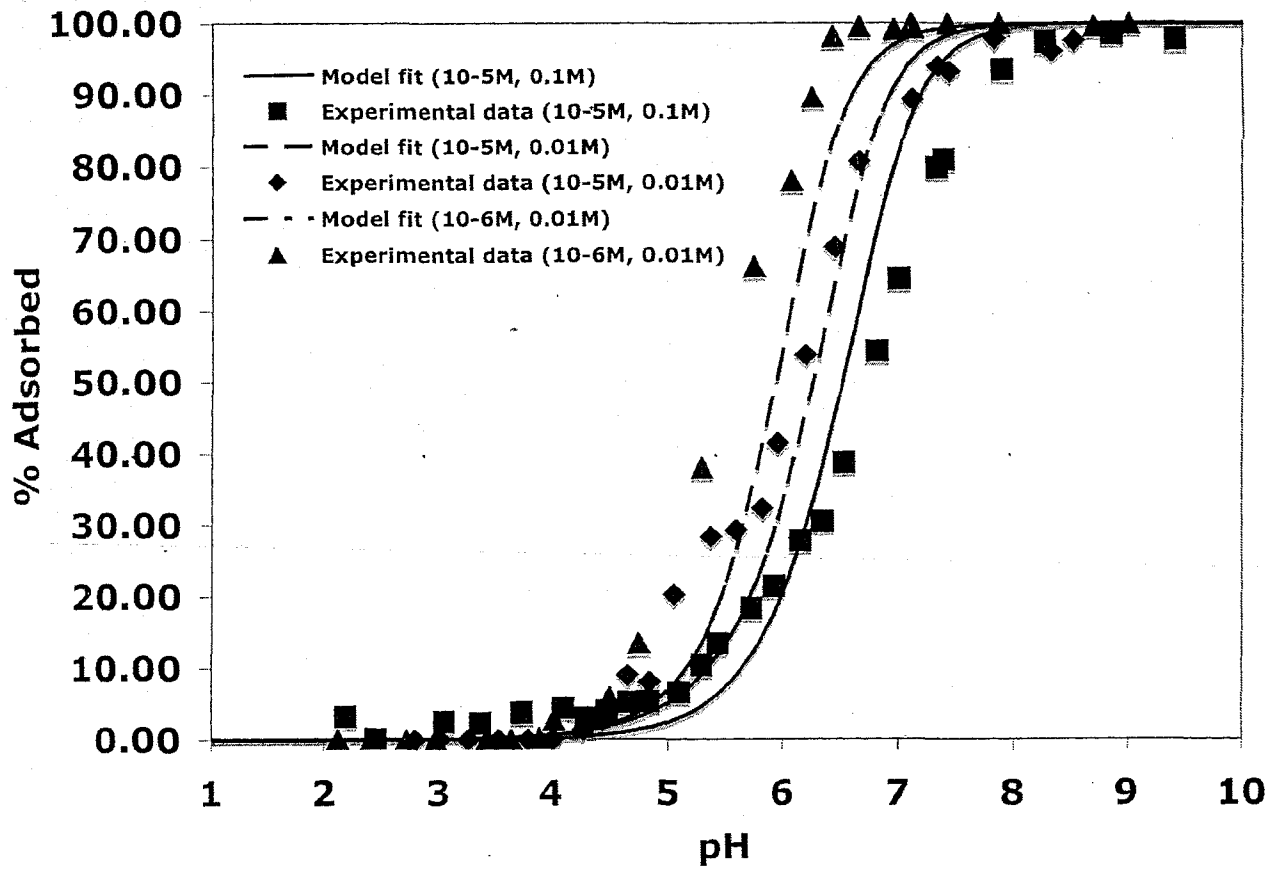


Figure 4.10. Model fits for all three experiments using the average log K for Pb adsorption derived from the three edges.

### Adsorption of Pb on KGa-1B

There is generally agreement in the literature that the surface charge of kaolinite results from both permanent or pH-independent and variable or pH-dependent charges (Sposito, 1984; Schulthess and Huang, 1990; Brady et al., 1996; Huertas et al., 1998; Angove et al., 1998; Ikhsan et al., 1999; Peacock and Sherman, 2005; Heidmann et al., 2005). Based on titration data and crystallographic data, many workers have suggested that the kaolinite surface sites contain reactive hydroxyl groups, possibly including both aluminol and silanol groups, present on edge surfaces of kaolinite. The silanol group ( $>\text{SiOH}$ ) is presumed to only deprotonate and contribute negative surface charge ( $>\text{SiO}^-$ ), but the aluminol group ( $>\text{AlOH}$ ) is presumed to protonate and deprotonate under environmentally relevant pH conditions, to produce both positive and negative charges, from  $>\text{AlOH}_2^+$  and  $>\text{AlO}^-$  respectively (Huang, 1971; Huang and Stumm, 1973; Carroll-Webb and Walthar, 1988). The other type of site for sorption is a cation exchange site, which is present on the basal planes of kaolinite. These types of sites have permanent negative charge due to isomorphic substitution of  $\text{Si}^{4+}$  by  $\text{Al}^{3+}$  in the tetrahedral sheets or isomorphic substitution of divalent cations for  $\text{Al}^{3+}$  in octahedral sheets (Heidmann et al., 2005). Heidmann et al. (2005) assumed that the edge surface area of KGa-2 was only  $4.76 \text{ m}^2/\text{g}$ , which is 20% of the total available surface area, in contrast to  $9.52 \text{ m}^2/\text{g}$  for face surface area (40%) as measured from BET analysis. They also suggested that due to the very small amount of isomorphic substitution in kaolinite, the cation exchange capacity (CEC) is very low for kaolinite, typically from 0.02-0.15 mol/kg. Schroth and Sposito (1997) similarly found a low CEC for kaolinite (0.0136 mol/kg). This value of CEC of kaolinite is very low compared to 2:1 clays (Newman and Brown, 1987; Huertas

et al., 1998). Moreover, the origin of this permanent structural charge, which is present on kaolinite, a 1:1 clay, is not clear (Brady et al., 1996; Schroth and Sposito, 1997). Some workers (Ferris and Jepson, 1975; Lim et al., 1980) have proposed that this permanent charge results from alumino-silicate gel coatings or smectite contamination in kaolinite.

Because kaolinite is a 1:1 type of clay mineral, and the permanent structural charge is very low compared to 2:1 type clay (e.g. montmorillonite has CEC of 80-120 cmol/kg compared to only 3-10 cmol/kg for kaolinite) (Brady, 1984), and due to the uncertainty regarding the formation of structural charge on 1:1 clay minerals (Ferris and Jepson, 1975; Lim et al., 1980; Brady et al., 1996; Schroth and Sposito, 1997), in this study the DDL model proposed by Benyahya and Garnier (1999), which does not include a cation exchange site, is used to model the experimentally derived adsorption edges. Moreover, as pointed out by Srivastava et al. (2005), Cu and Pb hydrolyze very easily, thus, these divalent cations interact more readily with hydroxyl groups. As a result, these cations (Cu and Pb) would be adsorbed more compared to cations like Zn and Cd, which do not readily hydrolyze. So, cations like Zn and Cd would interact only with exchange sites at low pH values, whereas even at low pH, Cu and Pb would interact mostly with variable charge hydroxyl sites. Furthermore, KGa-1B (used for this study) also does not contain any significant quantity of phyllosilicate impurities (Pruett and Webb (1993), so cation exchange sites are expected to be of minimal importance. Subsequent workers (Payne et al., 2004; Hizal and Apak, 2006) have also modeled metal adsorption data for kaolinite without using an exchange site.

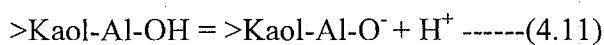
Adsorption of Pb on kaolinite is modeled in this study using a DDLM based on the model proposed by Benyahya and Garnier (1999). They used China Clay Supreme from

U.K., having surface area of 15 m<sup>2</sup>/g, which is similar to the surface area of KGa-1B (13.6 m<sup>2</sup>/g) used for this study. According to their model, kaolinite has two different types of variable charge sites, namely silanol and aluminol sites. Positively charged silanol groups were not included in the model, as according to previous workers (Huang, 1971; Huang and Stumm, 1973; Carroll-Webb and Walthar, 1988) >SiOH groups only deprotonate at environmentally relevant pH conditions. Each of type of surface hydroxyl site can take up Pb to form complexes. The exchange capacities for these two sites, as proposed by Benyahya and Garnier (1999), based on their titration data, are shown in Table 4.7.

Table 4.7 Exchange capacities for two site kaolinite surface, as proposed by Benyahya and Garnier (1999)

Site	Exchange capacity
>Kaolinite-(Si)-OH	3.57 μmol/m <sup>2</sup>
>Kaolinite-(Al)-OH	1.96 μmol/m <sup>2</sup>

Based on potentiometric surface titration data, Benyahya and Garnier (1999) suggest that the silanol and aluminol deprotonate and protonate according to the following reactions:



$$\log K = -7.68$$



$$\log K = 6.80$$



$$\log K = -3.52$$

Benyahya and Garnier (1999) optimized stability constants for the adsorption of divalent cations including Mn, Co, Cd and Zn on kaolinite. In this study, the sites, site densities, and protonation/deprotonation stability constants proposed by Benyahya and Garnier (1999) were used, together with the measured adsorption edges, to optimize stability constants for Pb adsorption on kaolinite. These two sites were assumed to adsorb Pb and form monodentate surface complexes according to the following reactions:



and



The log stability constants for reactions 4.14 and 4.15 were optimized (by eye using JCHESS) for each experimental adsorption edge measured in this study. The resulting stability constants were averaged, producing log stability constants of -2.33 and -1.0 (consistent for all sorbate/sorbent ratios), for reactions 4.14 and 4.15, respectively (Table 4.8).

Table 4.8 Best-fit log Ks for Pb adsorption on kaolinite based on a 2-site DDLM

Pb <sup>2+</sup> conc. in M	Electrolyte (NaNO <sub>3</sub> ) conc. in M	Log K >Kaol-Si-OPb <sup>+</sup>	Log K >Kaol-Al-OPb <sup>+</sup>
10 <sup>-5</sup>	0.1	-2.5	-1.0
10 <sup>-5</sup>	0.01	-2.5	-1.0
10 <sup>-6</sup>	0.01	-2.0	-1.0
AVERAGE		-2.33	-1.0

This approach produces a very good fit to the 10<sup>-5</sup> M Pb at ionic strengths of 0.1 or 0.01 M (Figures 4.11-4.13). For data measured with 10<sup>-6</sup> M Pb, a good fit cannot be produced for pH<4, but the fit is reasonable at higher pH (Figure 4.13). The average log Ks from the three edges produces reasonable fits to all three datasets, with an underestimate of adsorption for the 10<sup>-6</sup> M Pb data and an overestimate of adsorption for the 10<sup>-5</sup> M Pb data (Figure 4.14).

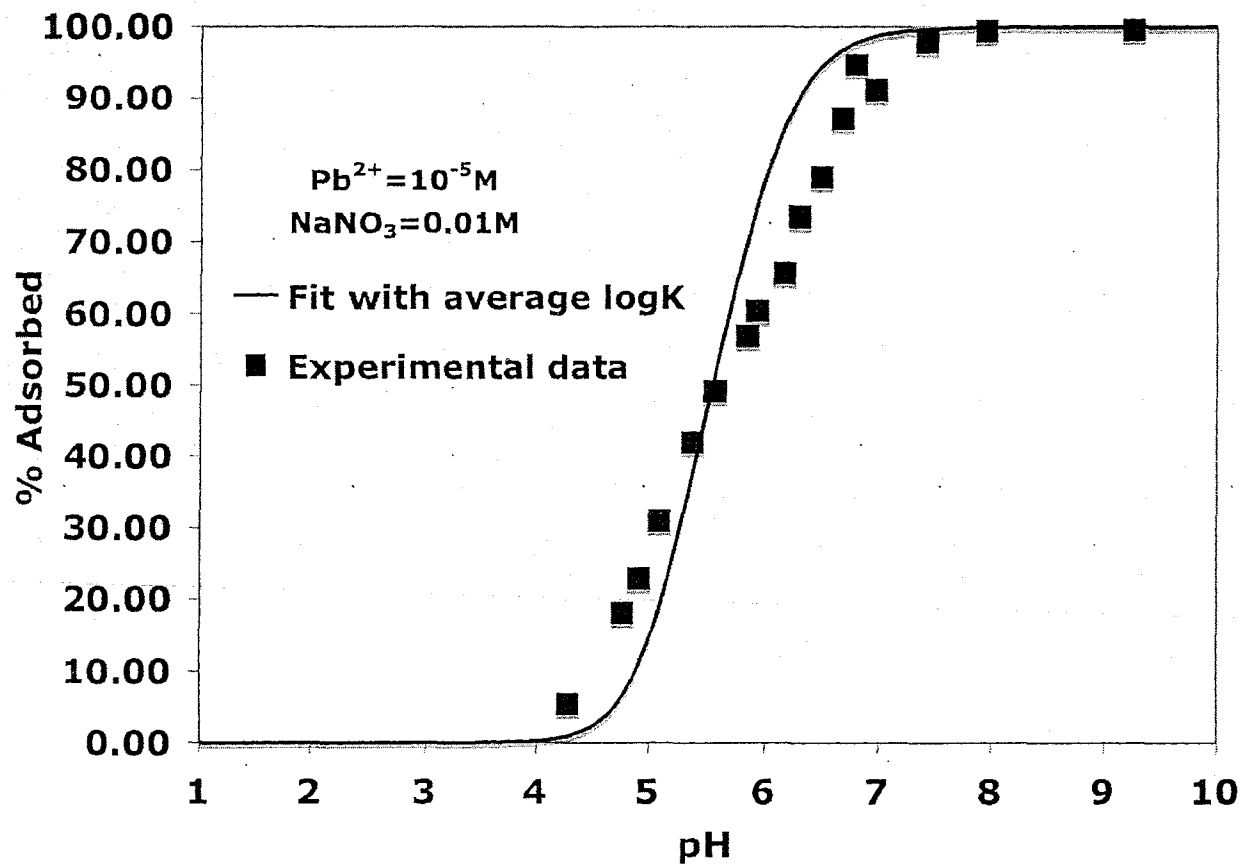


Figure 4.11. Experimental data (squares) for  $10^{-5} M$  Pb in  $0.01 M$   $NaNO_3$  and best DLM fit achieved by adjusting the log Ks for Pb adsorption on a two surface site model of kaolinite.

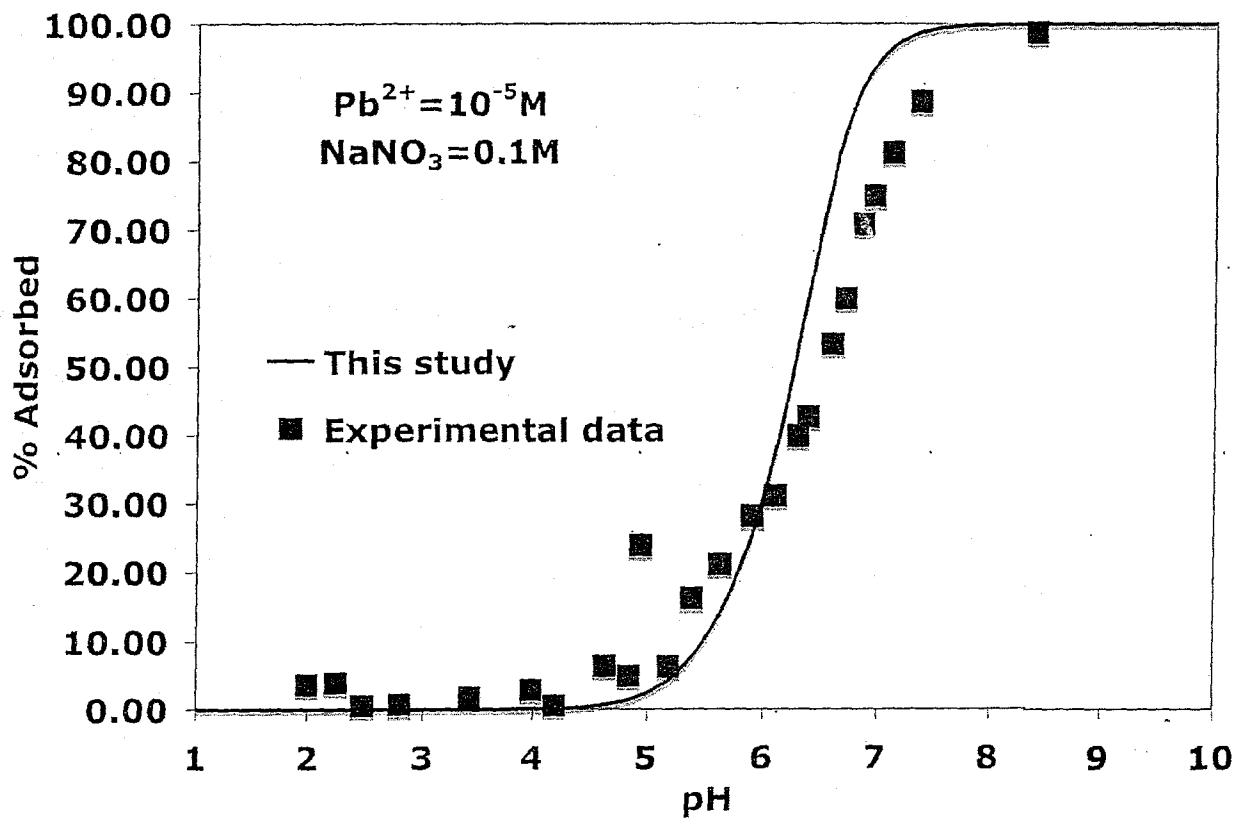


Figure 4.12. Experimental data (squares) for 10<sup>-5</sup> M Pb in 0.1M NaNO<sub>3</sub> and best DLM fit achieved by adjusting the log Ks for Pb adsorption on a two surface site model of kaolinite.

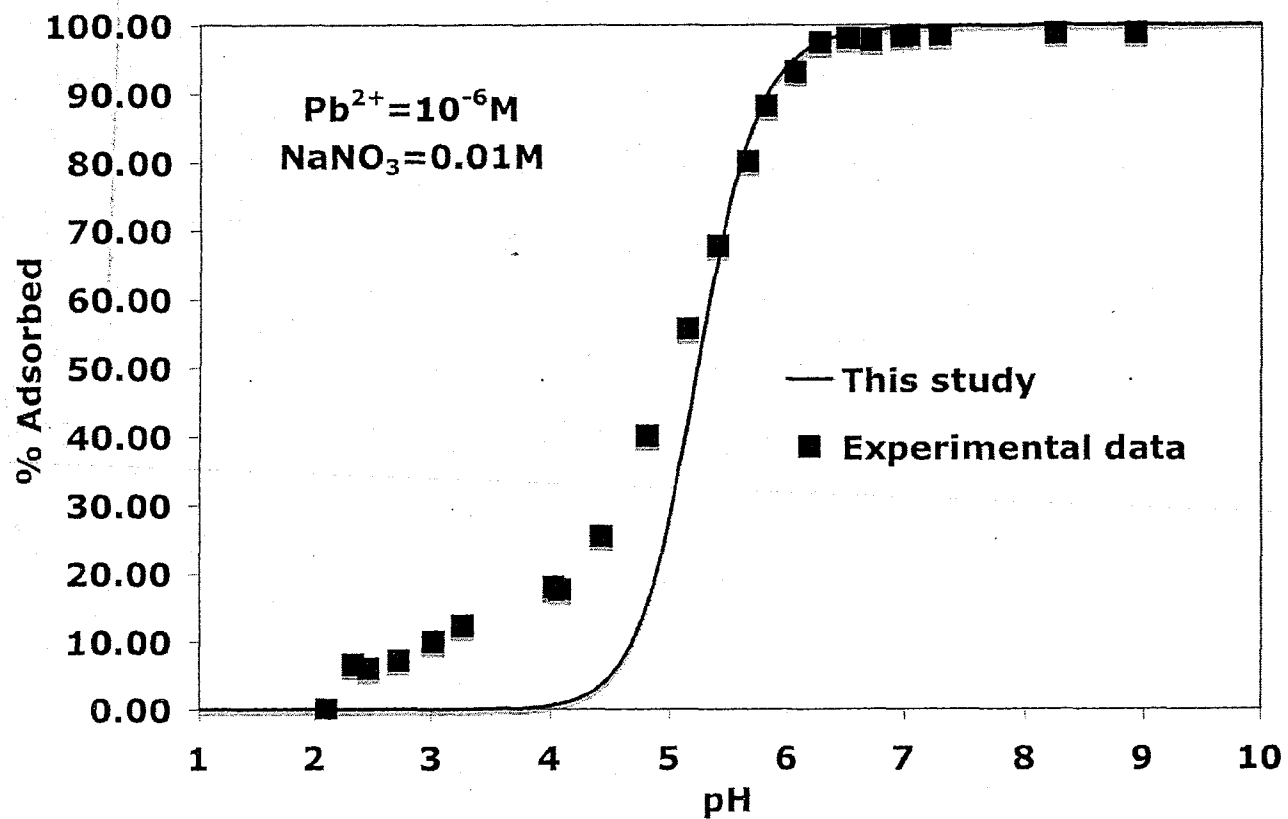


Figure 4.13. Experimental data (squares) for 10<sup>-6</sup> M Pb in 0.01 M NaNO<sub>3</sub> and best DLM fit achieved by adjusting the log Ks for Pb adsorption on a two surface site model of kaolinite.

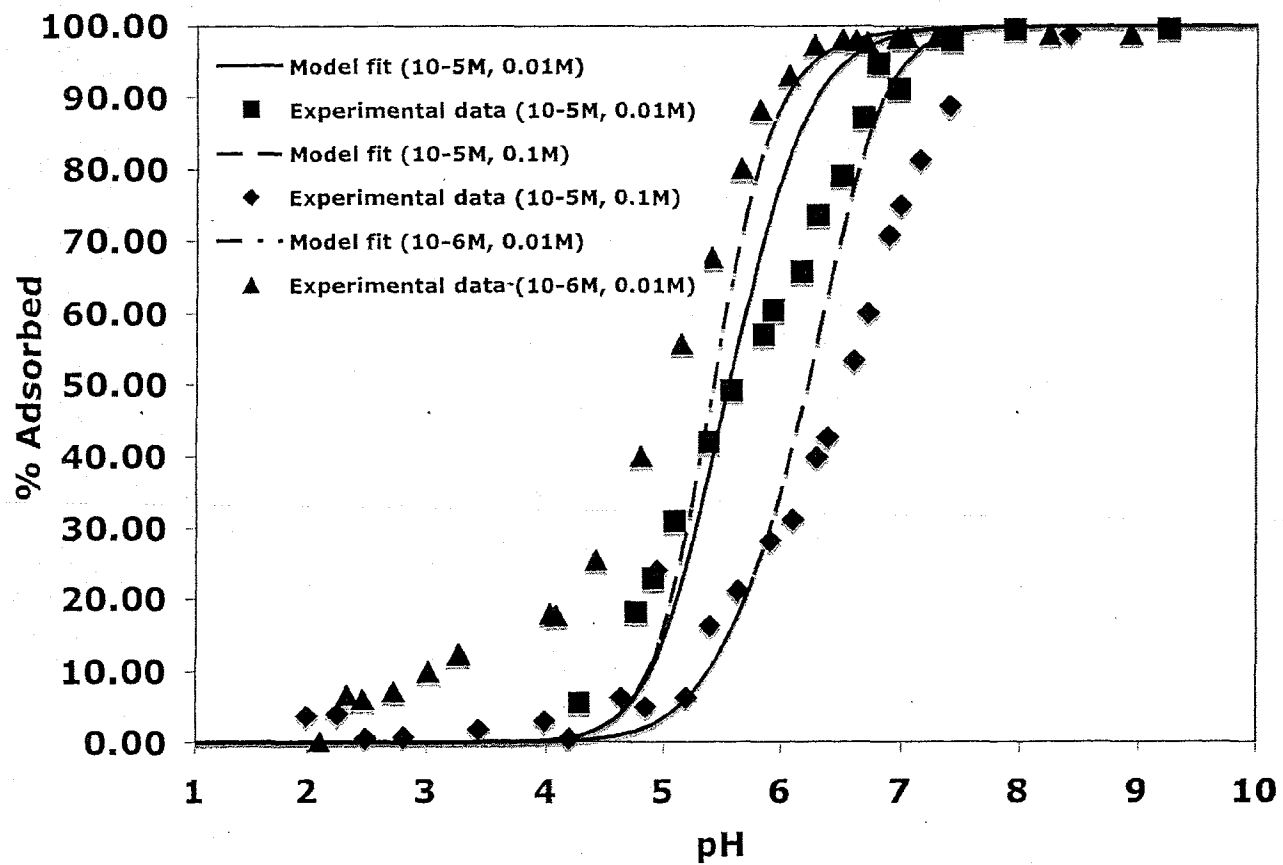


Figure 4.14. Model fits for all three experiments using the average log K for Pb adsorption derived from the three edges.

## Binary systems

As discussed in chapter 1, Davis et al. (1998) proposed two different methods, namely the component additivity and generalized composite models, for using a SCM approach for characterizing adsorption on environmental sorbents of mixed mineralogy. The component additivity approach assumes that the adsorption on complex mineral assemblages can be predicted using adsorption data derived from single pure mineral or organic phases. Thus, according to this model, if data are available for all the pure single phases in a mixture, and the abundances and surface areas of the minerals in the mixture are known, then a simple speciation calculation, not accounting for mineral-mineral interactions, should accurately predict Pb sorption on the mixed mineral assemblage. Experimental data has been derived in this study for binary assemblages of silica:HFO, kaolinite:HFO and kaolinite:silica as well as for ternary assemblages of various proportions. A goal of this study is to determine whether the component additivity can adequately predict these experimental data using well controlled mineral assemblages.

### HFO+silica system

Six systems with different silica to HFO ratios were modeled using the estimated average stability constants derived for each of the single solid systems. The silica to HFO ratios used were 1:1, 5:1, 10:1, 50:1, 100:1 and 500:1. The modeling was done using JCHESS 3.0 by incorporating the newly derived DDLM stability constants for Pb adsorption on HFO and silica into the JCHESS database. All binary experiments were conducted using 0.01 M NaNO<sub>3</sub> electrolyte in 10<sup>-5</sup> M Pb.

Table 4.9 Stability constants for Pb adsorption used for modeling of binary mixtures

Species	log K
$>\text{HFO}_{(s)}\text{-OPb}^+$	5.87
$>\text{HFO}_{(w)}\text{-OPb}^+$	2.03
$>\text{Silica-OPb}^+$	-2.46

The component additivity approach produces good agreement with the experimental data for all the HFO+silica ratios (Figures 4.15-4.22). Thus, it can be concluded that for the system HFO+silica, the component additivity approach works really very well. In other words, using single, pure solid adsorption data, the adsorption behavior of a mixture of these two phases can be accurately predicted, irrespective of their proportions.

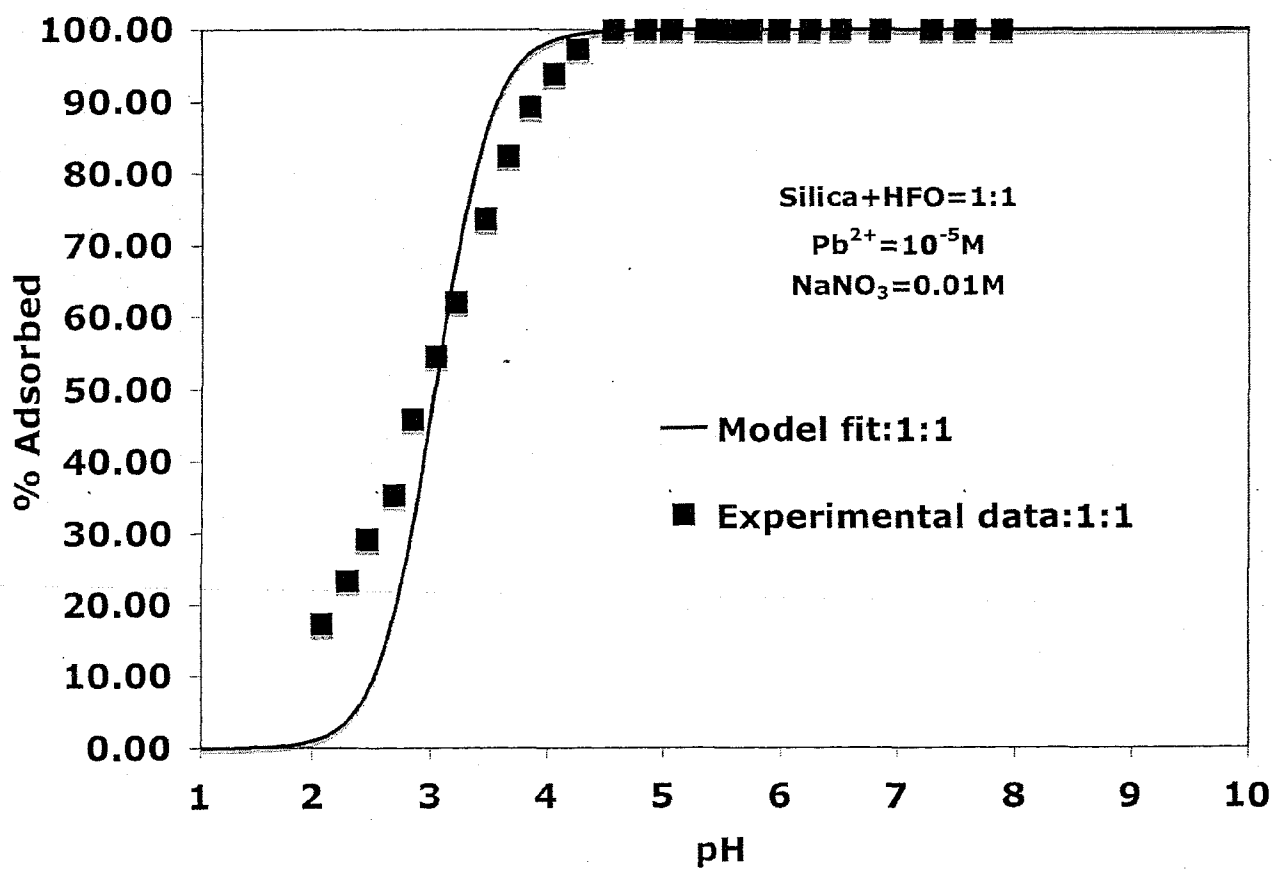


Figure 4.15. Predicted fit for a mixture of silica and HFO of 1:1 with 10<sup>-5</sup> M Pb in 0.01 M NaNO<sub>3</sub> based on thermodynamic parameters derived for the single solid systems.

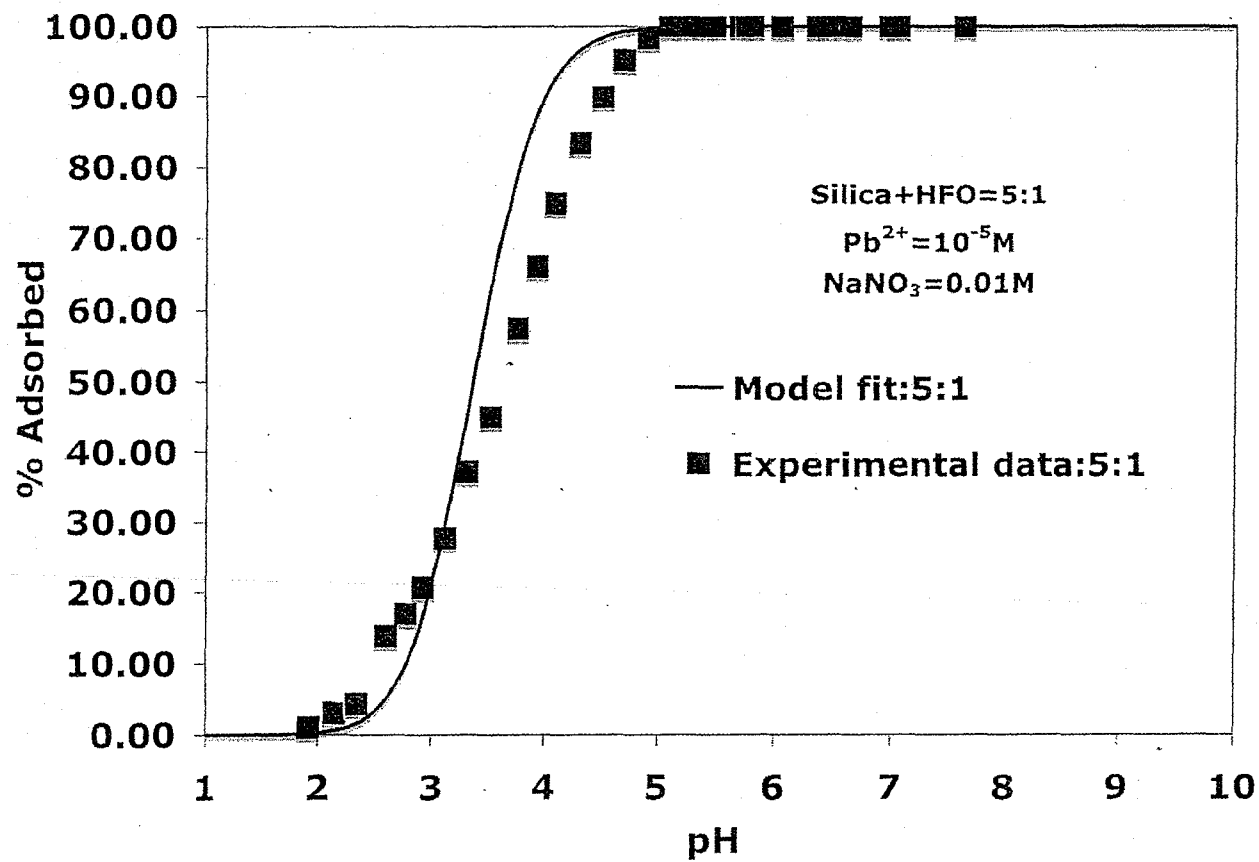


Figure 4.16. Predicted fit for a mixture of silica and HFO of 5:1 with  $10^{-5} M Pb$  in  $0.01 M NaNO_3$ , based on thermodynamic parameters derived for the single solid systems.

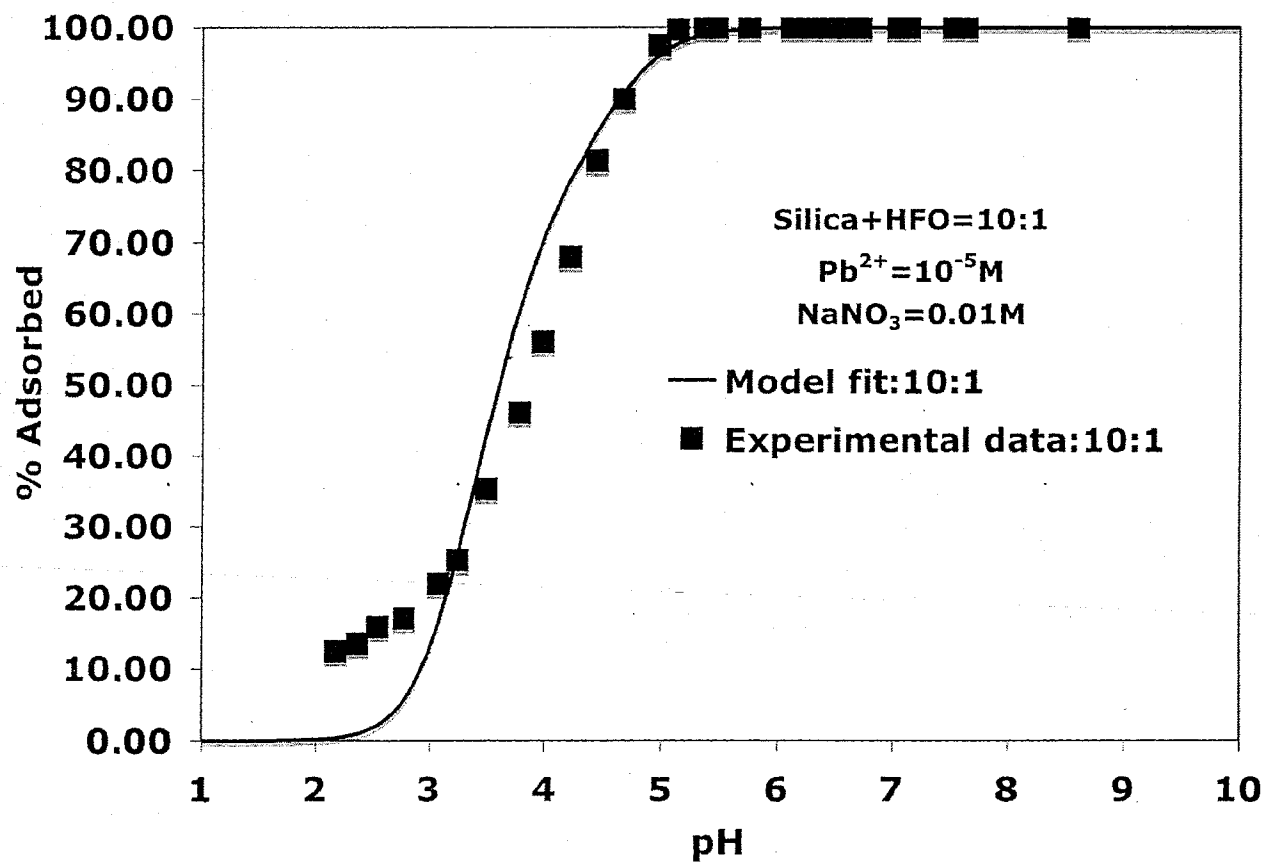


Figure 4.17. Predicted model fit for a mixture of silica and HFO of 10:1 with 10<sup>-5</sup> M Pb in 0.01 M NaNO<sub>3</sub> based on thermodynamic parameters derived for the single systems.

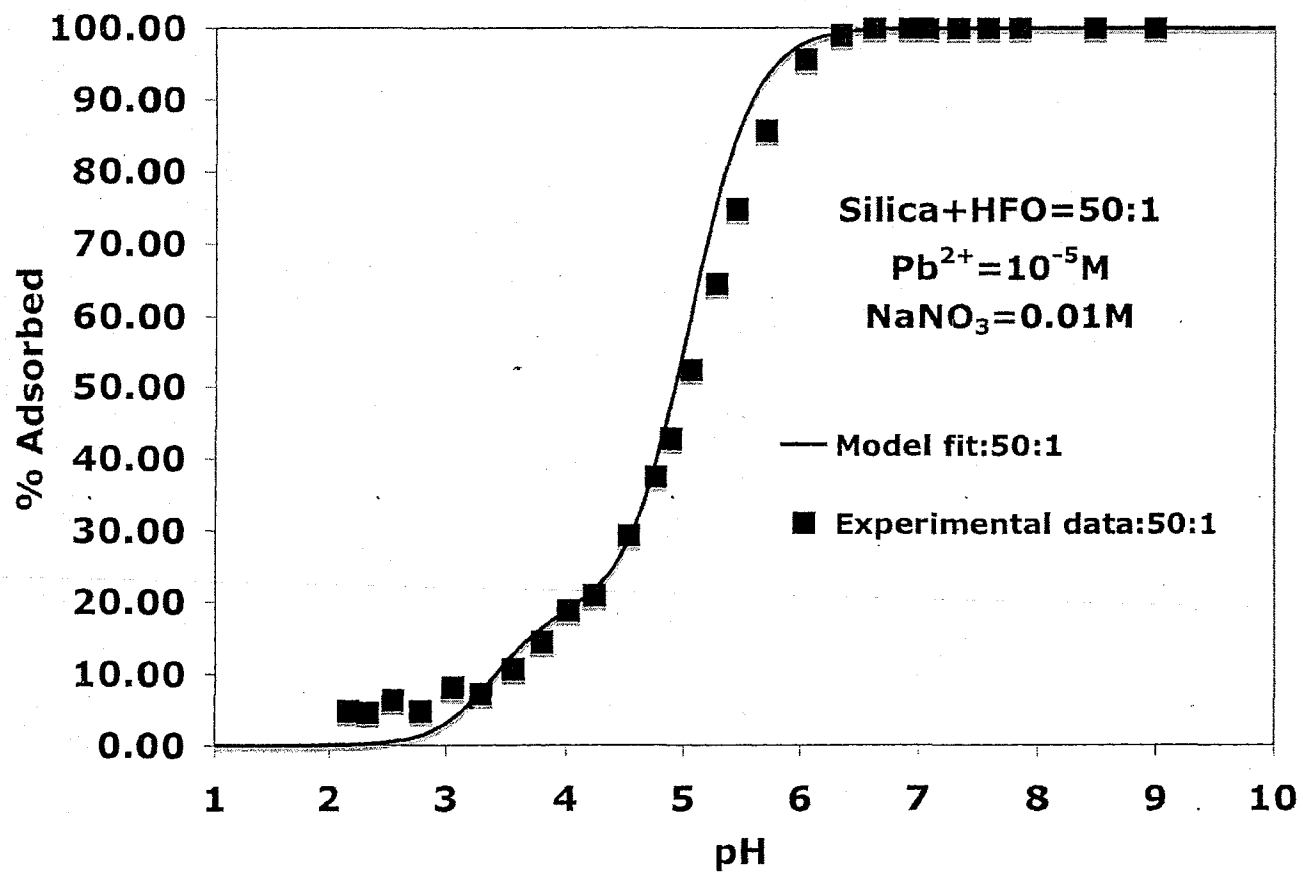


Figure 4.18. Predicted fit for a mixture of silica and HFO of 50:1 with  $10^{-5} M$  Pb in  $0.01 M$   $NaNO_3$  based on thermodynamic parameters derived for the single solid systems.

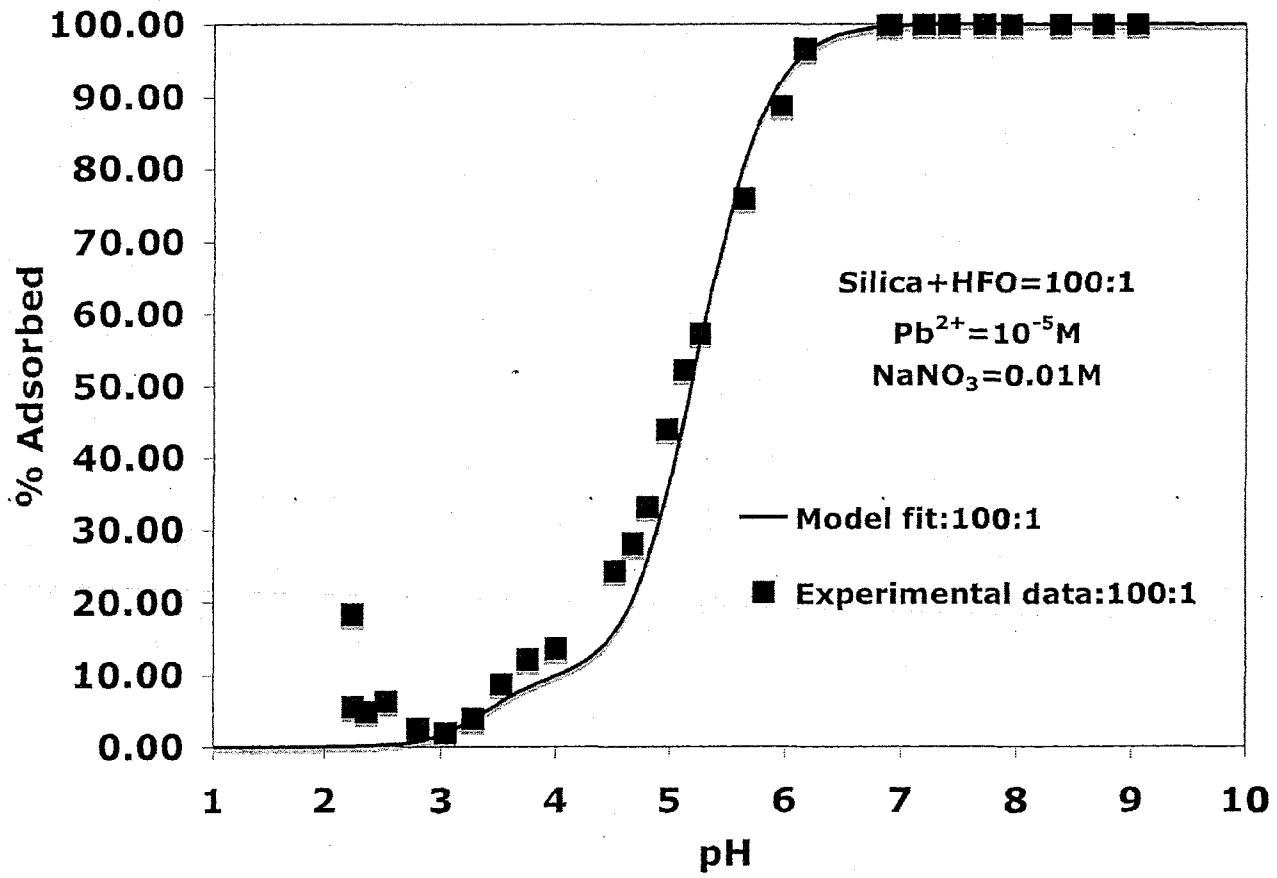


Figure 4.19. Predicted model fit for a mixture of silica and HFO of 100:1 with  $10^{-5} M Pb$  in  $0.01 M NaNO_3$  based on thermodynamic parameters derived for the single solid systems.

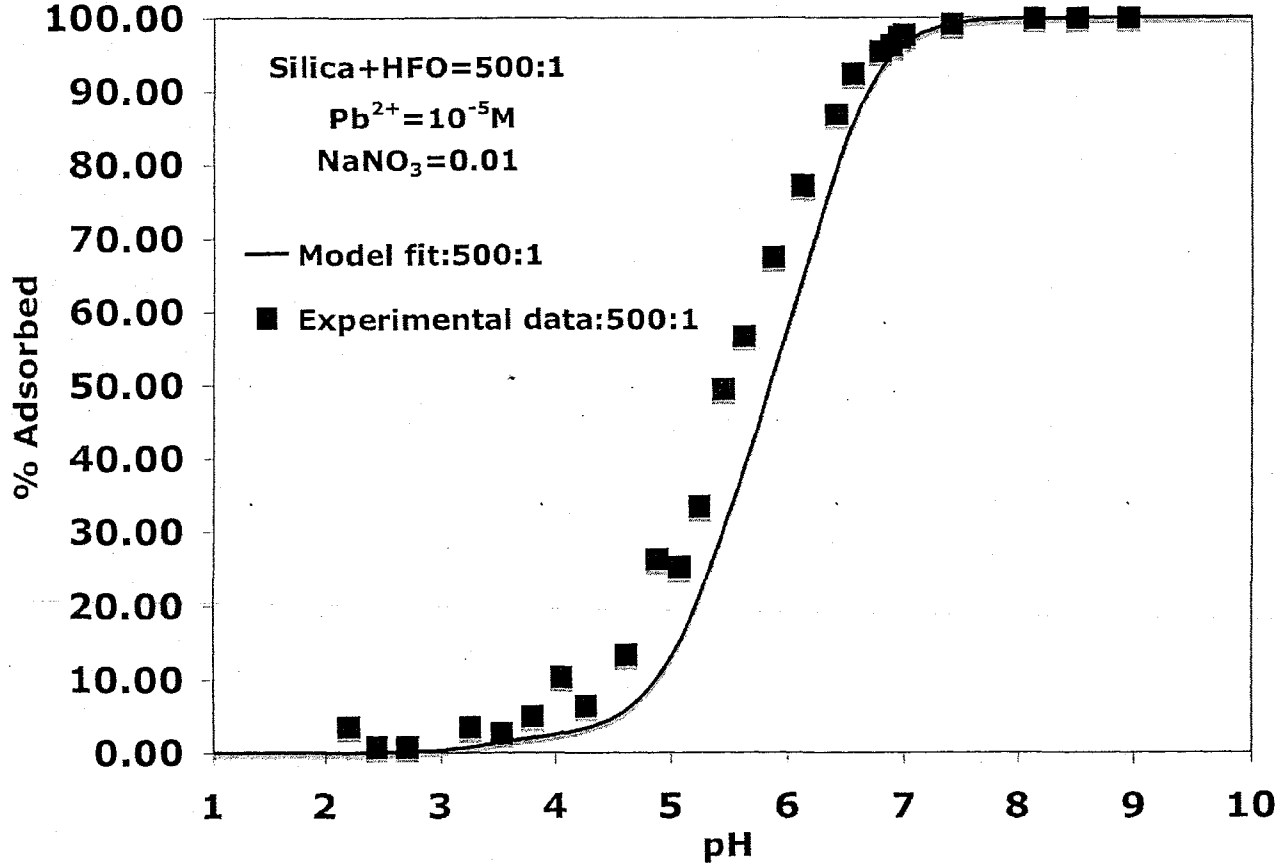


Figure 4.20. Predicted fit for a mixture of silica and HFO of 500:1 with  $10^{-5}$  M Pb in 0.01 M  $NaNO_3$  based on thermodynamic parameters derived for the single solid systems.

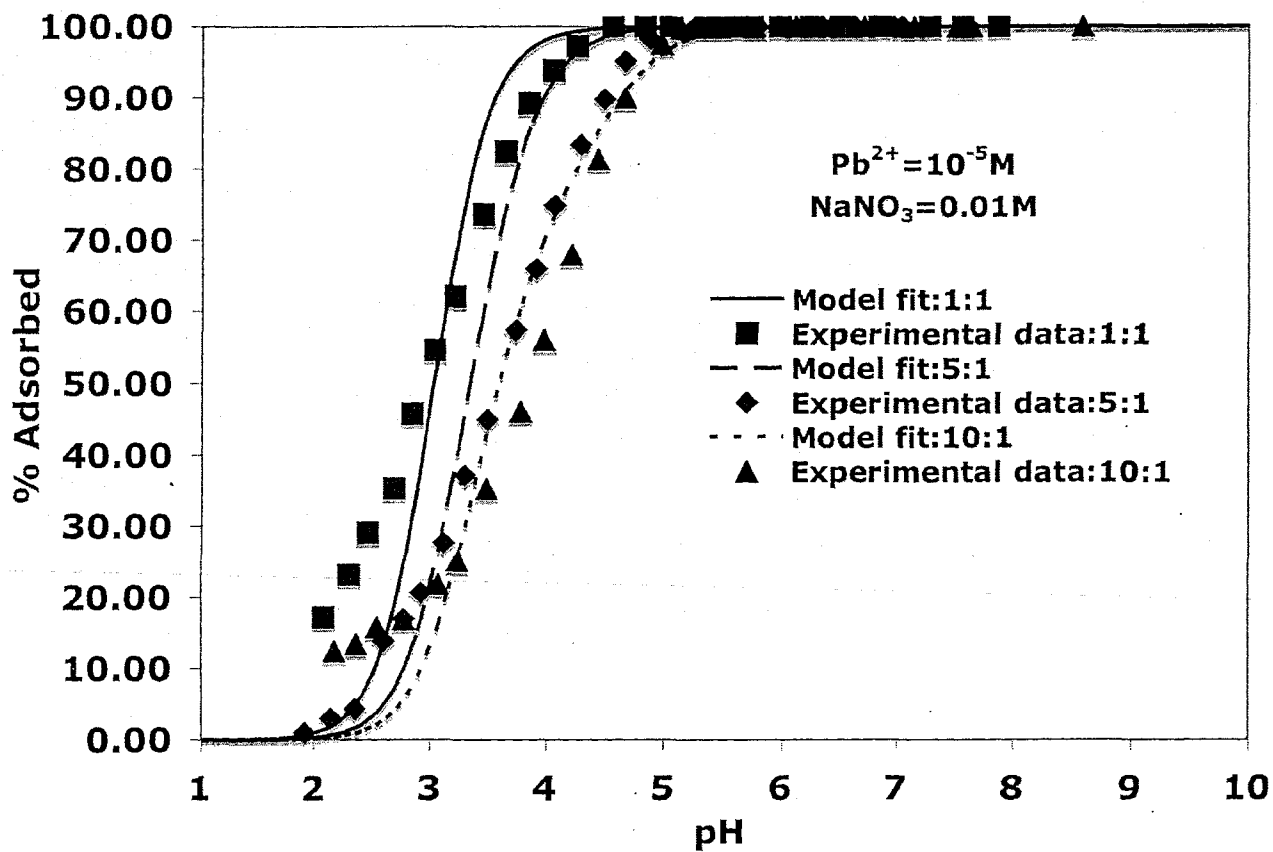


Figure 4.21. Predicted fits for mixtures of silica and HFO of 1:1, 5:1, and 10:1 with  $10^{-5}$  M Pb in 0.01 M  $NaNO_3$  based on thermodynamic parameters derived for the single solid systems.

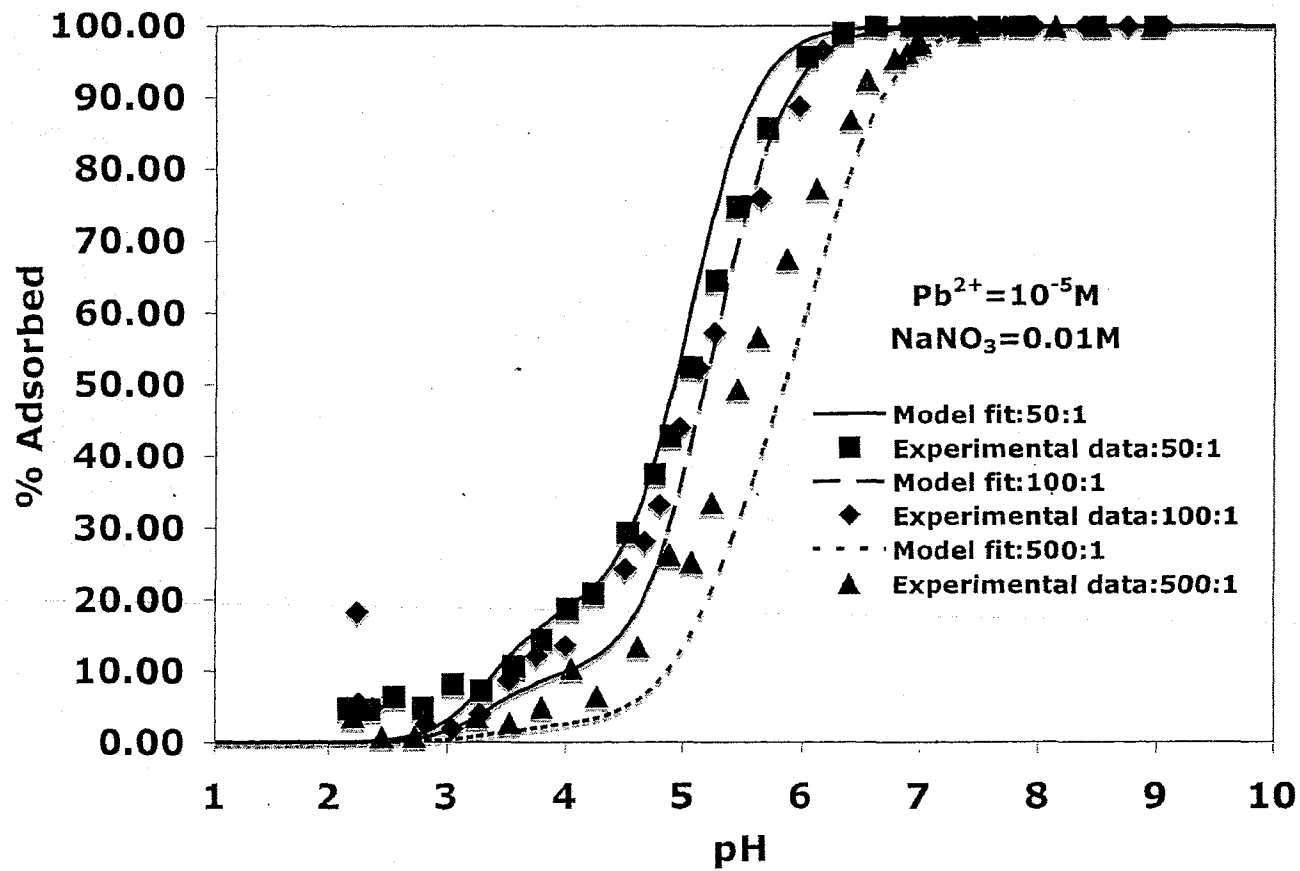


Figure 4.22. Predicted fits for mixtures of silica and HFO of 50:1, 100:1, and 500:1 with  $10^{-5} M$  Pb in 0.01 M  $NaNO_3$  based on thermodynamic parameters derived for the single solid systems.

### HFO+kaolinite (KGa-1B) system

Seven different sorbent-to-sorbent ratios (kaolinite to HFO) were measured and modeled using estimated average stability constants as derived from the single solid systems. The kaolinite to HFO ratios were 1:1, 5:1, 10:1, 50:1, 100:1, 500:1, and 5000:1. The modeling was done using JCHESS 3.0 by incorporating the new average DDLM stability constants (Table 4.10) into the JCHESS database. All the experiments were conducted under 0.01 M NaNO<sub>3</sub> electrolyte strength and the Pb concentrations were kept constant at 10<sup>-5</sup> M.

Table 4.10 Best fit log stability constants for Pb adsorption on HFO and kaolinite

Species	log K
>HFO <sub>(s)</sub> -OPb <sup>+</sup>	5.87
>HFO <sub>(w)</sub> -OPb <sup>+</sup>	2.03
>Kaolinite-(Si)-OPb <sup>+</sup>	-2.33
>Kaolinite-(Al)-OPb <sup>+</sup>	-1.0

The predicted fits for the binary system HFO + kaolinite are not in excellent agreement with the experimental data as they were for the HFO+silica system. The predicted fits get poorer as the amount of kaolinite is increased. Specifically, the model overpredicts adsorption somewhat compared to the experimental data for the 1:1 5:1, and 10:1 sorbent-to-sorbent experiments (Figures 4.23-4.25). However, at ratios of 50:1 and

greater, the scenario changes (Figures 4.26-4.31). For these ratios, the component additivity model predicts less adsorption than is measured. The predictions are best for the 1:1 system (Figure 4.23). This is also true for the system containing silica+kaolinite, which will be discussed in the next section of this chapter. This lack of agreement of the measured data with the component additivity model predictions cannot be explained by the fact that clay minerals like kaolinite may coat the surfaces of HFO and silica, decreasing the available sites for adsorption as proposed by Honeyman (1984). The results showed reverse effect compared to the study of Honeyman (1984). He studied Cd adsorption on mixture of montmorillonite and alumina, and found that a component additivity approach overestimated adsorption compared to experimental data. He explained this behavior as being caused by site exclusion due to the heterocoagulation between clay and alumina, which blocked the sites for adsorption. So, to properly model such binary mixtures, it is necessary to determine the quantity of sites blocked during the coagulation process. This study showed that as kaolinite increased in the system, the model undermines adsorption compared to experimental data. Therefore to explain this behavior this study needs a different explanation, as it does not show the effect of site exclusion. For pure kaolinite at 0.01 M NaNO<sub>3</sub> and 10<sup>-5</sup> M Pb, the single solid (kaolinite model) also overpredicts sorption a bit, especially at mid-pH, so this might be one source of overpredictions in systems containing kaolinite. However, the underprediction of adsorption at high kaolinite:HFO ratios requires a different explanation. Perhaps, the modeling of pure kaolinite is not adequate. Most probably, to model pure kaolinite data, we need to add ion exchange site onto kaolinite surface. This might explain why there is a mismatch between the experimental data and model fit at low pH for low Pb

concentration and low ionic strength. It appears that a simple component additivity model, not accounting for solid-solid interactions, inaccurately predicts the actual quantity of sites available for adsorption.

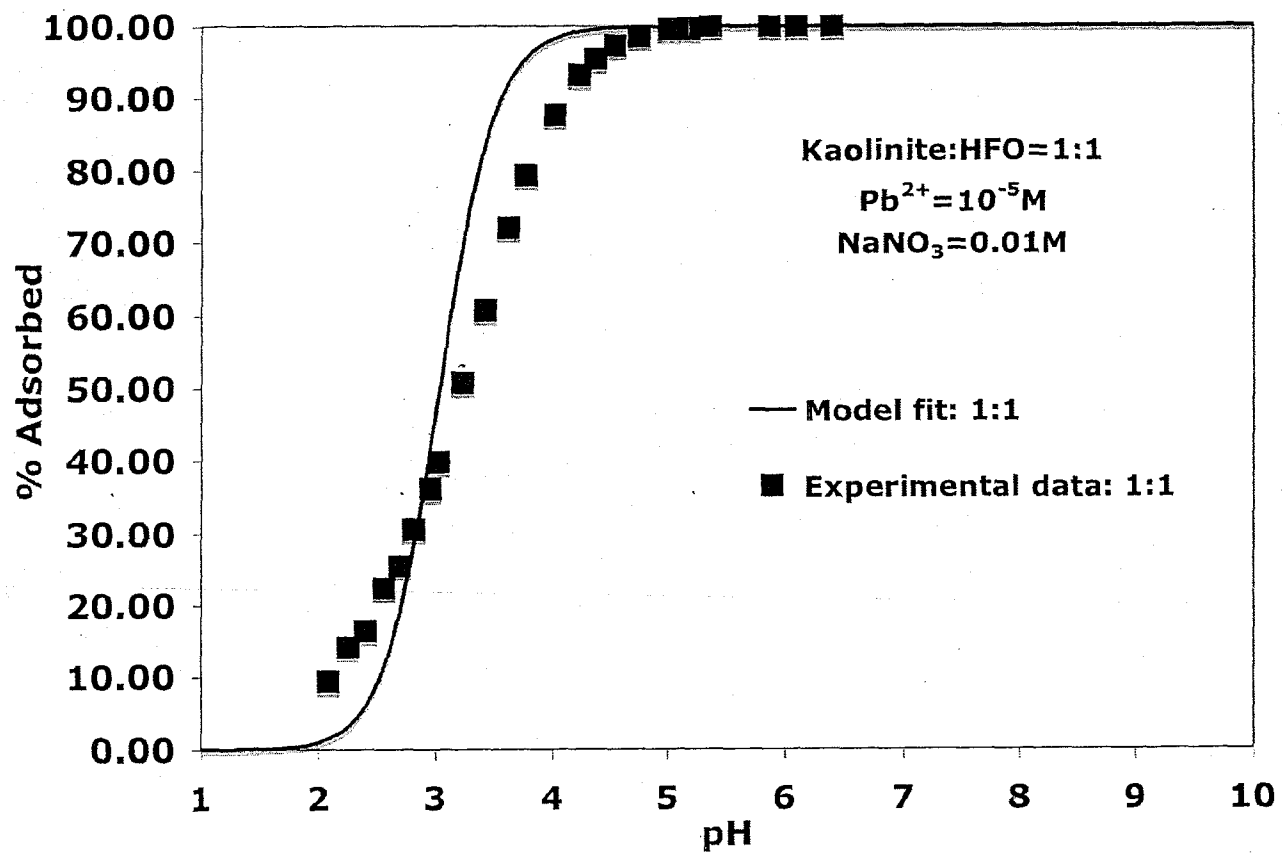


Figure 4.23. Predicted fit for a mixture of kaolinite and HFO of 1:1 with  $10^{-5}$  M Pb in 0.01 M NaNO<sub>3</sub> based on single system thermodynamic parameters.

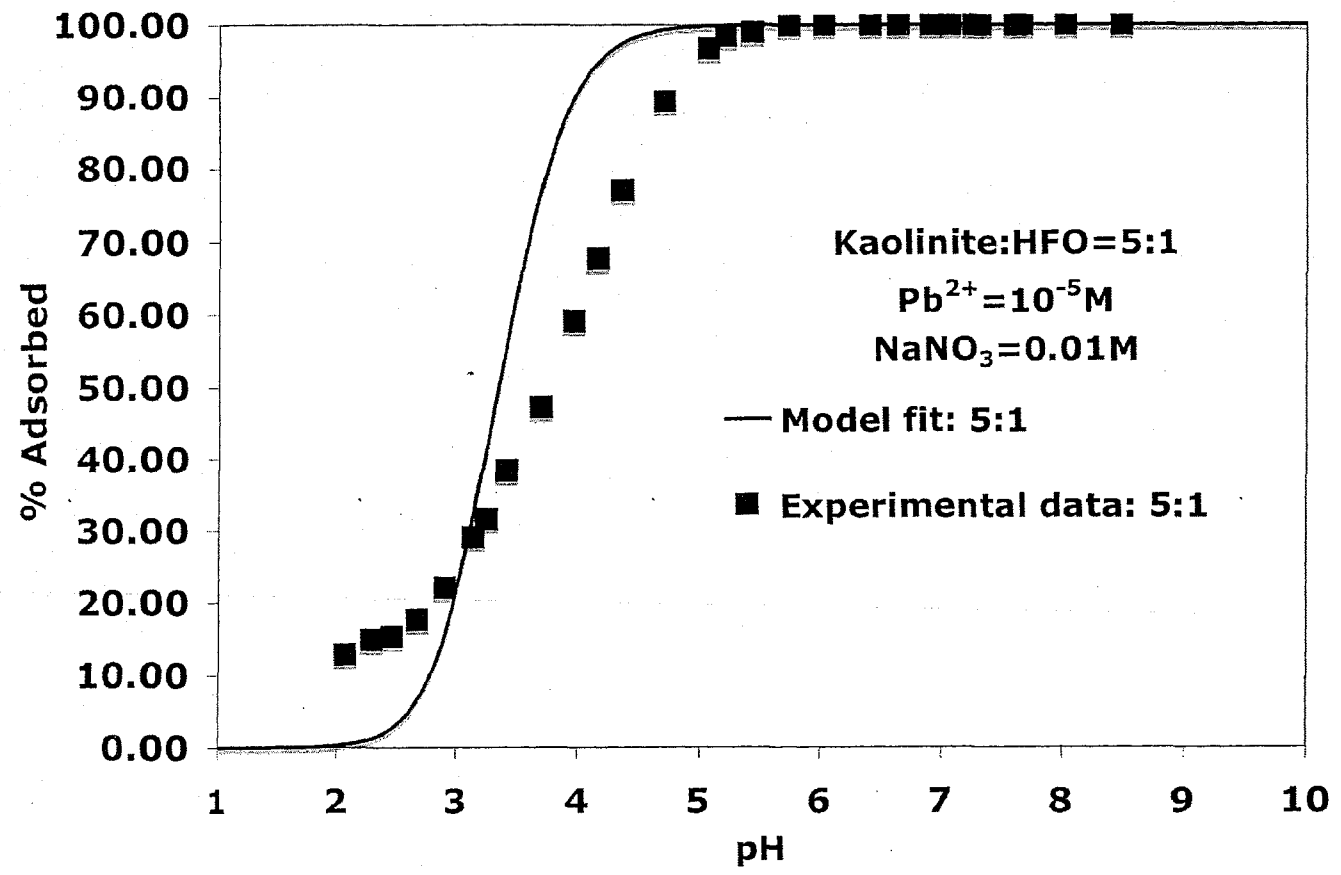


Figure 4.24. Predicted fit for a mixture of kaolinite and HFO of 5:1 with 10<sup>-5</sup> M Pb in 0.01 M NaNO<sub>3</sub> based on single system thermodynamic parameters.

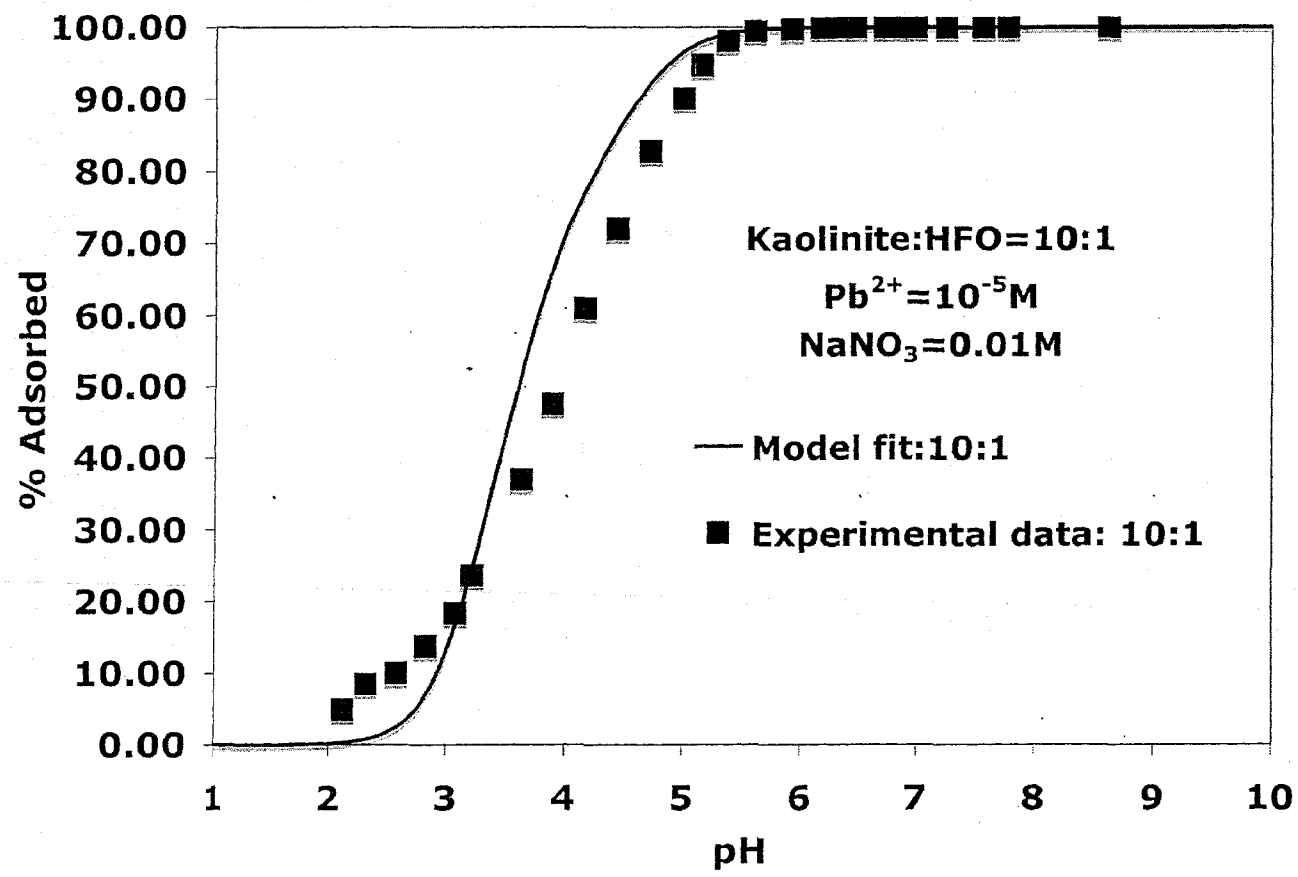


Figure 4.25. Predicted fit for a mixture of kaolinite and HFO of 10:1 with 10<sup>-5</sup> M Pb in 0.01 M NaNO<sub>3</sub> based on single solid system thermodynamic parameters.

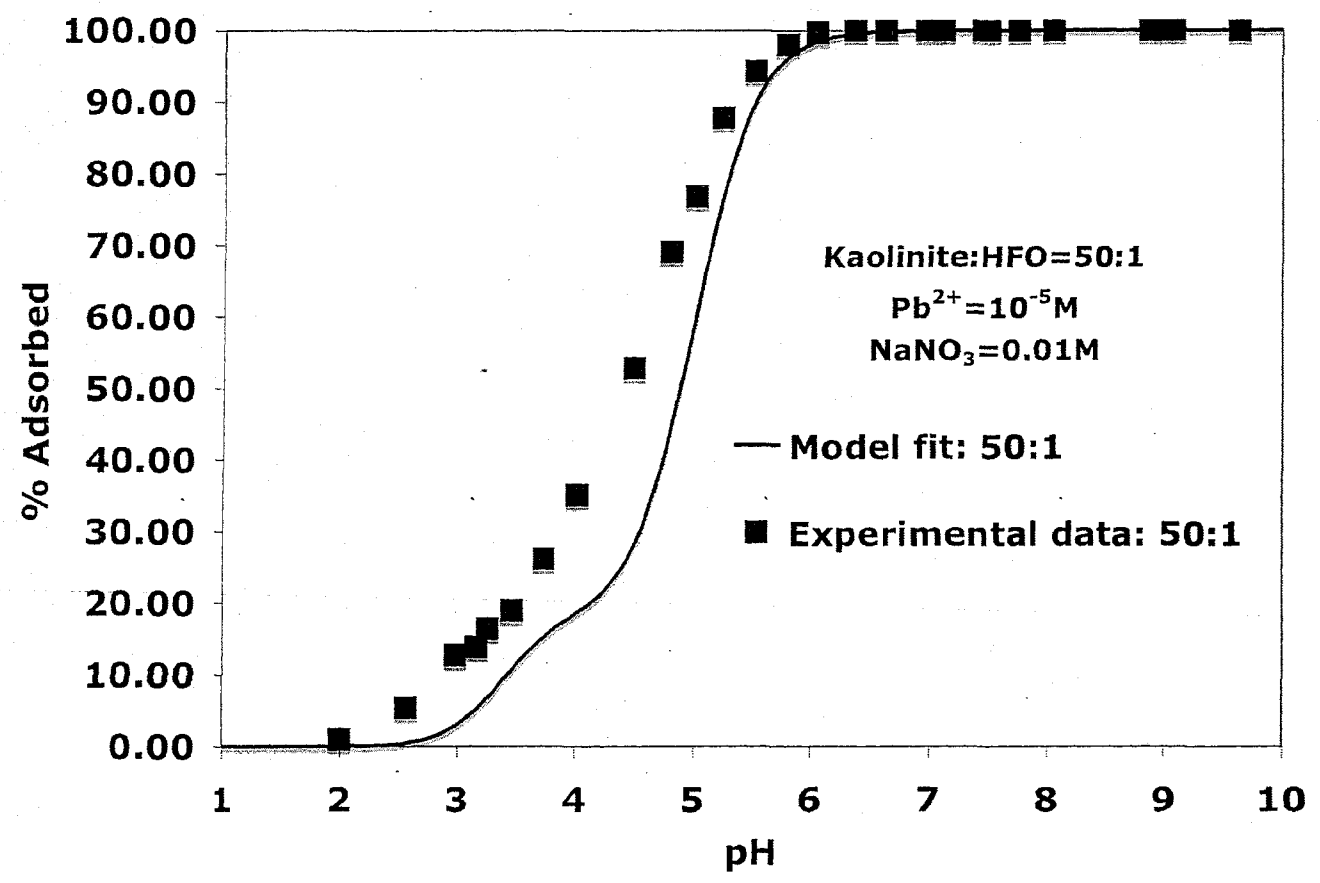


Figure 4.26. Predicted fit for a mixture of kaolinite and HFO of 50:1 with 10<sup>-5</sup> M Pb in 0.01 M NaNO<sub>3</sub> based on single solid system thermodynamic parameters.

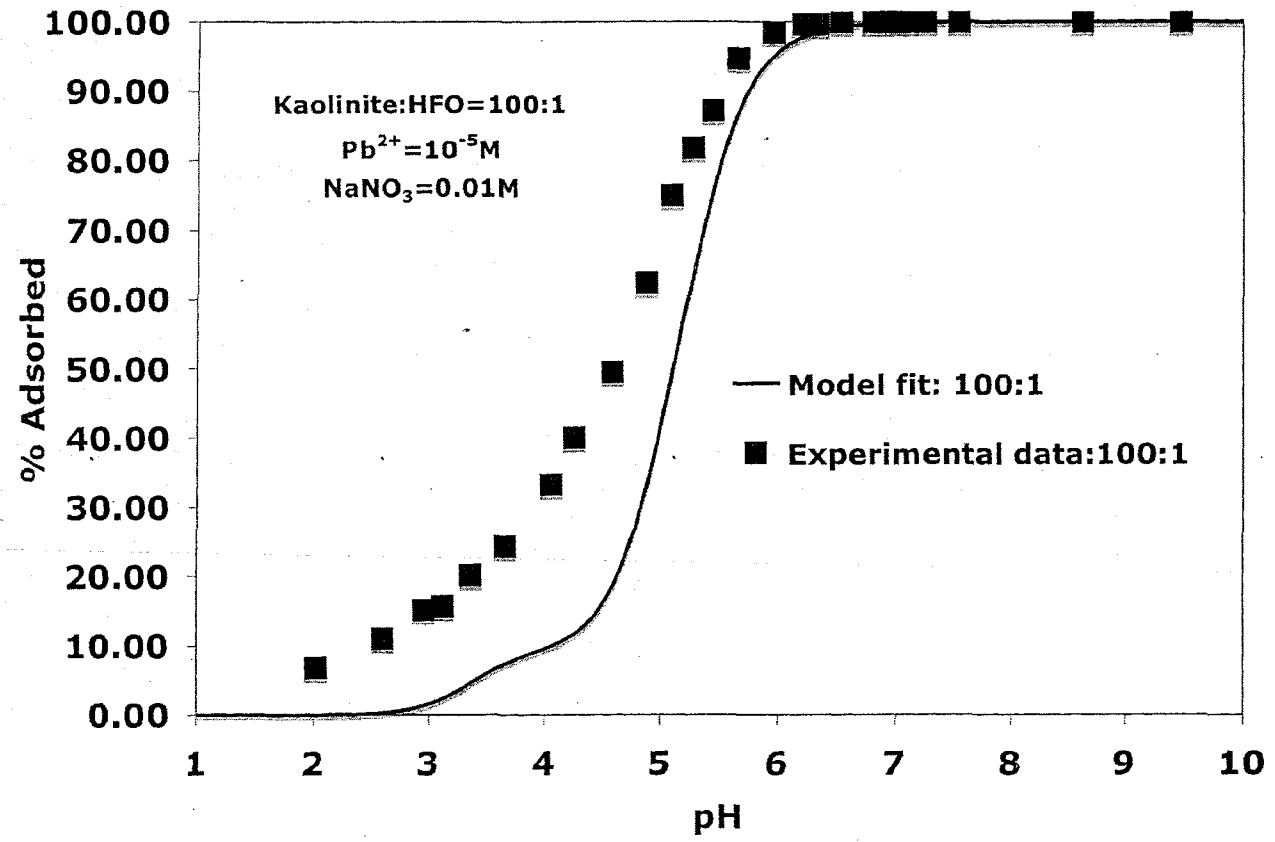


Figure 4.27. Predicted fit for a mixture of kaolinite and HFO of 100:1 with 10<sup>-5</sup> M Pb in 0.01 M NaNO<sub>3</sub> based on single solid system thermodynamic parameters.

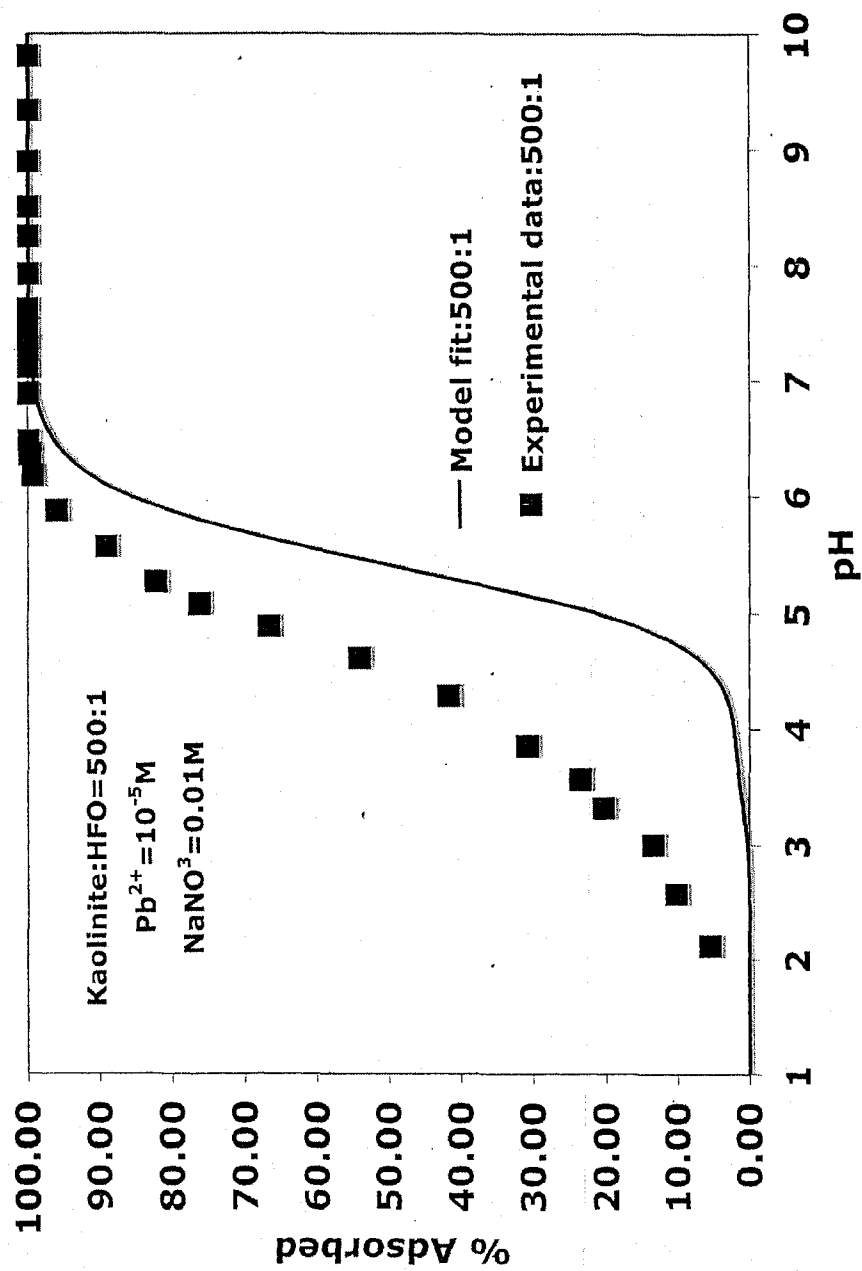


Figure 4.28. Predicted fit for a mixture of kaolinite and HFO of 500:1 with  $10^{-5}$  M Pb in 0.01 M  $NaNO_3$  based on single system thermodynamic parameters.

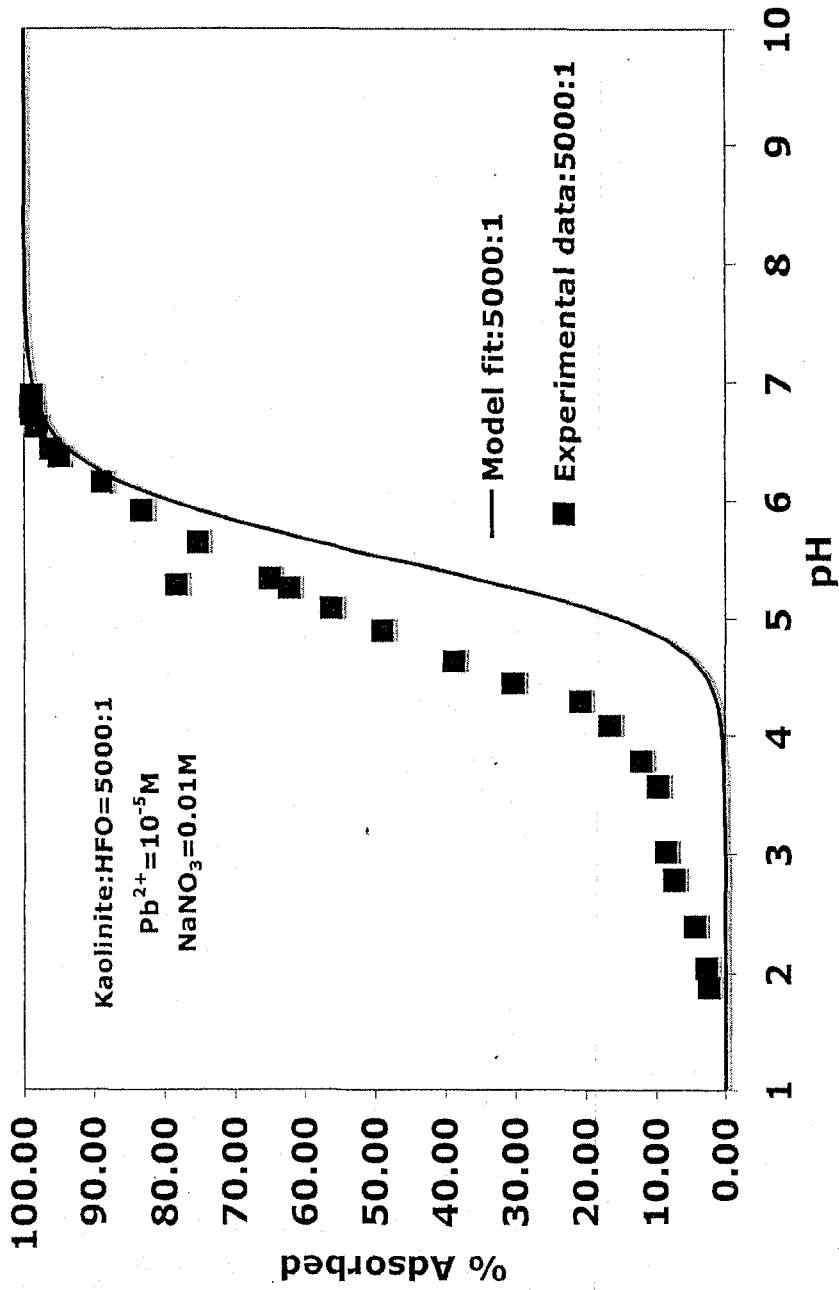


Figure 4.29. Predicted fit for a mixture of kaolinite and HFO of 5000:1 with  $10^{-5} M$  Pb in  $0.01 M$   $NaNO_3$  based on single solid system thermodynamic parameters.

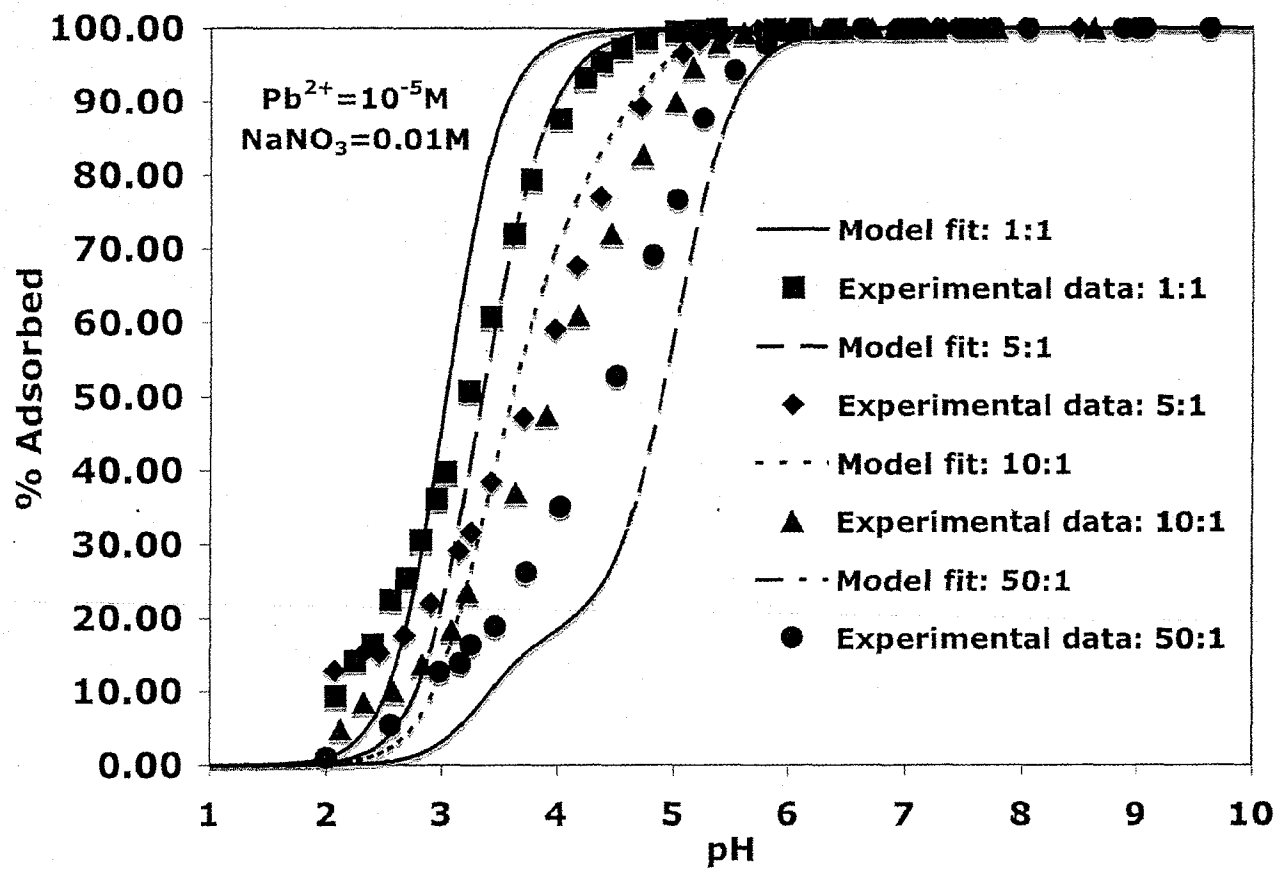


Figure 4.30. Predicted fits for mixtures of kaolinite and HFO of 1:1, 5:1, 10:1, and 50:1 with  $10^{-5} M$  Pb in  $0.01 M$   $NaNO_3$ , based on single solid system thermodynamic parameters.

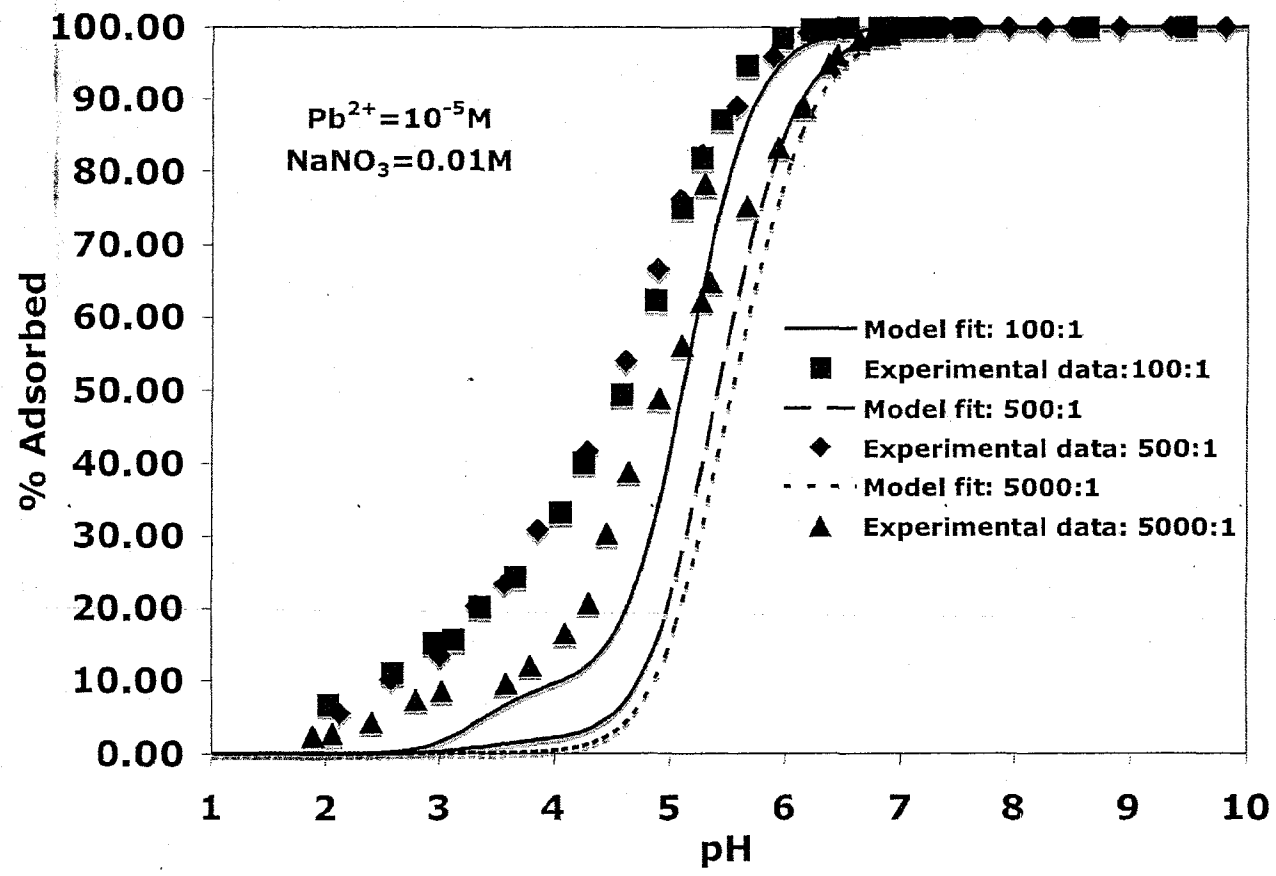


Figure 4.31. Predicted fits for mixtures of kaolinite and HFO of 100:1, 500:1, and 5000:1 with  $10^{-5} M$  Pb in 0.01 M  $NaNO_3$ , based on single solid system thermodynamic parameters.

### Kaolinite (KGa-1B)+silica system

Five different sorbent-to-sorbent ratios were studied for the kaolinite+silica system, namely 1:1, 10:1, 50:1, 0.1:1 and 0.01:1. All the experiments were conducted under 0.01 M NaNO<sub>3</sub> electrolyte strength and the Pb concentrations were kept constant at 10<sup>-5</sup> M. The results were modeled using the average best-fit stability constants for Pb adsorption on the pure kaolinite and silica colloids (Table 4.11).

Table 4.11 Stability constants for Pb adsorption on kaolinite and silica derived for the single solid systems and used for the binary system speciation calculations

Species	LogK
>Kaolinite-(Si)-OPb <sup>+</sup>	-2.33
>Kaolinite-(Al)-OPb <sup>+</sup>	-1.0
>Silica-OPb <sup>+</sup>	-2.46

The model predicts similar adsorption behavior compared to the experimental data (Figures 4.32-4.36). As the amount of kaolinite relative to silica increases, the model fit becomes poorer, whereas when the amount of silica in the system increases, the fit gets better. More interestingly, as seen in the previous system, namely HFO+kaolinite, with increasing kaolinite in the system, the predicted fit shows less adsorption compared to the experimental data. For example, at high kaolinite:silica ratios, for example 10:1 and 50:1, the model underpredicts adsorption compared to the experimental data. With increasing silica (i.e. lower kaolinite:silica ratios), the component additivity model overpredicts adsorption, but the fits for the 0.1:1 and

0.02:1 systems are improved considerably compared to the systems with larger quantities of kaolinite. As a result, the predictions are in very close proximity to the actual experimental data. Therefore, modeling results showed that, the component additivity approach could again predict adsorption of Pb very well in those mixed systems which contain negligible quantities of clay minerals. However, to model those systems which do contain significant amounts of clay minerals, a revised version of the component additivity model might be required to calculate the amount of available sites for adsorption. Also, as mentioned earlier, that the outcome of pure kaolinite modeling is not adequate, and a different SCM approach might provide better result. This also suggests that the generalized composite approach might produce better results than the component additivity approach, because it does not require information regarding the number and types of minerals present. So, a great follow up study might be to test whether the generalized composite approach could be used to predict Pb adsorption accurately for the solid mixtures, especially those with kaolinite, used in this study.

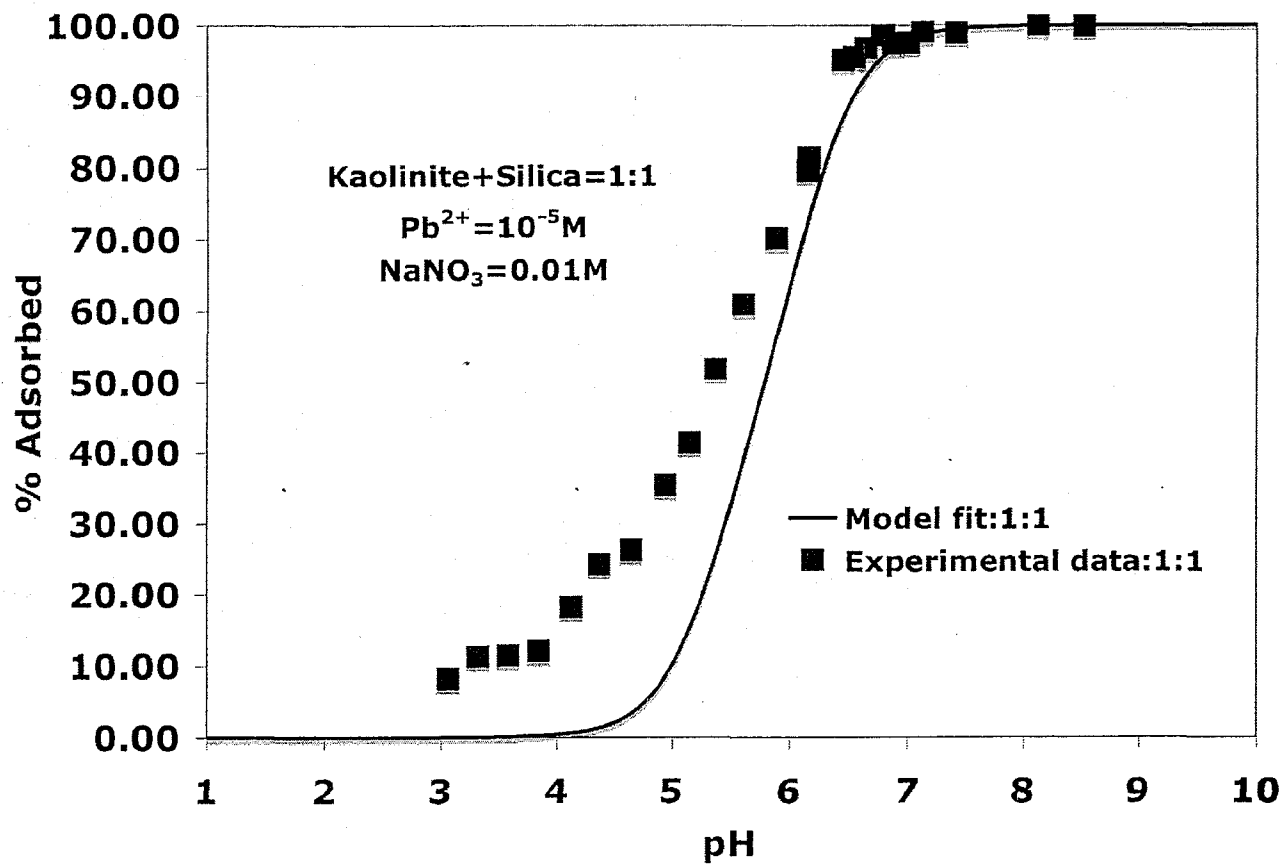


Figure 4.32. Predicted fit for a mixture of kaolinite and silica of 1:1 with 10<sup>-5</sup> M Pb in 0.01 M NaNO<sub>3</sub> based on single solid system thermodynamic parameters.

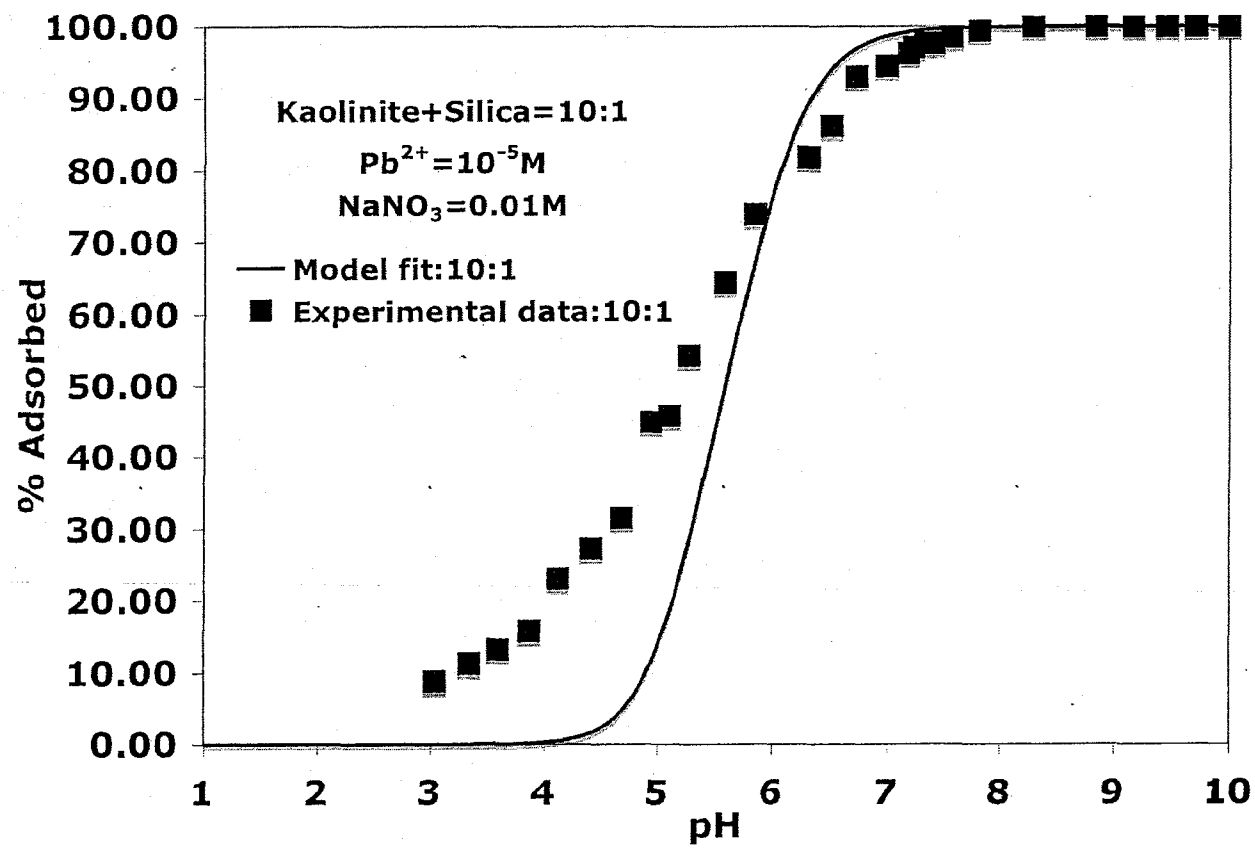


Figure 4.33. Predicted fit for a mixture of kaolinite and silica of 10:1 with  $10^{-5} M$  Pb in 0.01 M  $NaNO_3$  based on single solid system thermodynamic parameters.

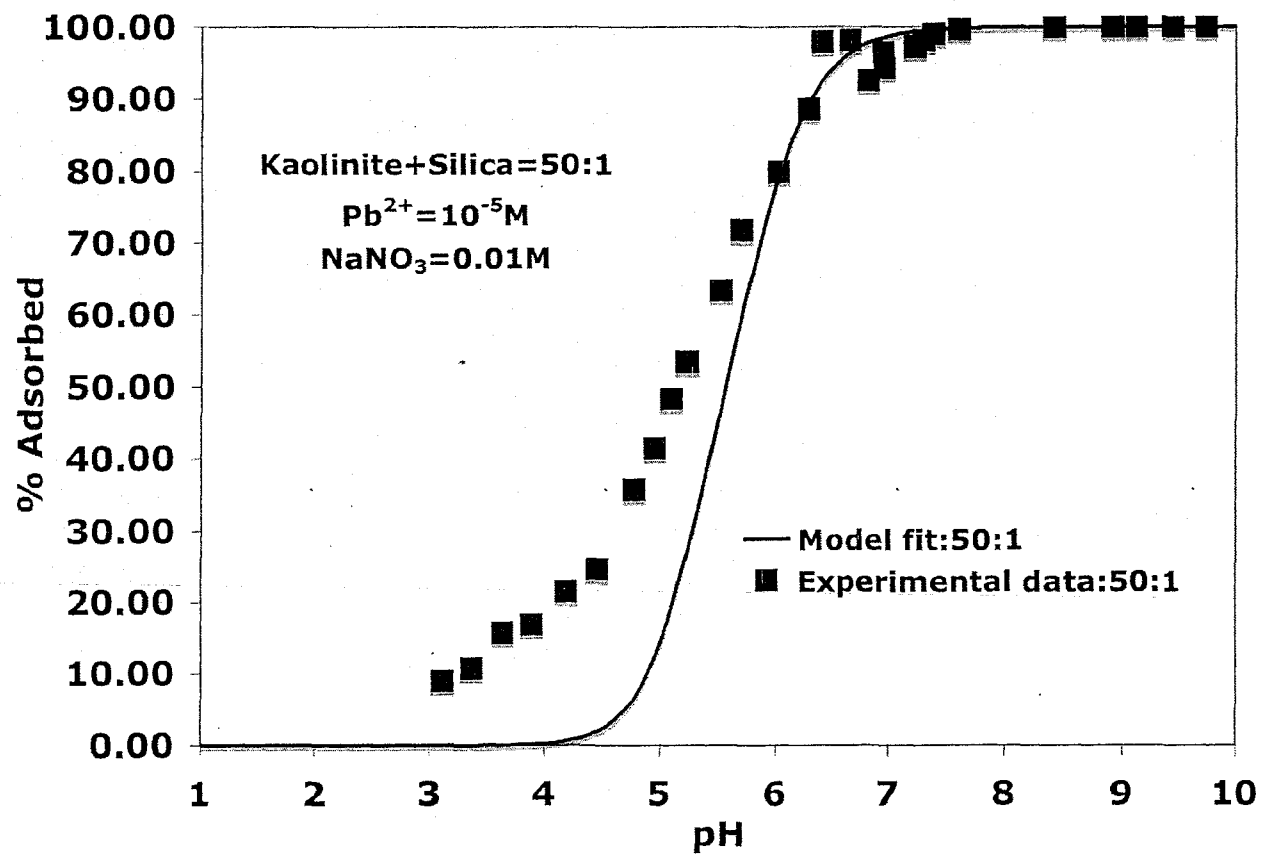


Figure 4.34. Predicted fit for a mixture of kaolinite and silica of 50:1 with  $10^{-5}$  M Pb in 0.01 M NaNO<sub>3</sub> based on single solid system thermodynamic parameters.

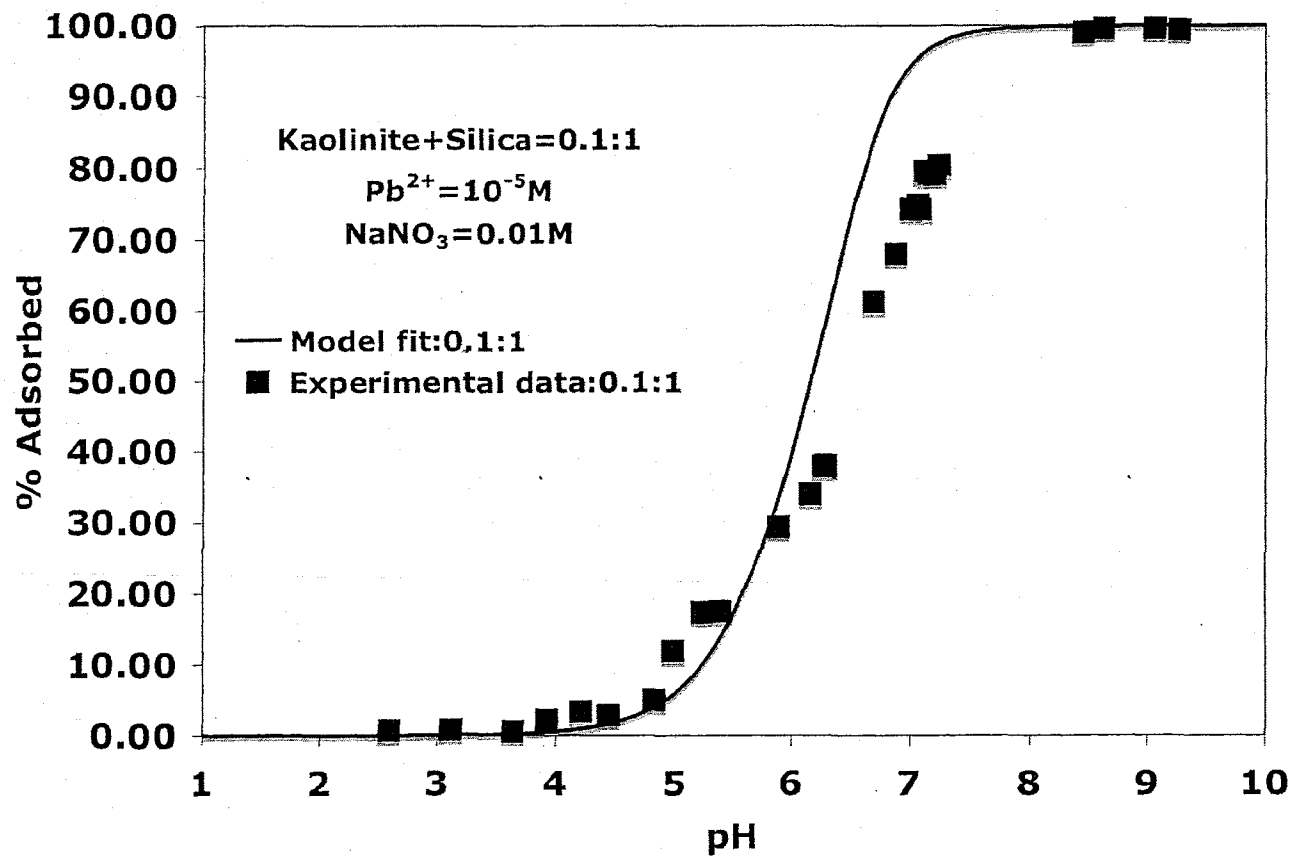


Figure 4.35. Predicted fit for a mixture of kaolinite and silica of 0.1:1 with 10<sup>-5</sup> M Pb in 0.01 M NaNO<sub>3</sub> based on single solid system thermodynamic parameters.

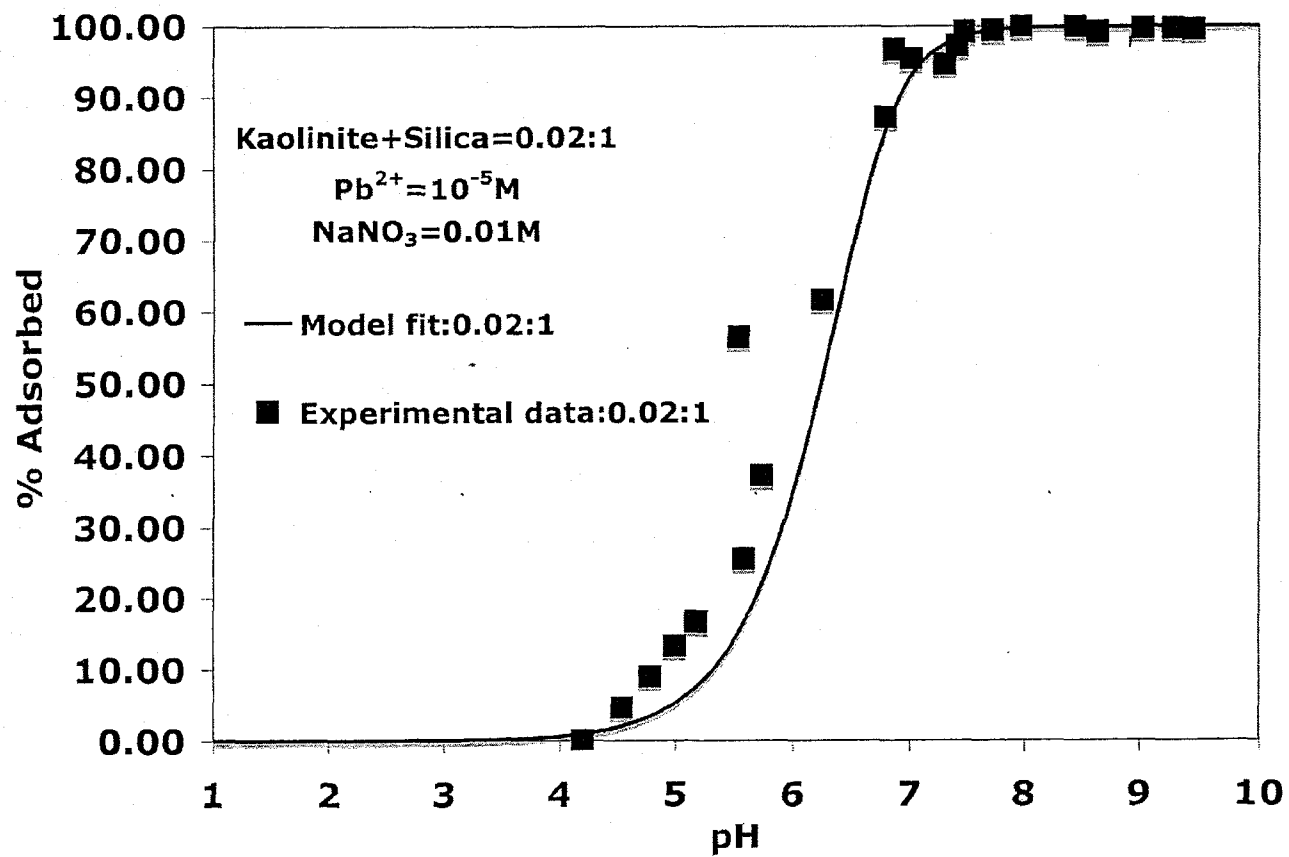


Figure 4.36. Predicted fit for a mixture of kaolinite and silica of 0.02:1 with 10<sup>-5</sup> M Pb in 0.01 M NaNO<sub>3</sub> based on single solid system thermodynamic parameters.

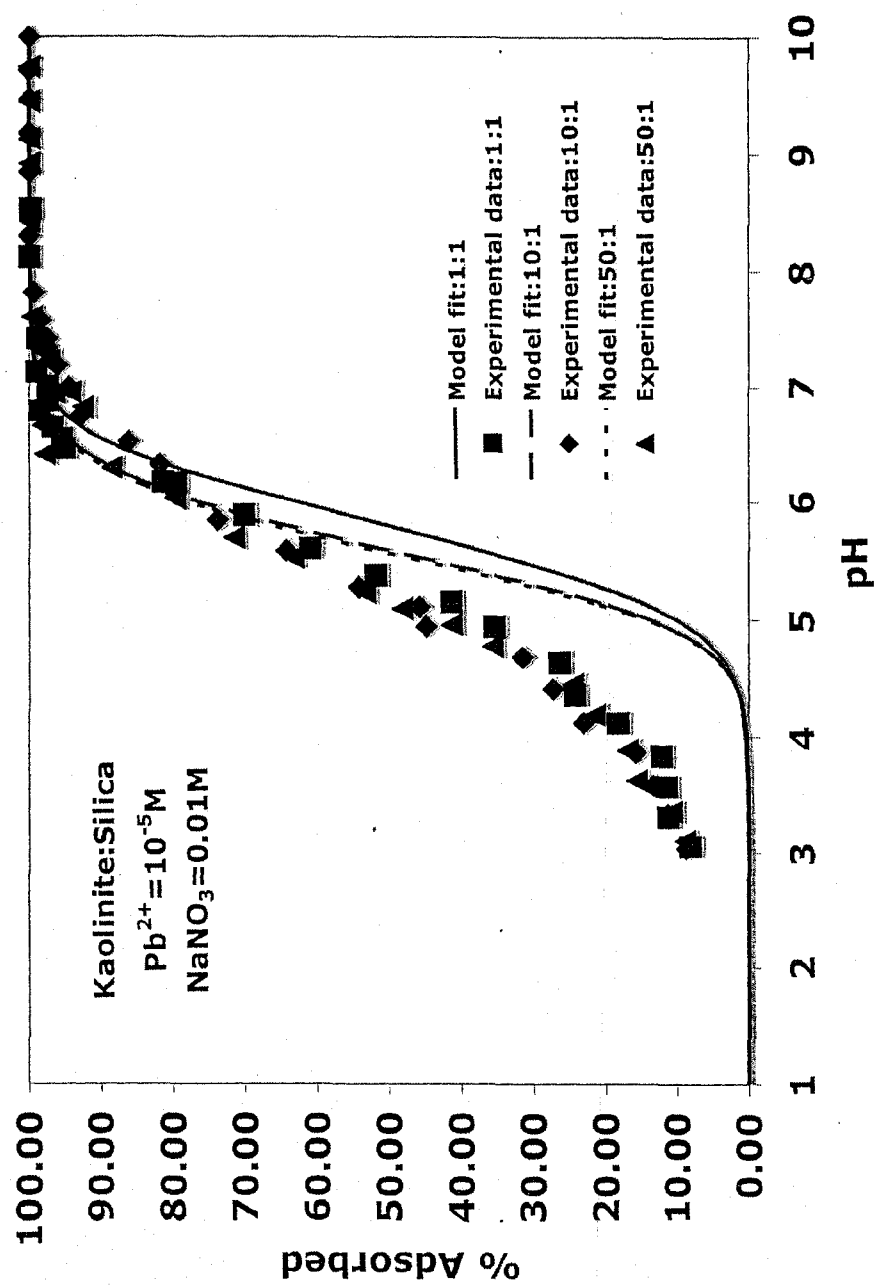


Figure 4.37. Predicted fits for mixtures of kaolinite and silica 1:1, 10:1 and 50:1 ratios with  $10^{-5} M Pb$  in  $0.01 M NaNO_3$ .

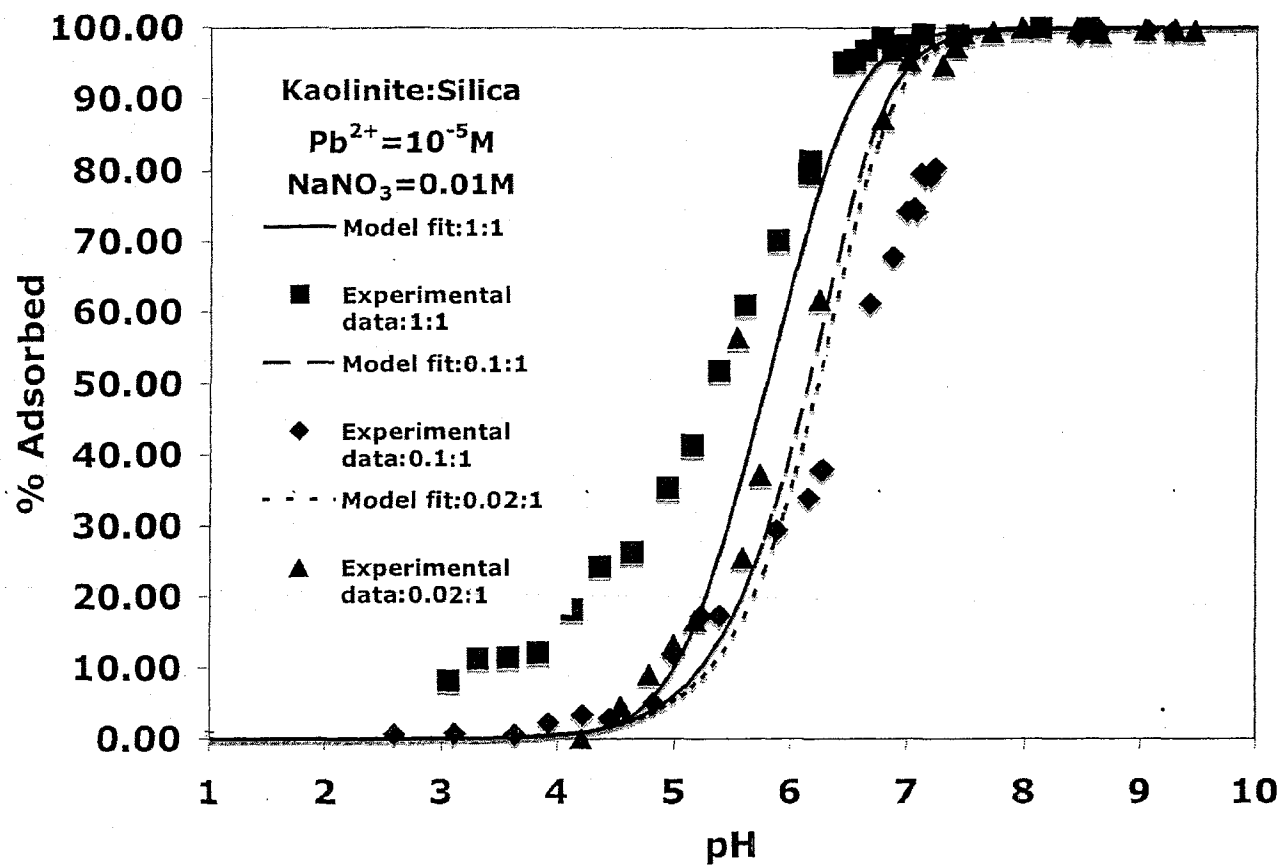


Figure 4.38. Model fits for mixture of kaolinite and silica for 1:1, 0.1:1 and 0.02:1 ratios with 10<sup>-5</sup> M Pb in 0.01 M NaNO<sub>3</sub>.

### Ternary systems

Two different ternary assemblages have been studied using a mixture of three single mineral phases, namely HFO, silica and kaolinite. The mixtures were chosen such that the ratio of these three minerals were 1:1:1 by their mass or 1:1:1 by their surface areas. JCHESS 3.0 was used for modeling as for the binary systems with the stability constants shown in Table 4.12. All the experiments were conducted under 0.01 M NaNO<sub>3</sub> electrolyte strength and the Pb concentrations were kept constant at 10<sup>-5</sup> M.

Table 4.12 Stability constant derived for single solid systems and used for modeling ternary mixtures

Species	log K
>HFO <sub>(s)</sub> -OPb <sup>+</sup>	5.87
>HFO <sub>(w)</sub> -OPb <sup>+</sup>	2.03
>Kaolinite-(Si)-OPb <sup>+</sup>	-2.33
>Kaolinite-(Al)-OPb <sup>+</sup>	-1.0
>Silica-OPb <sup>+</sup>	-2.46

The experimental data and the model fits are in excellent agreement for both these experiments (Figures 4.39-4.41). The model slightly underpredicts the 1:1:1 surface area data, and the predicted edge is a little too sharp for the 1:1:1 by mass experiment, but otherwise the fits are very good.

Figures 4.42 and 4.43 show the predicted surface species formed on the ternary mixtures as a function of pH. HFO surfaces were the prime adsorbent for Pb at any given pH in both ternary mixtures. For the ternary mixture with a ratio 1:1:1 by mass (Figure 4.42), most of the Pb was adsorbed onto the strong site, and the contribution from all other surface sites, including the weak site of HFO, have negligible influence on Pb adsorption. The scenario changes for the 1:1:1 mixture by surface area. Here, the influence of HFO was still predominant, but the adsorption occurred primarily on the weak site instead of strong site. The contribution to total adsorption from the surfaces of the other solids remains negligible. The dominance of the weak site in one instance and the strong site of HFO in the other can be explained by the different site densities of strong and weak sites on HFO. The strong site has a site density of just  $0.078 \mu\text{mol}/\text{m}^2$ , compared to  $3.11 \mu\text{mol}/\text{m}^2$  for weak site. So, for a mixture of 1:1:1 by mass, there is plenty of surface area and sites available for adsorption. As a result, most of the adsorption occurs on the strong site, as the strong site has a much higher stability constant (5.87) compared to the weak site (2.03). On the other hand, for a mixture of 1:1:1 by surface area, the amount of available strong sites decreases drastically, owing to the fact that this site has a very low site density. But for the weak site, enough sites are still available for the Pb to adsorb, and moreover this site has much higher stability constant compared to those for Pb surface complexes on the other two solids, namely silica and kaolinite. This is a nice demonstration of the experimental as well as the modeling results, showing that this modeling approach can predict very well the speciation of different Pb species onto ternary assemblages. This also proves again that HFO is by far the strongest adsorbent.

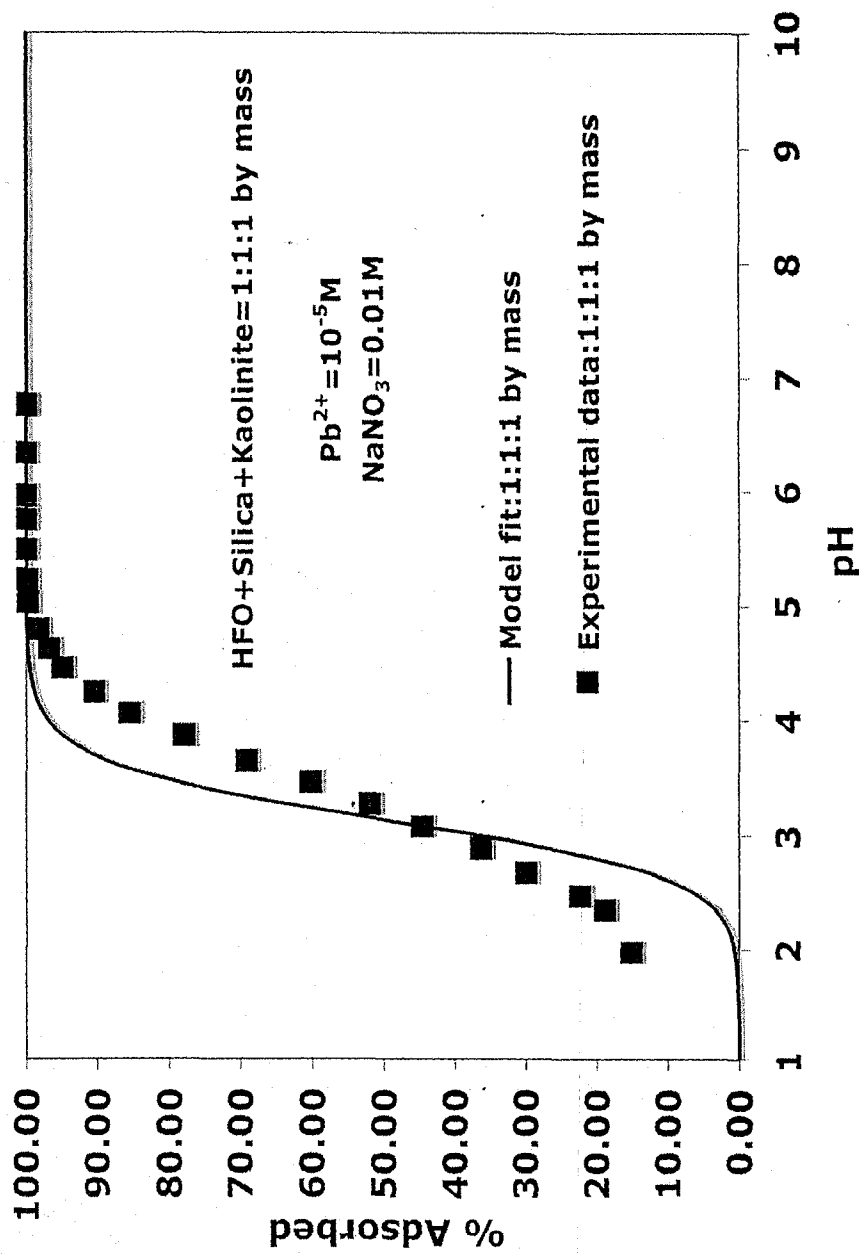


Figure 4.39. Model fit for 1:1:1 ratio by mass with  $10^{-5}M$  Pb in  $0.01M$   $NaNO_3$ .

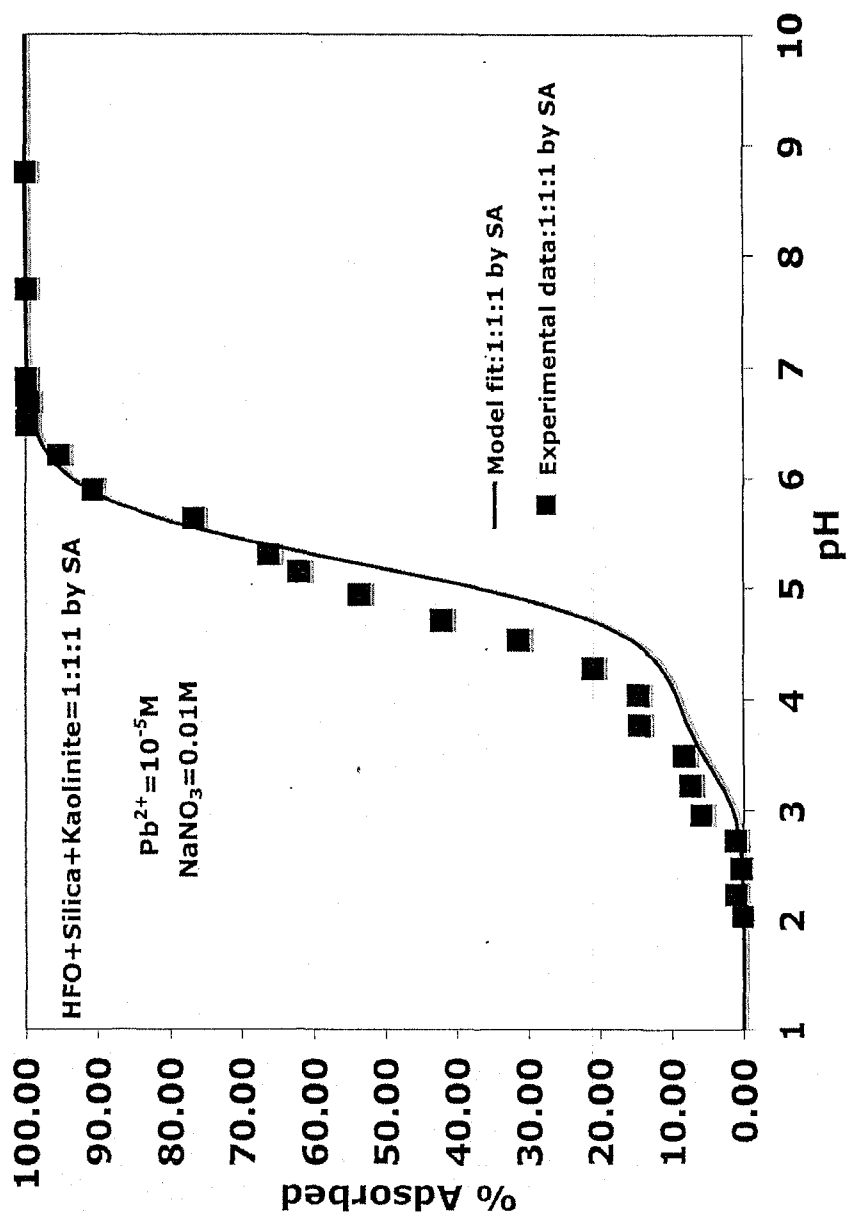


Figure 4.40. Model fit for 1:1:1 by surface areas with  $10^{-5} M Pb$  in  $0.01 M NaNO_3$ .

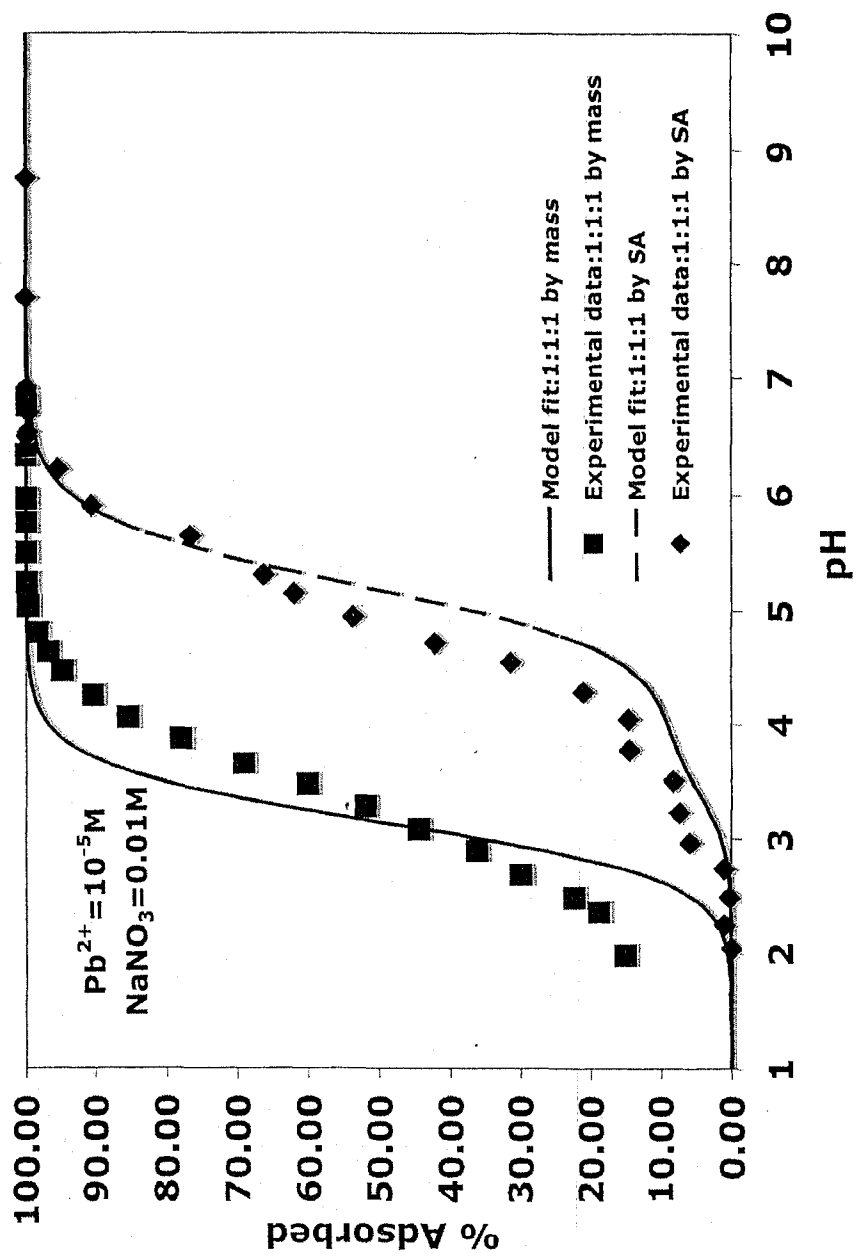


Figure 4.41. Model fit for ternary system for all ratios with  $10^{-5} M$  Pb in  $0.01 M$   $NaNO_3$ .

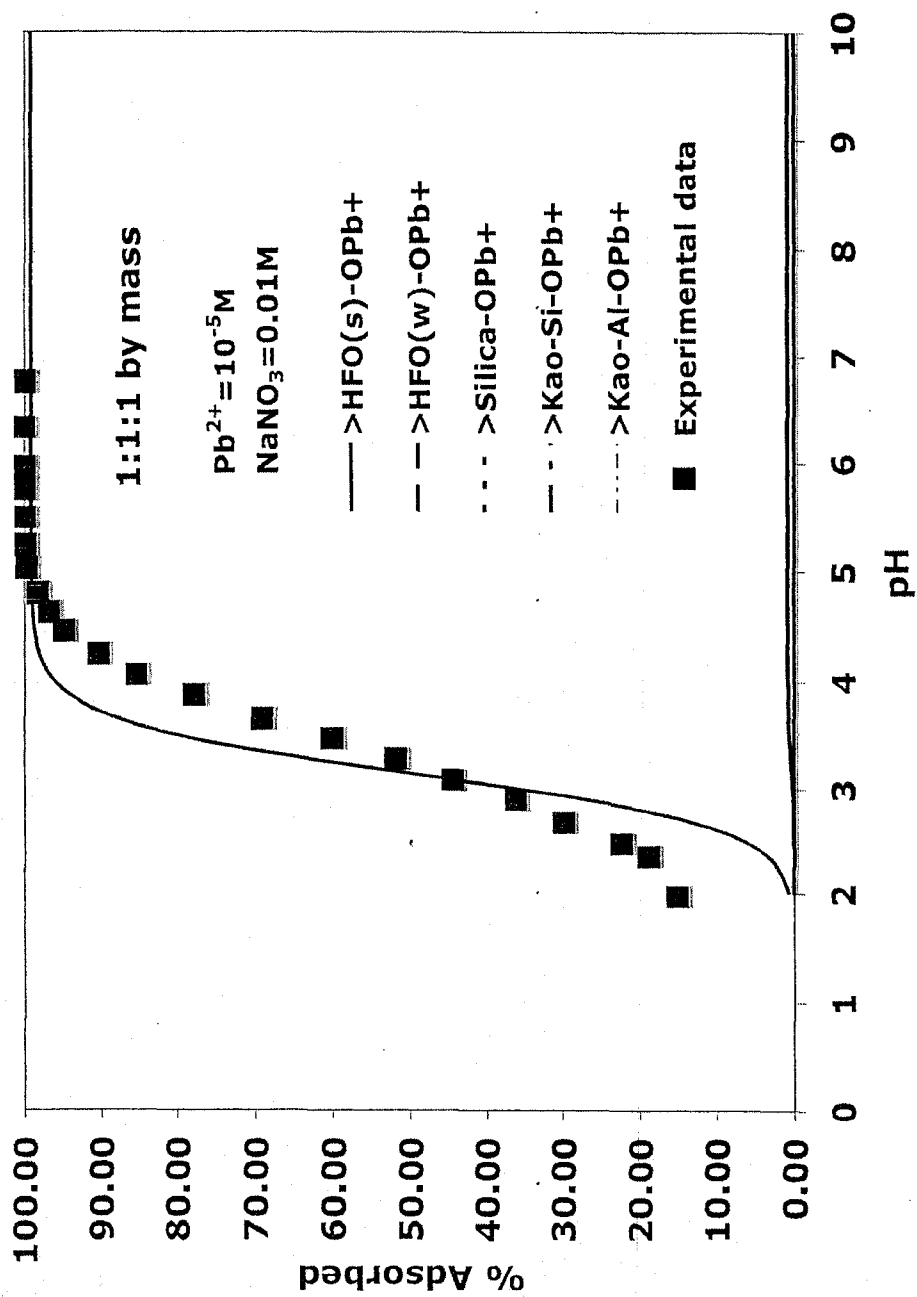


Figure 4.42. Percentage of adsorbed Pb species for a 1:1:1 mixture by mass.

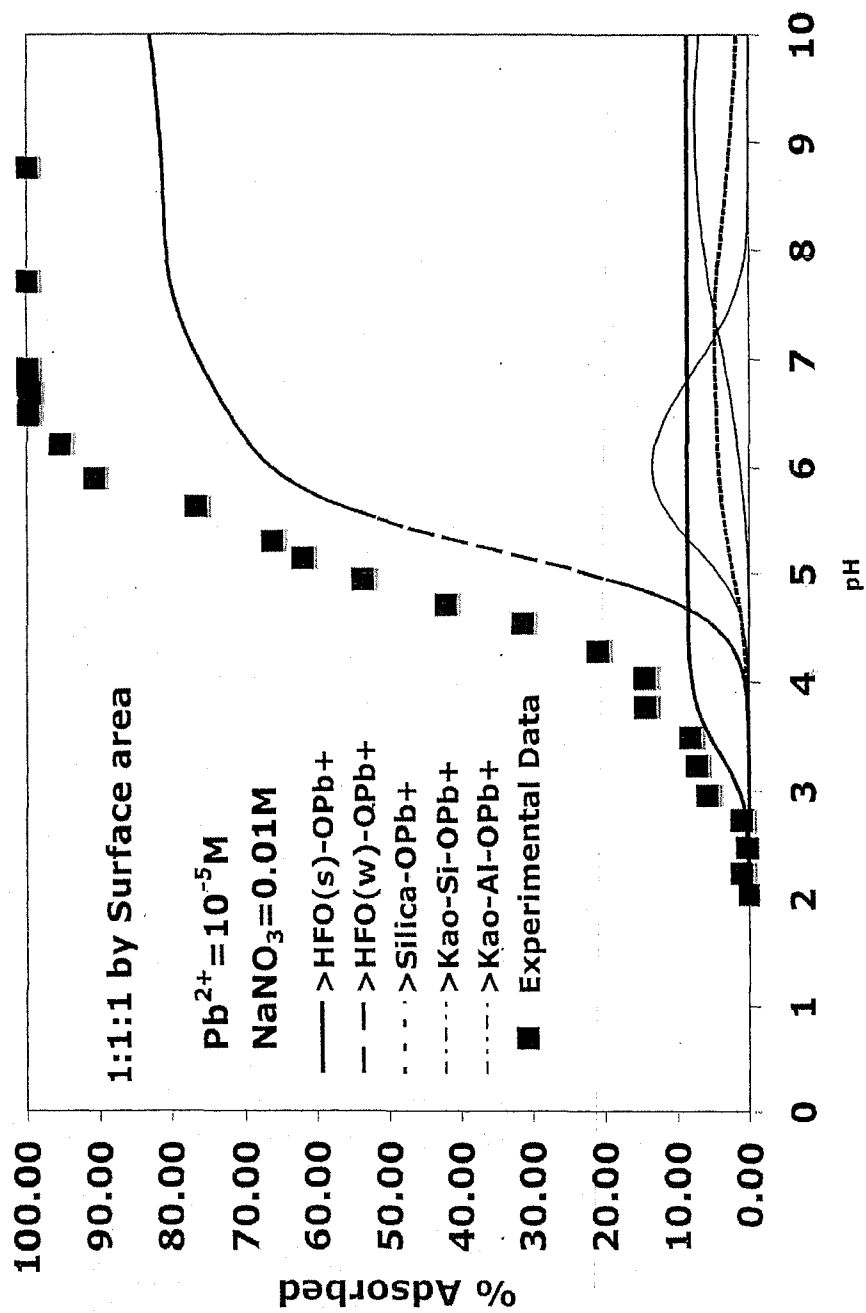


Figure 4.43. Percentage of adsorbed Pb species for a 1:1:1 mixture by surface area.

## CHAPTER V

## SUMMARY AND CONCLUSION

Lead is one of the toxic metals that can cause many human health problems, not only in children, but also in adults. In the United States, children age six or under are the most seriously effected victims according to the EPA and NHANES (Schwartz, 1994); see also Chapter 1). So, undoubtedly it is very important to understand the fate and transport of lead in natural systems, especially in soils and ground waters. It has been proven that the toxicity of heavy metals, including lead, is typically greatest when the metals are present as uncomplexed or free ions in solution. Metal toxicity typically decreases as metals become complexed with organic compounds, bind to surfaces (i.e. are adsorbed) or become lattice bound or co-precipitated (Allen et al., 1980; Anderson et al., 1990). Because adsorption plays a major role in determining both the toxicity and the potential mobility of toxic metals such as Pb, it is important to quantify how environmental factors including pH, Eh, solution composition and temperature impact lead and heavy metal adsorption.

Surface Complexation Models (SCMs) have been shown to predict the adsorption behavior of sorbates like Pb on many environmentally-relevant sorbents (e.g. HFO, clays, aluminosilicates) better than more empirical approaches (e.g., partition coefficient, Langmuir isotherms, Freundlich isotherms, etc) (Bethke and Brady, 1999; Domenico and Schwartz, 1998). Nonetheless, hydrogeologists often rely on simple partition coefficients ( $K_d$  values) to explain the movement of metals through ground water aquifers. This approach is typically used because it works very well with non-ionized organic molecules, is mathematically simple to apply and there is a lack of relevant

thermodynamic surface complexation data to describe natural systems (Stumm and Morgan, 1996). Unfortunately, however, there are many problems with using the  $K_d$  approach for describing metal speciation in the environment. For example, this approach cannot account for saturation effects, mass balance, competing ions, changes in solution composition, etc, which can cause inaccurate predictions of metal speciation and predictions of metal bioavailability and mobility (Davis and Kent, 1990; Domenico and Schwartz, 1998; Bethke and Brady, 1999).

Because the empirical approaches do not always provide accurate assessments of the variability, mobility and availability of metals in an aquifer, thermodynamically based surface complexation methods have been developed to quantify adsorption (Davis and Kent, 1990; Dzombak and Morel, 1990). The SCM approach is capable of predicting metal adsorption behavior on mineral surfaces as a function of pH, solute concentrations and ionic strength of electrolytes in well controlled laboratory experiments (Dzombak and Morel, 1990, Hayes et al., 1991). However, a problem with the SCM approach is that although there are many previous studies, which have accounted for the adsorption of various metals on pure mineral phases, very few studies have assessed adsorption of metals on mixed mineral assemblages. Other problems associated with applying SCMs to natural sediments are typically a lack of data regarding the nature and the numbers of mineral phases that are present in any given natural system (Padmanabhan and Mermut, 1996). Natural systems are much more complex than typical, single solid experimental systems and moreover mineral surfaces may contain a wide variety of different functional groups. In addition, the composition of aqueous solutions in natural systems is typically more complex than in experimental systems, which can make it more difficult to predict

intrinsic stability constants for surface reactions for sediment surfaces when they depend on solution parameters such as electrolyte composition or ionic strength (Davis et al., 1998). To develop surface complexation models that can accurately predict adsorption under both laboratory and natural conditions, it is first necessary to show that single solid SCM parameters can be used to model simple mineral assemblages. If this can be shown, then to apply SCMs to natural systems will require estimates of (a) the composition of natural mineral assemblage surfaces, including surface areas and densities of various surface functional groups, and (b) mass law and mass balance equation for the minerals within the assemblage which significantly influence metal adsorption on the mixture (Davis et al., 1998).

The primary goal of this study was to test whether Pb adsorption on well controlled model mixtures of environmentally-relevant solids could be modeled as a function of pH and total Pb concentration using the component additivity SCM approach. Thus, adsorption of lead was quantified not only on single mineral phases, but also on binary and ternary mixtures of solids. Pure HFO, silica and kaolinite were chosen as the single mineral phases, because these three phases are common constituents of natural soils and sediments. Measured adsorption edges for the single solid systems showed that HFO is by far the strongest adsorbent for Pb of the three phases chosen for study at all measured pH values. Adsorption of Pb is not affected significantly by changes in ionic strength from 0.001 to 0.1 M for HFO, but a strong ionic strength dependence, with decreasing Pb adsorption at higher ionic strength, is noted for silica and kaolinite. This suggests that Pb forms strong inner-sphere complexes on HFO surfaces and weaker complexes on both silica and kaolinite. Good model fits to the experimental data for pure solid systems could

be achieved using a DLM calibrated with the individual adsorption edges. The HFO/Pb system was modeled with the 2-site model proposed by Dzombak and Morel (1990). However, to accurately represent the experimental results of this study, the log stability constant for Pb adsorbing on the strong site had to be changed from 4.65 to 5.87. This change produces an excellent fit to all the experimental edges (with varying sorbate/sorbent ratio and ionic strengths). Silica data have been modeled satisfactorily using the single site DLM proposed by Sverjensky and Sahai (1996), although the model ionic strength dependence was somewhat less than observed experimentally. Pb on kaolinite data has been modeled using a 2-site model based on that proposed by Benyahya and Garnier (1999), with a deprotonating silanol site and an amphoteric aluminol site. This again produces a satisfactory fit to the experimental data, except for data at  $\text{pH} < 4$  for  $10^{-6}$  M Pb and an ionic strength of 0.01 M.

Results of the binary system experiments showed that a very small amount of HFO has a strong influence on Pb adsorption. Increasing either silica or kaolinite in the system shifts the adsorption edges towards the pure silica or kaolinite systems, respectively. However, edges measured for 500:1 or 5000:1 ratios of kaolinite or silica to HFO never reach the pure silica or kaolinite edges. Ternary systems also showed preference of Pb adsorption for HFO surfaces compared to the other two minerals.

A significant goal of this study was to model the experimental datasets for the mixed system using a component additivity approach based on the thermodynamic stability constants derived for the single mineral systems. Predicted adsorption edges using this approach for the binary mixtures containing HFO and silica are in excellent agreement with experimental data. Fits are less impressive when kaolinite is present in the system.

This might reflect that the model proposed for this study is not sufficiently robust. Further study could be completed using an ion exchange site (not variable charge) to see if fits for the binary systems are improved. Although the simple component additivity model can predict data for the 1:1 systems containing kaolinite reasonably well, as the amount of kaolinite relative to HFO or silica increases, the fits became poorer. This adsorption behavior cannot be explained by the fact that the clay minerals like kaolinite, coated over the surfaces of HFO and silica, decreasing the available sites for adsorption, as proposed by Honeyman (1984). Actually, results of this study showed the reverse effect. Although the cause of this behavior is not entirely clear, one difficulty is indicated by the pure kaolinite model. For pure kaolinite at 0.01 M  $\text{NaNO}_3$  and  $10^{-5}$  M Pb, the same conditions used for the binary and ternary mixtures, the SCM used in this study overpredicts Pb sorption a bit, especially at mid-pH, so this might be the source of overpredictions in binary and ternary systems with kaolinite. However, the underpredictions at high kaol/HFO require a different explanation. Perhaps the kaolinite modeling is not adequate in this study. To properly model the data, this study might need an ion exchange site on kaolinite. At lower pH value, the prediction of Pb adsorption cannot be modeled properly using variable charge site for lower Pb concentration. So, presumably, this might be the source of these mismatches of experimental data and model fit.

Nonetheless, predicted edges using the simple component additivity approach are quite reasonable for ternary assemblages. In systems comprised of 1:1:1 silica:kaolinite:HFO by either mass or surface area, the HFO dominated Pb adsorption in the system. HFO surfaces played a major role in adsorbing Pb at any given pH in the ternary

mixtures. For a ternary mixture with a ratio 1:1:1 by mass, most of the Pb was predicted to adsorb onto the strong site. Contributions from the other surface sites from other solids (even the weak site of HFO) do not have any significant influence on Pb adsorption at all for this mixture. This scenario changes when the 1:1:1 mixture by surface area is considered. Nonetheless, the influence of HFO was still prominent. However, for this mixture, most of the adsorption occurred on the weak site instead of the strong site because of the larger quantity of Pb relative to the available HFO surface area. Contributions from the other solids remained insignificant.

From this study it can be concluded that if the single system has been studied well enough to derive adequate stability constants for the protonation, deprotonation, and metal adsorption reactions, then adsorption of Pb can be predicted reasonably well for mixed solid assemblages. Although the predictions are somewhat off when kaolinite is present in the system, it is still clear that the simple component additivity SCM approach could be an important first step for estimation of the adsorptive behavior of Pb in natural systems. Thus, this study should provide an excellent foundation for understanding the fate and transport of metal pollutants like Pb in the environment.

In particular, the results of this study could be applied to natural systems, which are mainly composed of iron oxides and hydroxides along with silica and clay minerals. If the mineralogy of the sediment is not known, and if there are many more mineral phases present, which also contribute significantly to Pb adsorption, then further work will be necessary to apply this approach. However, if the mineralogy of the sediments is well established, then this study could provide a foundation for testing predictions of adsorption for more complex systems. There are data for other single solid systems (e.g.

Pb adsorption on goethite, hematite, Mn oxides). Adding thermodynamic data derived for these and other single systems to speciation calculations, could provide an even more rigorous test of the component additivity approach. Future studies could be conducted using more complex mixtures (i.e. with more mineral phases, together with organic materials) of the most common naturally occurring substances in shallow soils and sediments to test whether the experimental data can be fitted well with this modeling approach. If this works well, then the next logical step would be to find natural sediment, containing many of the tested mineral phases, and conduct experimental adsorption experiments to see whether the results are similar to those for artificially created mineral assemblages. Future studies should also continue to compare model predictions from the generalized composite approach with those of the component additivity approach to determine the approach that works best for specific systems.

APPENDIX A: Adsorption of Pb HFO

$10^{-4}$  M in 0.01M NaNO<sub>3</sub> (Fig. 3.1)

pH	% Adsorbed
1.86	2.852852853
2.12	8.708708709
2.22	12.61261261
2.37	16.61661662
2.52	20.67067067
2.69	24.77477477
2.88	31.18118118
3.05	38.58858859
3.23	47.6976977
3.47	59.97497497
3.67	69.3043043
4	83.43843844
4.22	91.13613614
4.68	98.19119119
4.91	99.27127127
5.12	99.68518519
5.37	99.88488488
5.63	99.92692693
6.03	99.74524525
6.16	99.98748749
6.38	99.97147147

$10^{-5}$  M in 0.01M NaNO<sub>3</sub> (Fig. 3.1)

pH	% Adsorbed
1.94	14.92537313
2.2	28.35820896
2.32	35.5120947
2.58	49.81986619
2.75	57.19505919
2.85	63.21667524
3.07	75.16212043
3.35	86.52599074
3.66	94.1482244
3.84	96.43335049
4.07	98.30159547
4.27	99.1610911
4.44	99.45445188
4.67	99.79927946
4.81	99.92794647
4.97	99.89706639
5.23	99.95367988
5.44	99.96397324
5.73	99.9485332
6	99.88162635
6.52	99.91250643

APPENDIX A (Contd.): Adsorption of Pb on HFO

$10^{-6}$ M in 0.1M NaNO<sub>3</sub> (Fig. 3.1)

pH	% Adsorbed
2.1	0
2.28	0
2.51	0
2.99	39.31034483
3.38	75.41871921
3.53	82.90640394
4.01	95.89162562
4.27	97.87684729
4.67	99.02955665
4.96	99.63546798
5.16	99.44827586
5.17	99.59605911
5.12	99.42857143
5.55	99.62561576
6.52	99.66995074
6.7	99.54187192

$6.8 \cdot 10^{-7}$ M in 0.1M NaNO<sub>3</sub> (Fig. 3.1)

pH	% Adsorbed
2.14	0
2.28	6.600425834
2.4	20.72391767
2.51	28.60184528
2.63	38.26117814
2.77	48.33215046
2.9	57.11852378
2.99	64.18026969
3.14	73.6053939
3.29	80.24840312
3.46	88.53797019
3.6	92.53371185
3.73	94.86728176
3.88	96.78921221
3.98	97.53655075
4.12	98.40880057
4.25	98.90773598
4.38	99.25762952
4.51	99.46770759
4.62	99.64868701
4.78	99.82682754
4.86	100.1036196
4.99	99.9418027
5.1	99.97799858
5.34	99.91341377
5.65	100.0943932
5.74	99.94748048
6.02	100.0283889
6.25	99.98580554
6.66	100.0099361

APPENDIX A (Contd.): Adsorption of Pb HFO6.10<sup>-8</sup>M in 0.001M NaNO<sub>3</sub> (Fig. 3.1)

pH	% Adsorbed
2.15	0
2.4	29.13509061
2.57	45.98023064
2.72	56.44975288
2.85	69.12685338
2.96	74.70345964
3.1	83.36902801
3.23	88.76441516
3.4	93.26194399
3.55	96.0214168
3.68	97.59472817
3.84	98.46787479
3.98	99.41515651
4.08	98.24546952
4.23	99.9752883
4.4	100.0906096
4.55	99.63756178
4.68	100.0988468
4.86	100.2883031
5.51	100.7166392
5.7	100.3130148

APPENDIX B: Adsorption of Pb on silica

$10^{-5}$ M in 0.1M NaNO<sub>3</sub> (Fig. 3.2)

pH	% Adsorbed
2.18	3.179723502
2.44	0.046082949
3.05	2.488479263
3.37	2.304147465
3.74	3.686635945
4.1	4.423963134
4.3	2.995391705
4.48	3.963133641
4.67	5.253456221
4.83	5.299539171
5.09	6.589861751
5.29	10.36866359
5.43	13.41013825
5.72	18.29493088
5.92	21.38248848
6.15	27.83410138
6.34	30.46082949
6.53	38.70967742
6.81	54.30875576
7	64.43317972
7.33	79.83410138
7.39	80.83410138
7.89	93.47926267
8.27	97.35483871
8.85	98.47004608
9.41	97.70506912

$10^{-5}$ M in 0.01M NaNO<sub>3</sub> (Fig. 3.2)

pH	% Adsorbed
2.79	0
3.01	0
3.26	0
3.53	0
3.79	0
4.01	0
4.27	1.350649351
4.44	2.701298701
4.66	8.987012987
4.84	8.051948052
5.05	20.25974026
5.37	28.36363636
5.59	29.24675325
5.82	32.36363636
5.95	41.35064935
6.19	53.72467532
6.44	68.78961039
6.66	80.66493506
7.11	89.36103896
7.33	94.01558442
7.43	93.25714286
7.82	97.93246753
8.32	96.07272727
8.51	97.60519481
8.84	98.85194805

APPENDIX B (Contd.): Adsorption of Pb on silica $10^{-6}$ M in 0.01M NaNO<sub>3</sub> (Fig. 3.2)

pH	% Adsorbed
2.11	0
2.4	0
2.71	0
2.97	0
3.42	0
3.64	0
3.89	0.25
4.02	2.85
4.28	1.95
4.5	6
4.75	13.5
5.29	38.05
5.74	66.2
6.07	78.05
6.24	89.7
6.42	98.2
6.65	99.595
6.95	99.2
7.1	100
7.12	99.4
7.42	100
7.86	100
8.69	99.6
9	100

## APPENDIX C: Adsorption of Pb on Ward's kaolinite

 $10^{-4}$ M in 0.01M NaNO<sub>3</sub> (Fig. 3.3)

pH	% Adsorbed
1.92	5.695067265
2.08	7.174887892
2.24	8.340807175
2.46	8.430493274
2.62	8.385650224
2.84	9.282511211
2.99	9.820627803
3.14	9.417040359
3.33	3.901345291
3.49	11.92825112
3.79	12.91479821
4.04	12.33183857
4.16	16.14349776
4.35	21.92825112
4.56	18.16143498
4.7	32.33183857
4.83	30.76233184
4.9	34.84304933
5.06	38.92376682
5.17	44.03587444
5.22	45.69506726
5.56	54.03587444
6	66.78475336

 $10^{-5}$ M in 0.01M NaNO<sub>3</sub> (Fig. 3.3)

pH	% Adsorbed
1.97	0
2.18	0
2.32	0
2.46	0
2.69	0
2.86	0
3.01	0
3.17	0
3.35	0.079194652
3.49	-0.218071284
3.6	5.920763647
3.78	13.69458128
3.91	2.674971926
3.98	-7.019852361
4.16	2.819943291
4.25	14.50651299
4.49	19.66102512
4.7	21.32493175
4.74	19.90962551
4.86	32.61069562
4.9	60.60539414
5.05	36.30296991
5.1	48.13485703
5.23	46.62895046
5.37	100.0104983
5.53	88.69844889
5.75	84.90147783
5.88	75.49364573

APPENDIX C (Contd.): Adsorption of Pb on Ward's kaolinite $10^{-6}$ M in 0.01M NaNO<sub>3</sub> (Fig. 3.3)

pH	% Adsorbed
2.38	0
2.58	0
2.79	2.003462775
3.04	0
3.18	0
3.39	5.876678604
3.62	9.30378981
3.82	13.28325404
3.98	19.36988272
4.16	22.71062271
4.4	31.60297623
4.53	39.40208965
4.68	43.32208531
5.6	63.43880721
5.33	83.09489388
5.59	87.71098005
5.85	96.97812565
5.86	93.16914
6.47	99.57980342
6.5	99.76977672

APPENDIX D: Adsorption of Pb on KGa-1B

$10^{-5}$ M in 0.01M NaNO<sub>3</sub> (Fig. 3.4)

pH	% Adsorbed
4.28	5.452674897
4.76	18.05555556
4.91	22.83950617
5.09	30.86419753
5.38	41.92386831
5.57	49.09465021
5.85	56.84156379
5.93	60.32921811
6.17	65.58127572
6.3	73.47736626
6.5	78.93518519
6.68	87.04218107
6.8	94.69650206
6.97	91.13168724
7.42	97.96296296
7.95	99.45473251
9.25	99.55761317

$10^{-5}$ M in 0.1M NaNO<sub>3</sub> (Fig. 3.4)

pH	% Adsorbed
1.72	-1.936702881
1.99	3.589985829
2.25	3.873405763
2.48	0.472366556
2.8	0.708549835
3.07	-1.369863014
3.42	1.747756259
3.98	2.881435994
4.19	0.472366556
4.63	6.329711856
4.84	4.912612187
4.94	23.90174776
5.19	6.235238545
5.39	16.15493623
5.63	21.11478507
5.91	28.10581011
6.1	31.08171941
6.3	39.82050071
6.39	42.56022674
6.6	53.22153991
6.72	59.88663203
6.89	70.71799717
6.99	74.88899386
7.15	81.23287671
7.4	88.68682097
8.42	98.68682097

APPENDIX D (Contd.): Adsorption Pb on KGa-1B $10^{-6}$ M in 0.01M NaNO<sub>3</sub> (Fig. 3.4)

pH	% Adsorbed
2.1	0
2.33	6.610337972
2.46	6.013916501
2.72	7.157057654
3.01	9.890656064
3.26	12.32604374
4.03	17.94234592
4.08	17.64413519
4.42	25.4473161
4.8	40.00994036
5.14	55.61630219
5.4	67.69383698
5.65	80.0695825
5.81	88.22067594
6.06	93.14115308
6.27	97.41550696
6.5	98.06163022
6.61	97.96222664
6.7	97.6640159
6.96	98.35984095
7.03	98.50894632
7.29	98.45924453
8.25	98.75745527
8.93	98.80715706

APPENDIX E: Adsorption Pb on HFO+silica

1:1 (Fig. 3.10)

pH	% Adsorbed
2.08	17.22084367
2.3	23.27543424
2.46	29.13151365
2.69	35.23573201
2.84	45.75682382
3.04	54.54094293
3.21	61.99503722
3.46	73.55831266
3.66	82.39702233
3.85	89.20595533
4.06	93.82133995
4.26	97.23473945
4.57	99.9817469
4.84	100
5.06	100
5.36	100
5.37	100
5.55	100
5.74	100
5.98	100
6.24	100
6.5	100
6.84	100
7.28	100
7.57	100
7.88	100

5:1 (Fig. 3.10)

pH	% Adsorbed
1.92	1.032608696
2.14	3.043478261
2.35	4.347826087
2.6	13.85869565
2.77	16.95652174
2.92	20.70652174
3.11	27.66304348
3.3	37.11956522
3.5	44.89130435
3.74	57.29891304
3.91	65.96195652
4.07	74.81521739
4.29	83.30434783
4.49	89.74456522
4.67	95.1125
4.88	98.28043478
5.07	100
5.26	100
5.46	100
5.68	100
5.78	100
6.04	100
6.34	100
6.43	100
6.62	100
6.96	100
7.04	100
7.62	100

APPENDIX E (Contd.): Adsorption of Pb on HFO+silica

10:1 (Fig. 3.10)

pH	% Adsorbed
2.17	12.48058001
2.36	13.46452615
2.54	15.84671155
2.77	16.98601761
3.07	21.90574832
3.24	25.27187985
3.49	35.26670119
3.78	46.09010875
3.98	56.02278612
4.21	67.90264112
4.44	81.28948731
4.67	89.92749871
4.98	97.51734852
5.14	99.71838426
5.36	100
5.47	100
5.75	100
6.11	100
6.28	100
6.44	100
6.6	100
6.71	100
7.04	100
7.14	100
7.52	100
7.64	100
8.59	100

50:1 (Fig. 3.10)

pH	% Adsorbed
2.17	4.764173416
2.34	4.525964745
2.55	6.241067175
2.79	4.764173416
3.05	8.051453073
3.29	7.146260124
3.56	10.62410672
3.8	14.38780372
4.02	18.67555979
4.24	20.86707956
4.53	29.20438304
4.76	37.44640305
4.89	42.68699381
5.06	52.31062411
5.28	64.35921868
5.45	74.68794664
5.7	85.57884707
6.04	95.56407813
6.34	98.95378752
6.62	100
6.92	100
7.06	100
7.32	100
7.57	100
7.84	100
8.47	100
8.98	100

## APPENDIX E (Contd.): Adsorption of Pb on HFO+silica

100:1 (Fig. 3.10)

pH	% Adsorbed
2.25	5.507246377
2.37	4.782608696
2.54	6.280193237
2.81	2.512077295
3.04	1.884057971
3.28	3.913043478
3.52	8.647342995
3.75	12.12560386
4	13.57487923
2.24	18.30917874
4.51	24.25120773
4.67	28.01932367
4.8	33.09178744
4.97	43.8647343
5.12	52.16908213
5.26	57.16908213
5.64	75.83574879
5.97	88.65700483
6.17	96.55555556
6.88	99.83961353
6.91	100
7.19	100
7.41	100
7.71	100
7.95	100
8.38	100
8.75	100
9.05	100

500:1 (Fig. 3.10)

pH	% Adsorbed
2.2	3.582554517
2.44	0.778816199
2.71	0.830737279
2.96	-0.882658359
3.25	3.478712357
3.53	2.699896158
3.8	4.880581516
4.05	10.33229491
4.27	6.386292835
4.62	13.34371755
4.88	26.22014538
5.07	25.18172378
5.24	33.33333333
5.45	49.31983385
5.62	56.51090343
5.87	67.40913811
6.12	77.1443406
6.41	86.76531672
6.55	92.34683281
6.78	95.41069574
6.88	96.24974039
6.95	97.28400831
6.99	97.63499481
7.41	99.11214953
8.13	99.89839045
8.51	100
8.95	100

APPENDIX F: Adsorption of Pb on HFO+KGa-1B

1:1 (Fig. 3.11)

pH	% Adsorbed
2.08	9.305689489
2.25	14.12729026
2.4	16.34522662
2.56	22.37222758
2.69	25.40983607
2.81	30.52073288
2.95	36.06557377
3.03	39.72999036
3.23	50.72324012
3.42	60.72324012
3.62	71.96239151
3.77	79.30568949
4.02	87.58437801
4.23	93.21600771
4.37	95.41947927
4.54	97.28061716
4.75	98.56316297
5.01	99.56605593
5.18	99.66730955
5.37	99.9710704
5.87	100
6.1	100
6.4	100

5:1 (Fig. 3.11)

pH	% Adsorbed
2.07	12.83075387
2.29	14.82775836
2.46	15.22715926
2.67	17.62356465
2.9	22.01697454
3.14	29.10634049
3.25	31.60259611
3.42	38.39241138
3.7	47.07938093
3.97	59.05641538
4.16	67.61857214
4.36	77.01947079
4.71	89.30604094
5.07	96.67998003
5.21	98.41238143
5.43	98.98652022
5.73	99.85022466
6.02	99.98502247
6.4	100
6.63	100
6.9	100
7.06	100
7.26	100
7.31	100
7.6	100
7.66	100
8.02	100
8.48	100

## APPENDIX F (Contd.): Adsorption of Pb on HFO+KGa-1B

10:1 (Fig. 3.11)

pH	% Adsorbed
2.12	4.849084612
2.32	8.461157843
2.58	9.945571499
2.83	13.7060861
3.08	18.30776843
3.22	23.60217714
3.63	36.96190005
3.9	47.50123701
4.17	60.93023256
4.45	71.99901039
4.72	82.69173676
5.01	90.0544285
5.16	94.71548738
5.38	98.06036616
5.61	99.41613063
5.92	99.75754577
6.17	99.95051954
6.31	100
6.46	100
6.71	100
6.9	100
6.98	100
6.99	100
7.25	100
7.56	100
7.77	100
8.62	100

50:1 (Fig. 3.11)

pH	% Adsorbed
2	0.989068194
2.56	5.361790734
2.98	12.64966163
3.16	13.84695471
3.25	16.34565331
3.46	18.89640812
3.73	26.18427902
4.02	35.03383654
4.5	52.77459656
4.81	69.02134305
5.02	76.70484123
5.25	87.72514315
5.53	94.28422697
5.8	97.96980739
6.05	99.62519521
6.37	100
6.63	100
6.97	100
7.03	100
7.12	100
7.45	100
7.5	100
7.75	100
8.05	100
8.87	100
9	100
9.07	100
9.63	100

APPENDIX F (Contd.): Adsorption of Pb HFO+KGa-1B

100:1 (Fig. 3.11)

pH	% Adsorbed
2.02	6.666666667
2.59	10.95238095
2.95	15.0952381
3.12	15.57142857
3.36	20.0952381
3.66	24.23809524
4.05	33.14285714
4.25	39.95238095
4.58	49.33333333
4.87	62.18095238
5.09	74.90952381
5.27	81.67619048
5.44	87.04285714
5.66	94.66190476
5.96	98.43333333
6.21	99.65714286
6.33	99.63809524
6.53	100
6.8	100
6.87	100
6.93	100
6.94	100
7.02	100
7.09	100
7.25	100
7.54	100
8.62	100
9.47	100

500:1 (Fig. 3.11)

pH	% Adsorbed
2.12	5.424409844
2.57	10.14565545
3	13.41034656
3.32	20.24108488
3.57	23.45554997
3.85	30.73832245
4.28	41.58714214
4.61	53.93269714
4.89	66.55449523
5.08	76.12757408
5.27	82.15971873
5.57	88.97538925
5.88	95.90155701
6.18	99.24660974
6.36	99.66348569
6.48	99.95981919
6.89	100
7.11	100
7.3	100
7.36	100
7.46	100
7.63	100
7.93	100
8.25	100
8.5	100
8.9	100
9.34	100
9.81	100

APPENDIX F (Contd.): Adsorption of Pb on HFO+KGa-1B5000:1 (Fig.3.11)

pH	% Adsorbed
1.88	2.315047811
2.05	2.667337695
2.4	4.277805737
2.79	7.347760443
3.02	8.505284348
3.58	9.612481127
3.79	12.02818319
4.09	16.55762456
4.3	20.68444892
4.45	30.24660292
4.64	38.75188727
4.9	48.86763966
5.09	56.09964771
5.26	62.09864117
5.29	78.25868143
5.34	64.83643684
5.65	75.18369401
5.92	83.2259688
6.15	88.78711626
6.37	94.92702567
6.44	96.13990941
6.63	98.25868143
6.74	98.97332662
6.76	98.93809763
6.8	99.12934071
6.89	99.01358832

APPENDIX G: Adsorption of Pb on KGa-1B+silica

1:1 (Fig. 3.12)

pH	% Adsorbed
3.06	8.172147002
3.32	11.31528046
3.58	11.41199226
3.84	12.08897485
4.12	18.23017408
4.36	24.22630561
4.64	26.25725338
4.94	35.25145068
5.15	41.2959381
5.37	51.73597679
5.6	60.94294004
5.88	70.07736944
6.15	79.57930368
6.16	81.31044487
6.45	95.10154739
6.54	95.46421663
6.64	96.70938104
6.78	98.53094778
6.87	97.40377176
7	97.49081238
7.12	99.04110251
7.41	98.87137331
8.12	100
8.52	99.84932302

10:1 (Fig. 3.12)

pH	% Adsorbed
3.04	8.727272727
3.34	11.22077922
3.59	13.24675325
3.87	15.84415584
4.12	23.01298701
4.41	27.22077922
4.68	31.42857143
4.94	44.83116883
5.1	45.71428571
5.27	54.15064935
5.58	64.28051948
5.84	73.88051948
6.31	81.79220779
6.51	86.13506494
6.73	92.95064935
6.99	94.4987013
7.18	96.1974026
7.23	97.03376623
7.33	97.57142857
7.41	97.61038961
7.57	98.50493506
7.81	99.35168831
8.29	100
8.84	100
9.17	99.98126234
9.46	99.90846753
9.71	100
10	100

## APPENDIX G (Contd.): Adsorption of Pb on KGa-1B+silica

50:1 (Fig. 3.12)

pH	% Adsorbed
3.11	8.937437934
3.36	10.72492552
3.63	15.69016882
3.89	16.88182721
4.19	21.49950348
4.45	24.52830189
4.77	35.60079444
4.95	41.36047666
5.09	48.16285998
5.23	53.34657398
5.52	63.30188679
5.69	71.67328699
6.02	79.83614697
6.28	88.54021847
6.4	97.9652433
6.65	98.13108242
6.81	92.53723932
6.94	96.50446872
6.95	94.30983118
7.22	97.24925521
7.3	98.11569017
7.38	99.05412115
7.6	99.63743793
8.42	100
8.91	99.98127607
9.12	100
9.44	100
9.74	100

0.1:1 (Fig. 3.12)

pH	% Adsorbed
2.59	0.688637482
3.11	0.836202656
3.36	-1.032956222
3.63	0.63944909
3.92	2.213477619
4.21	3.344810625
4.44	2.852926709
4.82	5.017215937
4.98	11.90359075
5.22	17.31431382
5.38	17.41269061
5.88	29.31628136
6.15	33.84161338
6.26	37.7766847
6.28	37.92424988
6.68	61.11657649
6.87	67.79636006
6.99	74.12690605
7.05	74.648303
7.07	74.10723069
7.11	79.47368421
7.14	79.16871618
7.19	79.09985243
7.23	80.30496803
8.44	98.99754058
8.62	99.57678308
9.05	99.56040334
9.26	99.37088047

APPENDIX G (Contd.): Adsorption of Pb on KGa-1B+silica

0.02:1 (Fig.3.12)

pH	% Adsorbed
3.06	-5.706666667
3.27	-2.186666667
3.57	-7.093333333
3.8	-4.8
4.02	-1.92
4.2	0
4.54	4.586666667
4.78	9.066666667
4.99	13.33333333
5.17	16.74666667
5.53	56.43733333
5.58	25.54666667
5.73	37.17333333
6.24	61.68
6.78	87.168
6.85	96.78506667
7	95.52213333
7.29	94.71946667
7.4	97.3408
7.46	99.26666667
7.71	99.44053333
7.96	100
8.43	100
8.63	99.23946667
9.02	99.71152
9.28	99.70501333
9.45	99.60165333

APPENDIX H: Adsorption of Pb HFO+KGa-1B+silica

1:1:1 by mass (Fig. 3.13)

pH	% Adsorbed
1.98	15.0617284
2.36	18.81481481
2.48	22.32098765
2.68	29.87654321
2.89	36.19753086
3.08	44.39506173
3.28	51.81234568
3.47	60.06419753
3.65	69.01728395
3.87	77.85679012
4.06	85.35308642
4.25	90.35555556
4.46	94.86419753
4.63	96.78518519
4.8	98.30024691
5.03	99.71432099
5.23	99.89051852
5.49	100
5.75	100
5.96	100
6.33	100
6.75	100
6.77	100

1:1:1 by surface area (Fig. 3.13)

pH	% Adsorbed
2.04	0
2.24	1.018848701
2.48	0.254712175
2.73	1.018848701
2.96	5.858380031
3.23	7.335710647
3.5	8.252674478
3.77	14.46765155
4.04	14.56953642
4.28	20.9373408
4.54	31.32959755
4.71	42.12939379
4.94	53.64238411
5.14	61.95109526
5.3	66.18441161
5.63	76.61232807
5.89	90.61640346
6.21	95.44625573
6.48	100
6.52	99.83876719
6.69	99.68665308
6.75	100
6.82	100
6.89	100
6.9	100
7.7	100
8.75	100

## BIBLIOGRAPHY

- Adriano, D.C., 2001, Trace Elements in Terrestrial Environments; Biogeochemistry, Bioavailability and Risk of Metals, Springer-Verlag, New York.
- Allen, H.E., Hall, R.H., and Brisbin T., D., 1980, Environmental Science and Technology, v.14, p.441-443.
- Anderson, P.R., and Benjamin M.M., 1990, Surface and Bulk Characteristics of Binary Oxide suspensions, Environmental Science and Technology, v.24, p.692-698.
- Anderson, W.C., 1993, Innovative site remediation technology: Soil washing/soil flushing, v.3, WASTECH, American Academy of Environmental Engineers, Annapolis, MD.
- Angove, M.J., Johnson, B.D., and Wells, J.D., 1998, The Influence of Temperature on the Adsorption of Cadmium (II) and Cobalt (II) on Kaolinite, Journal of Colloid and Interface Science, v.204, p.93-103.
- Appelo, C.A.J., Vander Weiden, M.J.J., Tournasaat, C., and Charlet, L., 2002, Surface complexation of ferrous iron and carbonate on ferrihydrite and mobilization of arsenic, Environmental Science and Technology, v.36, p.3096-3103.
- Baldwin, D.R., and Marshall, W.J., 1999, Heavy metal poisoning and its laboratory investigation, Annals of Clinical Biochemistry, Review article, v.36, p.267-300.
- Bancroft, G.M. and Hyland M.M., 1990, Spectroscopic studies of adsorption/reduction reactions of aqueous metal complexes on sulfide surfaces, In: M.F. Hochella and A.F. White (ed.), Mineral-water interface geochemistry, Reviews in mineralogy, Mineralogical Society of America, v.23, p.511-558.
- Barnett, M.O., Jardine, P.M., and Brooks, S.C., 2002, U(VI) Adsorption to Heterogeneous Subsurface Media: Application of a Surface Complexation Model, Environmental Science and Technology, v.36, p.937-942.
- Benjamin, M.M., Hayes, K.F. and Leckie, J.O., 1982, Removal of toxic metals from power-generation waste streams by adsorption and coprecipitation, Journal of Water Pollution Control Federation, v.54, p.1472-1481.
- Benschoten, J.E.V., Young, W.H., Matsumoto, M.R., and Reed, B.E., 1998, A Nonelectrostatic Surface Complexation Model for Lead Sorption on Soils and Mineral Surfaces, Journal of Environmental Quality, v.27, p.24-30.

- Benyahya, L. and Garnier, J.M., 1999, Effect of Salicylic Acid upon Trace-Metal Sorption ( $\text{Cd}^{\text{II}}$ ,  $\text{Zn}^{\text{II}}$ ,  $\text{Cu}^{\text{II}}$  and  $\text{Mn}^{\text{II}}$ ) onto Alumina, Silica, and Kaolinite as a Function of pH, *Environmental Science and Technology*, v.33, p.1398-1407.
- Bertsch, P.M. and Seaman, J.C., 1999, Characterization of complex mineral assemblages: Implication for contaminant transport and environmental remediation, *Proceeding of National Academy of Sciences, USA*, colloquium paper, v.96, p.3350-3357.
- Bethke, C.M. and Brady, P.V., 1999, How  $K_d$  Approach Undermines Ground Water Cleanup, *Ground Water*, v.38, n.3, p.435-443.
- Bodek, I., Lyman, W.J., Reehl, W.F., and Rosenblatt, D.H., 1988, *Environmental Inorganic Chemistry: Properties, Processes and Estimation Methods*, Pergamon Press, Elmsford, NY.
- Borden, D. and Giese, R.F., 2001, Baseline Studies of the Clay Minerals Society Source Clays: Cation Exchange Capacity Measurements by the Ammonia-Electrode Method, *Clays and Clay Minerals*, v.49, n.5, p.444-445.
- Borggaard, O.K., Jorgensen, S.S., Moberg, J.P., 1990, Influence of organic matter on phosphate adsorption by aluminium and iron oxides in sandy soils, *Journal of Soil Science*, v.41, p.443-449.
- Brady, N.C., 1984, *The nature and properties of soils*, 9<sup>th</sup> ed, Macmillan Publication Company, New York.
- Brady, P.V., Cygan, R.T., and Nagy, K.L., 1996, Molecular Controls on Kaolinite Surface Charge, *Journal of Colloid and Interface Science*, v.183, p.356-364.
- Brody, D.J., Prikle, J.L., Kramer, R.A., Flegal, K.M., Matte, T.D., Gunter, E.W., and Paschall, D.C., 1994, Blood Lead Levels in the US Population, *Journal of the American Medical Association*, v.274, n.4, p.277-283.
- Brown, P.L. and Markich, S.J., 2000, Evaluation of the Free Ion Activity Model of Metal-Organism Interaction: Extension of the Conceptual Model, *Aquatic Toxicology*, v.51, p.177-194.
- Brunauer, S., Emmett, P.H., and Teller, E., 1938, Adsorption of gases in multimolecular layers, *Journal of Physical Chemistry*, v.60, p.309-319.
- Carroll-Webb, S.A. and Walther, J.V., 1988, A surface complex reaction model for the pH-dependence of corundum and kaolinite dissolution rates, *Geochimica et Cosmochimica Acta*, v.52, p.2609-2623.

- Chantawong, V., Harvey, N.W., and Bashkin, V.N., 2003, Comparison of Heavy Metal Adsorptions by Thai Kaolin and Ball Clay, *Water, Air and Soil Pollution*, v.148, p.111-125.
- Chen, C.C., Coleman, M.L., and Katz, L.E., 2005, Bridging the Gap between Macroscopic and Spectroscopic Studies of Metal Ion Sorption at the Oxide/Water Interface: Sr(II), Co(II) and Pb(II) Sorption to Quartz, *Environmental Science and Technology*, v.40, n.1, p.142-148.
- Christl, I. and Kretzschmar, R., 1999, Competitive sorption of copper and lead at the oxide-water interface: Implications for surface site density, *Geochimica and Cosmochimica Acta*, v.63, n.19/20, p.2929-2938.
- Cornell, R.M. and Schwertmann, U., 1991, *Iron oxides in the Laboratory, Preparation and Characterization*, VCH, New York.
- Coston, J.A., Fuller, C.C., and Davis, J.A., 1995, Pb<sup>2+</sup> and Zn<sup>2+</sup> adsorption by a natural aluminum- and iron-bearing surface coating on an aquifer sand, *Geochimica and Cosmochimica Acta*, v.59, n.17, p.3535-3547.
- Coughlin, B.R. and Stone, A.T., 1995, Nonreversible Adsorption of Divalent Metal Ions (Mn<sup>II</sup>, Co<sup>II</sup>, Ni<sup>II</sup>, Cu<sup>II</sup>, and Pb<sup>II</sup>) onto Goethite: Effects of Acidification, Fe<sup>II</sup> Addition, and Picolinic Acid Addition, *Environmental Science and Technology*, v.29, p.2445-2455.
- Cowan, C.E., Zachara, J.M., Smith, S.C., and Resch, C.T., 1992, Individual Sorbent Contributions to Cadmium Sorption on Ustisols of Mixed Mineralogy, *Soil Science Society of America Journal*, v.56, p.1084-1094.
- Craw, D., Chappel, D., Reay, A., 1999, Environmental mercury and arsenic sources in fossil hydrothermal systems, Northland, New Zealand, *Environmental Geology*, v.39, no.8, p.875-887.
- Davis, J.A. and Hem, J.D., 1989, The surface chemistry of aluminum oxides and hydroxides, In: *The environmental Chemistry of Aluminum*, G.A. Sposito (ed), CRC press, Boca Raton, FL, p.185-289.
- Davis, J.A. and Kent, D.B., 1990, Surface complexation modeling, In: M.F. Hochella and A.F. White (ed.), *Mineral-water interface geochemistry*, Reviews in mineralogy, Mineralogical Society of America, v.23, p.177-260.
- Davis, J.A., Coston, J.A., Kent, D.B., and Fuller C.C., 1998, Application of the Surface Complexation Concept to Complex Mineral Assemblages, *Environmental Science and Technology*, v.32, p.2820-2828.

- Domenico, P.A. and Schwartz, F.W., 1998, *Physical and Chemical Hydrology*, 2<sup>nd</sup> ed, Wiley, New York.
- Dixit, S. and Van Cappellen, P., 2002, Surface chemistry and reactivity of biogenic silica, *Geochimica et Cosmochimica Acta*, v.66, n.14, p.2559-2568.
- Dyer, J.A., Trivedi, P., Scrivner, N.C., and Sparks, D.L., 2003, Lead Sorption onto Ferrihydrite 2, *Surface Complexation Modeling, Environmental Science and Technology*, v.37, p.915-922.
- Dzombak, D.A. and Morel, F.M.M., 1987, Adsorption of inorganic pollutants in aquatic systems, *Journal of Hydraulic Engineering*, v.113, p.430-475.
- Dzombak, D.A. and Morel, F.M.M., 1990, *Surface Complexation Modeling, Hydrous Iron Oxide*, Wiley.
- Elzinga, E.J., and Sparks, D.L., 2002, X-ray adsorption spectroscopy study of the effects of pH and ionic strength on Pb(II) sorption to amorphous silica, *Environmental Science and Technology*, v.36, p.4352-4357.
- Evanko, R.C. and Dzombak, D.A., 1997, *Remediation of Metals-Contaminated Soils and Groundwater, Technology Evaluation Report, Ground-Water Remediation Technologies Center, Series TE-97-01*, p.1-61.
- Evans, L.J., 1989, Chemistry of Metal Retention by Soils, *Environmental Science and Technology*, v.23, p.1046-1056.
- Ferris, A.P. and Jepson, W.V., 1975, The exchange capacities of kaolinite and the preparation of homoionic clays, *Journal of Colloid Interface Science*, v.51, p.245-259.
- Fetter, C.W., 1994, *Applied Hydrogeology, Third Edition*, Prentice Hall, Upper Saddle River, NJ 07458.
- Fuller, C.C., and Davis, J.A., 1989, Influence of coupling of sorption and photosynthetic processes on trace element cycles in natural waters, *Nature*, v.340, p.52-54.
- Fulton, J.R., McKnight, D.M., Foreman, C.M., Cory, R.M., Stedmon, C., and Blunt, E., 2004, Change in the fulvic acid redox state through the oxycline of a permanently ice-covered Antarctic lake, *Aquatic Sciences*, v.66, n.4, 27-46.
- Ganor, J., Cama, J., and Metz, V., 2003, Surface protonation data of kaolinite-reevaluation based on dissolution experiments, *Journal of Colloid and Interface Science*, v.264, p.67-75.

- Graveling, G.J., Ragnarsdottir, K.V., Allen, G.C., Eastman, J., Brady, P.V., Balsley, S.D., and Skuse, D.R., 1997, Controls on polyacrylamide adsorption to quartz, kaolinite, and feldspar, *Geochimica et Cosmochimica Acta*, v.61, n.17, p.3515-3523.
- GuhaMazumdar, D.N., Dasgupta, J., Chakraborty, A.K., Chatterjee, A., Das, D., and Chakraborty, D., 1992, Environmental Pollution and chronic arsenicosis in South Calcutta, *Bulletin WHO*, v.70, n.4, p.481-485.
- Gunneriusson, L., Lovgren, L., and Sjoberg, S., 1994, Complexation of Pb(II) at the goethite ( $\alpha$ -FeOOH)/water interface: The influence of chloride, *Geochimica et Cosmochimica Acta*, v.58, n.22, p.4973-4983.
- Hayes, K.F., 1987, Equilibrium, spectroscopic, and kinetic studies of ion adsorption at the oxide/aqueous interface, Ph.D. thesis, Stanford University, Stanford, CA.
- Hayes, K.F., Redden, G., Wendell, E., and Leckie, J.O., 1991, Surface complexation models: An evaluation of model parameter estimation using FITEQL and oxide mineral titration data, *Journal of Colloid Interface Science*, v.142, n.2, p. 448-469.
- Heidmann, I., Christl, I., and Kretzschmar, R., 2005, Sorption of Cu and Pb to kaolinite-fulvic acid colloids: Assessment of sorbent interactions, *Geochimica et Cosmochimica Acta*, v.69, n.7, p.1675-1686.
- Heidmann, I., Christl, I., Leu, C., and Kretzschmar R., 2005, Competitive sorption of protons and metal cations onto kaolinite: experiments and modeling, *Journal of Colloid and Interface Science*, v.282, p.270-282.
- Hochella, M.F., Jr. and White, A.F., 1990, Mineral water interface geochemistry, In *Mineralogical Society of America, Reviews in Mineralogy*, v.23, p.1-16.
- Hoffman, A., Pelletier, M., Michot, L., Stradner, A., Schurtenberger, P., and Kretzschmar, R., 2004, Characterization of the pores in hydrous ferric oxide aggregates formed by freezing and thawing, *Journal of Colloid and Interface Science*, v.271, p.163-173.
- Honeyman, B.D., 1984, Cation and anion adsorption at the oxide/solution interface in systems containing binary mixtures of adsorbents: An investigation of the concept of adsorptive additivity, Ph.D. thesis, Stanford University, Stanford, CA.
- Hizal, J., and Apak, R., 2006, Modeling of copper(II) and lead(II) adsorption on kaolinite-based clay minerals individually and in the presence of humic acid, *Journal of Colloid and Interface Science*, v.295, p.1-13.

- Huang, C.P., 1971, The chemistry of the aluminium oxide-electrolyte interface, Ph.D. thesis, Harvard University.
- Huang, C.P. and Stumm, W., 1973, Specific adsorption of cations on hydrous  $\gamma$ - $\text{Al}_2\text{O}_3$ , *Journal of Colloid and Interface Science*, v.43, p.409-420.
- Hudson, R.J. and Morel, F.M.M., 1993, Trace metal transport by marine microorganisms: Implication of metal coordination kinetics, *Deep-Sea Research*, v.40, p.129-150.
- Huertas, F.J., Chou, L., and Wollast, R., 1998, Mechanism of kaolinite dissolution at room temperature and pressure: Part 1. Surface speciation, *Geochimica et Cosmochimica Acta*, v.62, n.3, p.417-431.
- Hudson, R.J.M., 1998, Which aqueous species control the rates of trace metal uptake by aquatic biota? Observations and predictions of non-equilibrium effects, *Science Total Environment*, v.219, p.95-115.
- Ikhsan, J., Johnson, B.B., and Wells, J.D., 1999, A Comparative Study of the Adsorption of Transition Metals on Kaolinite, *Journal of Colloid and Interface Science*, v.217, p.403-410.
- Janusz, W., Patkowski, J., and Chibowski, S., 2003, Competitive adsorption of  $\text{Ca}^{2+}$  and  $\text{Zn}(\text{II})$  ions at monodispersed  $\text{SiO}_2$ /electrolyte solution interface, *Journal of Colloid and Interface Science*, v.266, p.259-268.
- Kehew, A.L., 2000, *Applied Chemical Hydrogeology*, Prentice Hall, Upper Saddle River, New Jersey.
- Kent, D.B., Tripathi, V.S., Ball, N.B., and Leckie, J.O., 1986, Surface-complexation modeling of radionuclide adsorption in sub-surface environments, Stanford Civil Engineering Tech, Report #294, Stanford, CA, also NUREG Report, CR-4897, SAND 86-7175 (1988).
- Koretsky, C.M., 2000, The significance of surface complexation reactions in hydrologic systems: a geochemist's perspective, *Journal of Hydrology*, v.230, p.127-171.
- Kovacevic, D., Pohlmeier, A., Ozbas, G., Narres, H.D., and Kallay, M.J.N., 2000, The adsorption of lead species on goethite, *Colloid and Surfaces, Physicochemical and Engineering Aspects*, v.166, p.225-233.
- Kraemer, S.M. and Hering J.G., 2004, Biogeochemical controls on the mobility and bioavailability of metals in soils and groundwater, *Aquatic Sciences*, v.66, p.1-2.

- Lackovic, K., Wells, J.D., Johnson, P.B., and Angove, M.J., 2004, Modeling the adsorption of Cd(II) onto kaolinite and Mulloorina illite in the presence of citric acid, *Journal of Colloid and Interface Science*, v.270, p.86-93.
- Leckie, J.O., Merrill, D.T., and Chow, W., 1985, Trace element removal from power plant waste streams by adsorption/precipitation with amorphous iron oxyhydroxide, In: *Separation of Heavy Metals and other Contaminants*, P.W. Peters and B.M. Kim (eds), *AIChE Symposium Series #243*, v.81, p.28-42.
- Lim, C.H., Jackson, M.L., Koons, R.D., and Helmke, P.A., 1980, Kaolins: Source of differences in cation-exchange capacities and cesium retention, *Clays and Clay Minerals*, v.28, p.223-229.
- Luoma, S.N. and Davis, J.A., 1983, Requirements for modeling trace metal partitioning in oxidized estuarine sediments, *Marine Chemistry*, v.12, p.159-181.
- Manceau, A., Schlegel, M., Nagy, K.L., and Charlet, L., 1999, Evidence for the formation of trioctahedral clay upon sorption of  $\text{Co}^{2+}$  on quartz, *Journal of Colloid and Interface Science*, v.220, p.181-187.
- Martinez, C.E. and McBride, M.B., 1998, Solubility  $\text{Cd}^{2+}$ ,  $\text{Cu}^{2+}$ ,  $\text{Pb}^{2+}$  and  $\text{Zn}^{2+}$  in Aged Coprecipitates with Amorphous Iron Hydroxides, *Environmental Science and Technology*, v.32, p.743-748.
- Morel, F.M.M. and Hudson, R.J.M., 1985, The geobiological cycle of trace elements in aquatic systems: Redfield revisited, In: *Chemical Processes in Lakes*, W. Stumm (ed), Wiley, New York, p.251-281.
- Newman, A.C.D. and Brown, G., 1987, The chemical constitution of clays, In *chemistry of clays and clay minerals* (ed. A.C.D. Newman), Mineral Society Monograph, v.6, p.1-128.
- Padmanabhan, E. and Mermut, A.R., 1996, Submicroscopic Structure of Fe-Coatings on Quartz Grains in Tropical Environments, *Clays and Clay Minerals*, v.44, p.801-810.
- Papini, M.P., Kahie, Y.D., Troia, B., and Majone, M., 1999, Adsorption of Lead at Variable pH onto a Natural Porous Medium: Modeling of Batch and Column Experiments, *Environmental Science and Technology*, v.33, p.4457-4464.
- Parks, G.A., 1990, Surface energy and adsorption at mineral/water interfaces: an introduction, In: Hochella M.F. Jr. and White, A.F., *Mineral-Water Interface Geochemistry*, *Reviews in Mineralogy*, Mineralogical Society of America, v.23, p.133-175.

- Payne, T.E., Davis, J.A., Lumpkin, G.R., Chisari, R., and Waite, T.D., 2004, Surface complexation model of uranyl sorption on Georgia kaolinite, *Applied Clay Science*, v.26, p.151-162.
- Peacock, C.L. and Sherman, D.M., 2005, Surface complexation model for multisite adsorption of copper (II) onto kaolinite, *Geochimica et Cosmochimica Acta*, v.69, n.15, p.3733-3745.
- Prelot, B., Janusz, W., Thomas, F., Villieras, F., Charmas, R., Piasecki, W., and Rudzinski, W., 2002, Adsorption of cadmium ions at the electrolyte/silica interface, I. Experimental study of surface properties, *Applied Surface Science*, v.196, p.322-300.
- Prikle, J.L., Brody, D.J., Gunter, E.W., Kramer, R.A., Paschall, D.C., Flegal, K.M., Matte, T.D., 1994, The Decline in Blood Lead Levels in the United States, *Journal of the American Medical Association*, v.274, n.4, p.284-291.
- Pruett, R.J. and Webb, H.L., 1993, Sampling and Analysis of KGa-1B Well-Crystallized Kaolin Source Clay, *Clays and Clay Minerals*, v.41, n.4, p.514-519.
- Puls, R.W. and Bohn, H.L., 1988, Sorption of Cadmium, Nickel, and Zinc by Kaolinite and Montmorillonite Suspensions, *Soil Science Society American Journal*, v.52, p.1289-1292.
- Rodda, D.P., Johnson, B.B., and Wells, J.D., 1996, Modeling the Effect of Temperature on Adsorption of Lead (II) and Zn (II) onto Goethite at Constant pH, *Journal of Colloid and Interface Science*, v.184, p.365-377.
- Samad, H.A. and Watson, P.R., 1998, An XPS study of the adsorption of lead on goethite ( $\alpha$ -FeOOH), *Applied Surface Science*, v.136, p.46-54.
- Sarkar, D., Essington, M.E., and Misra, K.C., 1999, Adsorption of Mercury(II) by Variable Charge Surfaces of Quartz and Gibbsite, *Soil Science Society of America Journal*, v.63, p.1626-1636.
- Schindler, P.W., Liechti, P., and Westall, J.C., 1987, Adsorption of copper, cadmium and lead from aqueous solution to the kaolinite/water interface, *Netherlands Journal of Agricultural Science*, v.35, p.219-230.
- Schindler, P.W. and Stumm, W., 1987, The surface chemistry of oxides, hydroxides and oxide minerals, In: W. Stumm (Ed.), *Aquatic surface chemistry*, Wiley Interscience, New York, p.83-110.
- Schroth, B.K. and Sposito, G., 1997, Surface charge properties of kaolinite, *Clays and Clay Mineral*, v.45, p.85-91.

- Schulthess, C.P. and Huang, C.P., 1990, Adsorption of Heavy Metals by Silicon and Aluminum Oxide Surfaces on Clay Minerals, *Soil Science Society American Journal*, v.54, p.679-688.
- Schwartz, I., 1994, Low Lead Level Exposure and Children's IQ: A meta-analysis and search for a threshold, *Environmental Research*, v.65, p.42-55.
- Shivkumar, K., Pande, A.K., and Biksham, G., 1997, Toxic trace element pollution in ground water around Patancheru and Bolaram industrial areas, Andhra Pradesh, India, a graphical approach. *Environmental Monitoring and Assessment*, v.45, p.57-80.
- Smith, L.A., Means, J.L., Chen, A., Alleman, B., Chapman, C.C., Tixier, J.S., Jr., Brauning, S.E., Gavaskar, A.R., and Royer, M.D., 1995, *Remedial Options for Metals-Contaminated Sites*, Lewis Publishers, Boca Raton, FL.
- Sparks, D.L., 2003, *Environmental Soil Chemistry*, Academic Press, San Diego, California.
- Sposito, G., 1984, *The Surface Chemistry of Soils*, Oxford University Press, New York.
- Sposito, G., 1989, *The Chemistry of Soils*, Oxford University Press, New York, p.277.
- Srivastava, P., Singh, B., and Angove, M., 2005, Competitive adsorption behavior of heavy metals on kaolinite, *Journal of Colloid and Interface Science*, v.290, p.28-38.
- Stumm, W., 1992, *Chemistry of the Solid-Water Interface: Process at the Mineral-Water and Particle-Water Interface*, Wiley-Interscience, New York.
- Stumm, W. and Morgan, J.J., 1996, *Aquatic Chemistry: Chemical Equilibria and Rates in Natural waters*, 3<sup>rd</sup> ed., Wiley, New York.
- Sverjensky, D.A. and Sahai, N., 1996, Theoretical prediction of single-site surface-protonation equilibrium constants for oxides and silicates in water, *Geochimica et Cosmochimica Acta*, v.60, n.20, p.3773-3797.
- Swedlund, P.J., Webster, J.G., Miskelly, G.M., 2003, The effect of SO<sub>4</sub> on the ferrihydrite adsorption of Co, Pb and Cd: ternary complexes and site heterogeneity, *Applied Geochemistry*, v.18, p.1671-1689.
- Traina, S.J. and Laperche, V., 1999, Contaminant bioavailability in soils, sediments and aquatic environments, *Proceedings of National Academy of Sciences. USA*, v.96, p.3365-3371.

- Trivedi, P., Dyer, J.A., and Sparks, D.L., 2003, Lead sorption onto Ferrihydrite. 1.A Macroscopic and Spectroscopic assessment, *Environmental Science and Technology*, v.37, p.908-914.
- van der Lee, J. and De Windt, L, 2002, CHESS Tutorial and Cookbook, Updated for version 3.0, Users Manual Nr, LHM/RD/02/13, Ecole des Mines de Paris, Fontainebleau, France.
- Wagner, H. M., 1991, Recent Trends In Human Lead Exposure. *New Horizons in Biological Dosimetry*, p.179-186.
- White, R., Feldman, R., and Travers, P., 1990, Neurobehavioral Effects of Toxicity Due to Metals, Solvents, and Insecticides. *Clinical Neuropharmacology*, v.13, n.5, p.392-412.
- Younger, P.L., 2000, Nature and practical application of heterogeneities in the geochemistry of Zn-rich alkaline mine water in and around Fe-Pb mine in the U.K., *Applied geochemistry*, v.15, p.1383-139.